5-2018

Multiscale investigation of the behavior of heart valve interstitial cells in response to pathological shape and mechanical stimulation

Ngoc Thien Lam
University of Arkansas, Fayetteville

Multiscale Investigation of the Behavior of Heart Valve Interstitial Cells in Response to Pathological Shape and Mechanical Stimulation

A dissertation submitted in partial fulfillment
of the requirements for the degree of
Doctor of Philosophy in Cell and Molecular Biology

by

Ngoc Thien Lam
University of Agriculture and Forestry, Vietnam
Bachelor of Science in Biotechnology, 2010

May 2018
University of Arkansas

This dissertation is approved for recommendation to the Graduate Council.

_____

Kartik Balachandran, Ph.D.
Dissertation Director

_____ _____

Suresh K Thallapuranam, Ph.D.
Committee Member

Gisela F Erf, Ph.D.
Committee Member

_____

Jeffrey C Wolchok, Ph.D.
Committee Member

ABSTRACT

Our works aim to provide an insight into how aortic valve interstitial cells (VICs) respond to pathological shape and mechanical stimulation as well as the potential signaling pathway that mediates these responses, using a multiscale approach. A single cell model was developed to investigate the effect of altered shape on valve cell function as valve cells were reported to significantly deform during the cardiac cycle. Single VICs were controlled to take on features with different width-to-length aspect ratios that corresponded to the steady-state shapes adopted by VICs when stretched to 0%, 10% and 20%, respectively. It appeared that single VIC reorganized their cytoskeleton and increased cellular activities, including contractility, metabolism, proliferation and pathological activation, in response to shape alterations. This study provided a fundamental understanding of VIC behavior at single cell level. In order to further examine valve cell pathophysiology, a more physiologically-relevant 3-dimensional (3D) stretchable model was developed to better simulate natural heart valve environment. We developed and characterized a collagen-based scaffold for dynamic culture of heart VICs. This 3D scaffold was porous, biocompatible and mechanically robust. For this reason, it was utilized as a culture model for the subsequent cell signaling study where the role of fibroblast growth factor on valve cell biology was examined in the presence of mechanical stretching stimulation. Stretch magnitudes of 10% and 20% were used to mimic healthy and pathological conditions, respectively. We reported that the Akt/mTOR pathway was up-regulated at elevated 20% stretch which was associated with increased cell proliferation/metabolism. Treatment with fibroblast growth factor 1/ fibroblast growth factor 2 (FGF1/FGF2) significantly altered cellular responses such that they aided in cell proliferation at 10% stretch while reduced cell proliferation at 20% stretch. FGF1/FGF2 treatment was also able to reduce expression of activated markers in pathologically stretched cells, suggesting that FGF1/FGF2 signaling might be a potential target

for drug therapies for heart valve treatment. Overall, this project provided a specific picture of how heart valve cells responded to pathological stimulations at multiscale levels and the involvement of FGF-receptor signaling. It is hoped that the knowledge gained from these studies could help to identify therapeutic targets for valvular disease treatment.

ACKNOWLEDGEMENTS

This dissertation is a result of a 7 year journey with a lot of ups and downs. To be able to get to this stage, I have received tremendous support from mentors, colleagues, friends and family.

First, I would like to gratefully thank my research advisor Dr. Kartik Balachandran for his willingness to welcome me to the laboratory and for his consistent support throughout my doctoral study.

I would like to express my sincere thanks to all the committee members, Dr. Suresh Kumar, Dr. Gisela Erf and Dr. Jeffrey Wolchok, for providing useful research advices and giving support for my fellowship application, and career development.

Dr. Kumar: I am thankful for always giving me support and encouragement when I needed. Thank you for giving me an opportunity to take part in your Fibroblast growth factor project.

I would also like to thank all the colleagues that I have had a chance to meet with, both from my old laboratory and from the current laboratory as well as colleagues across the CEMB and BMEG department. You made an important part of my doctoral life here at Fayetteville.

I would also like to thank all Vietnamese friends with whom I have had memorable moments of joy and laughter. A big thank to Tue Anh who has always been with me over the last few years. I am truly thankful for always having you listen to my daily stories and for always being available and helping me out when I needed it the most.

Finally, I own my deepest gratitude to my family, including mother Muot Nguyen, father Hung Lam, and sisters Hanh Lam and Quy Lam. Without them, I would not have enough strength to go this far.

Mom: although we are ocean apart and meet only thrice in the last 7 years, you are and will always be my strongest source of motivation. Without your unconditional love and sacrifice, I could have not been here today. This dissertation is for you to keep.

My sisters: I just want you to know that I am grateful for having you two as sisters. Every step that I have been through, I have been through it with you. Thank you for being with me in this journey, for believing in me and supporting me even when I did not believe in myself. I know that whatever I do, you will always be there for me. For that, I am forever grateful.

TABLE OF CONTENTS

LIST OF TABLES

LIST OF FIGURES

LIST OF ABBREVIATIONS

AR	Aspect ratio
AV	Aortic valve
BCA	Bicinchoninic acid assay
BSA	Bovine serum albumin
CAVD	Calcific aortic valve disease
DAPI	4’,6-diamidino-2-phenylindole
DMEM	Dulbecco’s modified eagle medium
DMSO	Dimethyl sulfoxide
ECG/ EKG	Electrocardiogram
ECM	Extracellular matrix
ET-1	Endothelin-1
FAD	Flavin adenine dinucleotide
FBS	Fetal bovine serum
FGF1	Fibroblast growth factor 1
FGF2	Fibroblast growth factor 2
FSS	Fluid shear stress
GAGs	Glycosaminoglycans
HMDS	Hexamethyldisilazane
Hsp47	Heat shock protein 47
5HTR2A	Serotonin receptor 2A
MMP-2	Matrix metalloproteinase-2
MMP-9	Matrix metalloproteinase-9
MTT	(3-(4, 5-dimethylthiazolyl-2)-2, 5-diphenyltetrazolium bromide
OP	Orientation parameter
PDMS	Polydimethylsiloxane
PEG	Polyethylene glycol
PFA	Paraformaldehyde
PLA	Polylactic acid
PLGA	Poly(lactic-co-glycolic acid)
PMT	Photomultiplier
PVDF	Polyvinylidene difluoride
SEM	Scanning electron microscopy
SHG	Second-harmonic generation
α-SMA	α-Smooth muscle actin
SM-MHC	Smooth muscle myosin heavy chain
TEMED	Tetramethylethylenediamine
TFM	Traction force microscopy
TGF-β1	Transforming growth factor-β1
VEC	Valvular endothelial cells
VIC	Valvular interstitial cells
VHD	Valvular heart disease
vSMC	Vascular smooth muscle cell

LIST OF PUBLISHED ARTICLES

CHAPTER 2:

Lam, N. T., T. J. Muldoon, K. P. Quinn, N. Rajaram, and K. Balachandran. 2016. Valve interstitial cell contractile strength and metabolic state are dependent on its shape. *Integr Biol (Camb)* 8 (10):1079-1089…….Published

CHAPTER 3:

Lam, N. T., H. Lam, N. M. Sturdivant, and K. Balachandran. 2017. Fabrication of a matrigel-collagen semi-interpenetrating scaffold for use in dynamic valve interstitial cell culture. *Biomed Mater* 12 (4):045013……..Published

CHAPTER 1

Introduction

1. THE HEART

1.1. The heart (Figure 1.1)

The human heart is roughly the size of a large closed fist that functions as the key organ in the circulatory system. It is the powerful muscle inside the chest that propels blood around the body as the heart beats. This blood carries oxygen and nutrients to every cell of the body while taking away carbon dioxide and waste products. There are four chambers that make up the heart: two upper chambers and two lower ones. The two upper chambers are the atria that are smaller and have thinner, less muscular walls than the ventricles. The two lower chambers are the ventricles that are larger and the stronger pumping chambers that propel blood out of the heart. A muscular wall called the septum divides the left and right sides of the heart. To prevent blood from flowing backwards into the heart, there is a system of one-way valves present in the heart. The atrioventricular valves which are between the atria and ventricles prevent backflow of the blood into the atria when the ventricle contracts. The atrioventricular on the right side of the heart is called the triscuspid valve while the one on the left side is called the mitral valve or the bicuspid valve. The semilunar valves include the pulmonary valve, located at the entrance to the pulmonary artery, and the aortic valve, located at the base of the aorta. The pulmonary valve opens to allow blood to be pumped from the heart to the lungs where it gets oxygenated and closes to prevent the backflow of blood from the pulmonary trunk into the right ventricle. Similarly, the aortic valve opens when the left ventricle squeezes to pump out blood into the aorta and closes to keep blood from going backward into the left ventricle. While the atrioventricular valves are attached to the chordae tendineae, the semilunar valves do not have chordea tendineae to hold them in place. Instead they are cup shaped and use the blood's pressure to open or close (Hinton and Yutzey 2011). The aortic valve will be the primary focus of this dissertation.

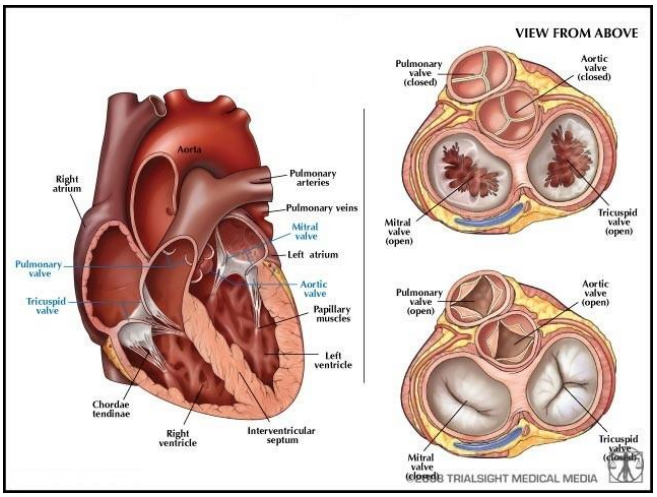

Figure 1.1: The heart and heart valves anatomy (adapted from http://thingscardiologistsnevertellyou.blogspot.com/2010/05/know-your-heart-structure-of-heart-and.html).

1.2. The Cardiac Cycle (Figure 1.2, 1.3)

The main function of the heart is to drive blood flow throughout the body. It acts as a pump using a series of contraction (systole) and relaxation (diastole) cycles of the heart muscle which occurs in a periodic pattern. During one heartbeat, 3 phases of the cardiac cycle take place: ventricular diastole/atrial systole, ventricular systole/atrial diastole and ventricular diastole/atrial diastole. In the first phase, both ventricles relax simultaneously while the left and right atria are filled with blood from the lungs and the circulation, respectively. Ventricular relaxation results in lower pressure in each ventricle compared to atrium above. The atria contract and pump blood into the ventricles through opened atrioventricular valves. The semilunar valves stay closed to keep blood from flowing retrograde into the heart. In phase 2, both atria relax after contraction while the ventricles contract simultaneously. The pressure of the ventricles forces the atrioventricular valves to close and the semilunar valves to open. Blood is simultaneously pumped into the lungs via the pulmonary artery and into the systemic circulation via the aorta. At the end of the ventricular contraction phase, both ventricles and atria enter phase 3 of the cardiac cycle. When the blood pressure in the ventricles falls below the aortic and pulmonary artery

pressures, the semilunar valves close to prevent the backflow of the blood. The atria are refilled as they relax and the cycle repeats (Fukuta and Little 2008).

The heart is able to beat in its regular rhythm through a unique electrical conduction system which includes the sinoatrial node, atrioventricular node, bundle of His, bundle branches, and Purkinje fibers. The sinoatrial node – the pacemaker of the heart, sends out an electrical signal through the walls of the atria causing them to contract. The signal travels down the atrioventricular node, through the bundle of His, down the bundle branches, and through the Purkinje fibers, causing the ventricles to contract (Christoffels and Moorman 2009; van Weerd and Christoffels 2016). The activity of these electrical impulses can be recorded and seen in the form of electrocardiogram (EKG or ECG). Hence, information from an electrocardiogram can be used to monitor the electrical activity in the heart.

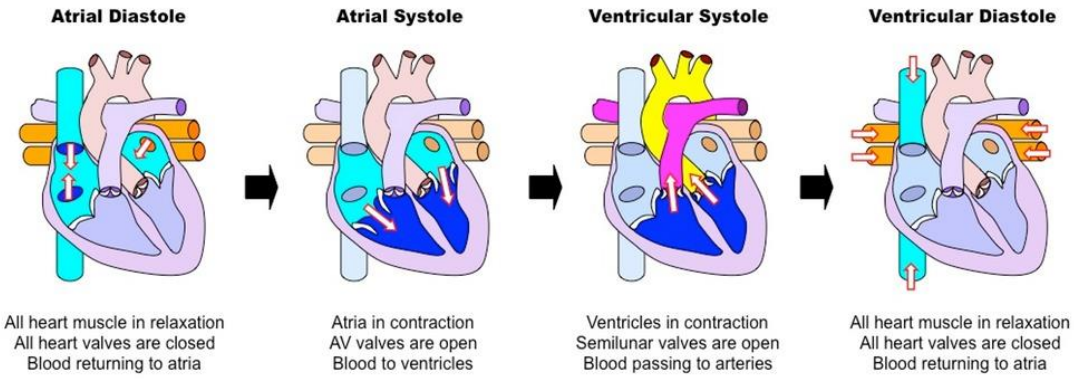

Figure 1.2: Summary of events of the cardiac cycle (adapted from https://pmgbiology.com/2015/02/17/cardiac-cycle-and-the-human-heart-a-understanding-for-igcse-biology/)

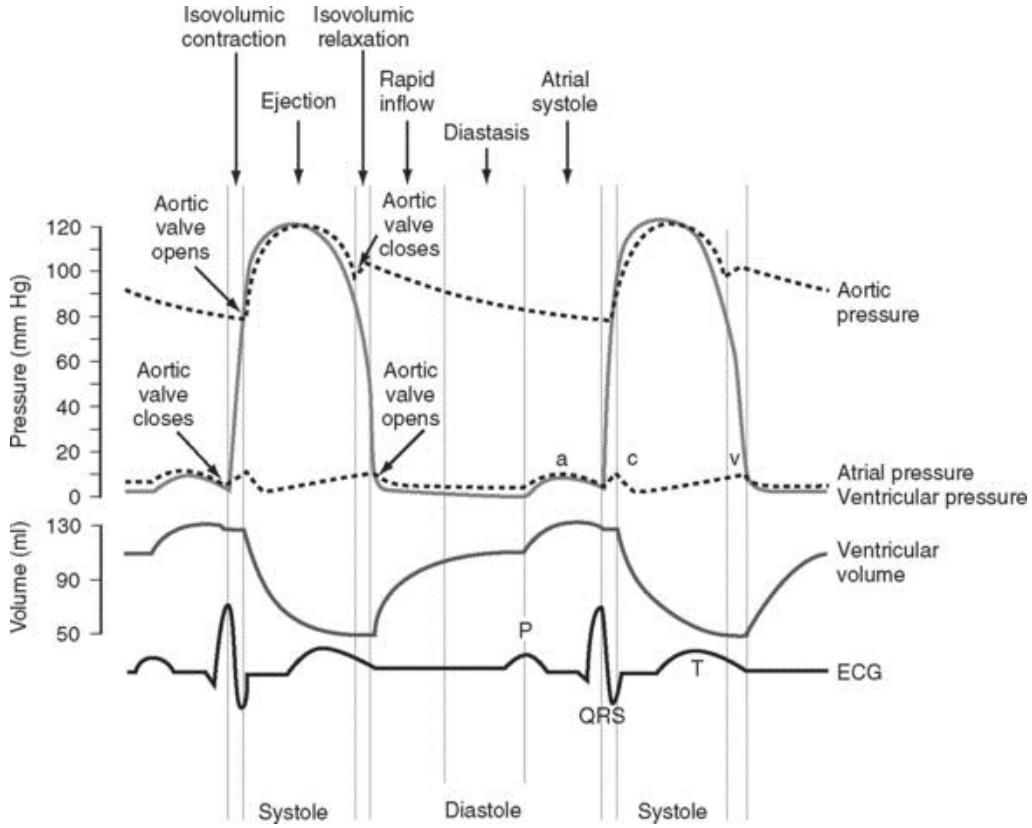

Figure 1.3: The relationship among pressure, volume and the ECG during the cardiac cycle (copied from https://thoracickey.com/physiology-and-pathophysiology/)

2. THE AORTIC HEART VALVE

As mentioned earlier, the heart has four valves: the tricuspid, pulmonary, mitral and aortic valves. They act like one-way gates, keeping the blood moving in the right direction. Heart valve disease occurs if one or more of the valves do not work properly. Such pathology can develop before birth (i.e. congenital heart valve disease), or can be acquired later in life. Congenital valve disease often affects the aortic or pulmonary valves, impairing proper formation of the tissue. They may have the wrong size or shape, or have leaflets that are not attached to the annulus correctly. Acquired or degenerative heart valve disease occurs in valves that were once normal and usually occurs in the aortic or mitral valves (Maganti et al. 2010).

Since our research focuses on the aortic valve only, the remaining sections will mainly provide background on aortic valve structure, its resident cells and an overview of aortic valve disease.

2.1. Aortic valve structure and function

The aortic valve (AV), lies at the junction between the aorta and the left ventricle, and is one of the main valves on the left side of the heart. It opens and closes more than 100,000 times per day to control blood flow between the heart and the body. The AV has three equal sized leaflets, or cusps: the left coronary cusp, the right coronary cusp, and the non-coronary cusp (Figure 1.4A) (Charitos and Sievers 2013). Each cusp is a few hundred microns thick and has 3 readily identifiable layers: the fibrosa, the spongiosa and the ventricularis (Figure 1.4B). Each layer has a distinct extracellular matrix composition and organization that confers unique mechanical and functional properties for the valves, allowing them to withstand the hemodynamic environment in the heart. In particular, the fibrosa layer, on the aortic surface, is the principle load-bearing layer due to the presence of circumferentially oriented Type I collagen fibers. The central layer, the spongiosa, is rich in glycoaminoglycans (GAGs) which aids in cushioning and lubrication between the top and the bottom layers. The ventricularis, on the ventricular side, is the thinnest of the 3 layers and contains radially aligned and elastic elastin fibers which extend and recoil as valves open and close (Wang, Leinwand, and Anseth 2014; Hinton and Yutzey 2011; Merryman and Schoen 2013).

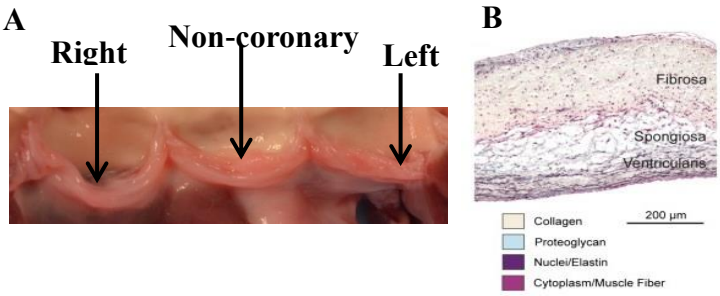

Figure 1.4: Porcine aortic valve (A), Movat's pentachrome histochemical staining of a porcine valve cusps, showing 3 distinct layers and composition of the ECM (B) ((Parvin Nejad et al. 2016)).

2.2. Cell populations in the aortic valve

Cardiac valves are composed of valvular endothelial cells (VECs) that cover the surfaces of the cusps and valvular interstitial cells (VICs) dispersed throughout the leaflets. They play an important role in maintaining normal valve architecture as well as physiological tissue homeostasis (Liu, Joag, and Gotlieb 2007).

2.2.1. Valvular Endothelial Cells

VECs line the surfaces of both sides of the valve leaflets and act as an interface between the cusp and the blood. VECs have been isolated and cultured *in vitro*. They appear cobblestone shaped in *in vitro* culture and express endothelial markers such as PECAM1, Von Willebrand Factor, and negative expression of α-smooth muscle actin (Gould and Butcher 2010).

Valve endothelial cells play an important role in regulating valve mechanics and function. Valvular leaflet degeneration and many valvular diseases have been traced to endothelial dysfunction and denudation (Leask, Jain, and Butany 2003). VECs align perpendicular to fluid flow *in vitro* and this alignment is mediated by the reorganization of focal adhesions within the cell via calpain- and Rho kinase signaling pathways (Butcher et al. 2004). Interestingly, VECs on each side of the valve appear to have different gene expression profiles as well as mechanical properties. Indeed, it was found that aortic valve disease is side-dependent, wherein AV calcification occurs more frequently in the fibrosa layer while the ventricularis side is more prone to inflammation. This side-dependency may also be due to the different local hemodynamic conditions on either side (Holliday et al. 2011).

Due to the close proximity between VEC and VICs, there exist mutual interactions in the form of paracrine signaling between these cells that regulate their phenotypes and functional behavior. Multiple co-culture models show that VICs can inhibit VEC endothelial-to-mesenchymal

transformation and VEC osteogenesis (Hjortnaes et al. 2015), while VECs appear to have a protective effect on VIC phenotype and function (Gould et al. 2014). VEC presence caused a decrease in VIC proliferation and stimulated VICs to undergo differentiation to a more quiescent phenotype (Butcher and Nerem 2006). Hence, being able to capture and study the reciprocal interactions between VEC-VIC *in vitro* will give useful insights into what really happens to these valve cells *in vivo*. The challenges with these studies come down to designing the experimental model that can mimic the *in vivo* cellular architecture of the aortic valve. Existing models are either direct co-culture, hydrogel-based or use transwell culture with complete lack of mechanical force stimulation (Richards et al. 2013; Gould et al. 2014; Tseng et al. 2014).

It has become increasingly evident that the VECs play a critical role in the pathogenesis of valvular heart disease. Continued research on VECs is crucial to our understanding of valvular heart disease and may elucidate novel treatment and prevention strategies for calcific aortic valve disease (CAVD) (Butcher and Nerem 2007).

2.2.2. Valvular Interstitial Cells

VICs are a dynamic and plastic cell population within the aortic valve that displays many unique characteristics, and provides structural integrity as well as mechanical durability for the valve. VIC isolation and culture *in vitro* have been well-established. Phenotypically, VIC population exhibits mixed characteristics of myofibroblast, fibroblast, and smooth muscle like cells (Taylor et al. 2003).

In the healthy valve, VICs are considered to be in a quiescent state. They are thought to maintain physiological valve structure and function although the exact homeostatic mechanisms are not known. Quiescent VICs are also hard to maintain in culture. Many lines of evidence suggest that VICs become activated when grown on tissue culture plastic and after several passages (Liu,

Joag, and Gotlieb 2007). Recently, addition of fibroblast growth factor 2 (FGF2) into cell culture media demonstrated promising outcomes in term of preserving the quiescent state of VICs *in vitro* (Latif et al. 2015; Porras et al. 2017). In injured or diseased valves, quiescent VICs are triggered to become activated VICs with prominent phenotypic characteristics of myofibroblast, including increased contractility, prominent stress fibers, ECM remodeling, proliferation, and migration. Activation of VICs is necessary as part of the natural repair process. However, if this process becomes dysregulated, activated cells would persist with proliferation and remodeling, leading to fibrosis, inflammation, and calcification (Liu, Joag, and Gotlieb 2007). Calcification restricts the motion of the leaflets, causing sclerosis and ultimately, stenosis (Merryman and Schoen 2013). During the pathogenesis of valve calcification, activated VICs undergo a phenotype transition to become osteoblast-like bone forming cells. Their presence has been well-described in calcified aortic valves (Leopold 2012; Rajamannan et al. 2011). It is worth noting that VICs do not normally promote calcification in culture. Addition of organic phosphates, bone morphogenetic proteins (BMPs) and/or transforming growth factor-β (TGF-β) has often been needed to induce osteogenic differentiation *in vitro* (Liu, Joag, and Gotlieb 2007).

VIC activation serves as an indicator of the early wound repair process and is associated with changes in the normal heart valve environment. Hence, understanding the regulation of VIC activation and the associated cellular responses is critical to understanding the pathobiology of heart valve diseases. *In vitro* studies have revealed several signaling mediators that promote VIC activation. Among them, the TGF-β signaling pathway is well-documented for its ability to activate VICs (Cushing, Liao, and Anseth 2005; Liu and Gotlieb 2008). TGF-β is secreted by numerous cell types including VICs. It presence is found in mitral valve prolapse and calcific aortic stenosis. Addition of TGF-β1 to cultured VICs effectively triggers VIC's differentiation

into active myofibroblasts, manifested by increasing α-SMA expression, promotion of stress fiber formation and contraction capacity (Walker et al. 2004). VICs are also sensitive to substrate stiffness and become activated if cultured on stiff substrates (about 2.5kPa) in 2D culture (Quinlan and Billiar 2012). Interestingly, it was also reported that human aortic VICs differentiated to an osteoblast-like cells with much higher alkaline phosphatase (ALP) activity and osteocalcin when they were cultured on low stiffness substrate (about 1kPa) (Duan et al. 2016). Although it is not very clear what stiffness value is considered to be pathogenic, it is worth noting that matrix stiffness alone is not sufficient to trigger valvulopathogenesis but works together with other factors to regulate VIC differentiation and calcification (Yip et al. 2009). Undoubtedly, mechanical forces belong to one of many factors that induce valve pathology.

The aortic valve is exposed to both hemodynamic forces and structural leaflet deformation as it opens and closes with every heartbeat. As a result, its resident cells, VICs in particular, continuously modulate their phenotypes and function to actively remodel cytoskeletal and ECM necessary for normal tissue homeostasis in this dynamic environment. Various *in vitro* models have set out to study how mechanical forces alter cellular function that could lead to valve pathology. The most common model is the use of native valve leaflets in *ex vivo* culture. It has been observed that when excised valve leaflets were subjected to 15% pathological circumferential cyclic tension and TGF-β treatment, VICs significantly increased activated marker, α-SMA expression and collagen biosynthesis after 2 weeks experiment (Merryman et al. 2007). In the same context, combination of stretch, TGF-β and osteogenic medium successfully induced these valve cusps to become calcified (Balachandran et al. 2010). Interestingly, it appeared that combined hemodynamic forces acted to maintain the quiescent phenotype of VICs and prevented expression of the activated contractile phenotype. It was observed that the increase

in α-SMA expression caused by elevated stretch was suppressed by the application of cyclic pressure while pressure alone significantly increased biosynthetic activity of valve leaflets but did not affect the expression of α-SMA (Thayer et al. 2011; Xing, Warnock, et al. 2004).

Although using whole valve leaflets to study the mechanobiological characteristics of valve cells provides a good model that represents the *in vivo* cell-ECM milieu, observations are typically confined to the tissue-level. More importantly, tissue-level studies cannot help to tease out the role of the various cellular components in the valve. Therefore, in order to get a big picture of valve mechanodynamics, there is a need to have more sophisticated experimental models that better characterize the valve at the cellular level.

2.3. Aortic Valve Disease

2.3.1. Valve Disease Etiology

Aortic valve disease occurs when the aortic valve does not function properly, and may be a condition present at birth or acquired over one's lifetime. The most common congenital aortic valve abnormality is called a bicuspid aortic valve that occurs when the valve has only two leaflets that are fused together instead of three. This prevents the valve from opening or closing completely (van der Wall 2015).

Acquired heart valve disease includes problems that develop with valves that were once normal. Acquired disease can be the result of an infection, such as infective endocarditis and rheumatic fever. It can also be caused by changes in the valve structure, such as stretching or tearing of the chordae tendineae or papillary muscles, fibro-calcific degeneration or dilatation of the valve annulus. Often the cause of acquired valve disease is unknown. Both congenital and acquired heart valve disease can cause stenosis or regurgitation (Maganti et al. 2010).

Aortic Valve Stenosis (Figure 1.5)

In the case of stenosis, the flaps (cusps) of the aortic valve may become thickened and stiff, or they may fuse together, causing narrowing of the aortic valve opening. The narrowed valve is not able to open fully, which reduces or blocks blood flow from the heart into the aorta and the rest of the body. The most common cause of acquired aortic stenosis is calcific degeneration, characterized by a slowly progressive, asymptomatic period that can last decades (Freeman, Crittenden, and Otto 2004). Recent studies have showed an association of aortic stenosis with atherosclerotic risk factors, suggesting that rather than a degenerative process alone, aortic stenosis is an active process akin to vascular atherosclerosis (Freeman, Crittenden, and Otto 2004).

Aortic Valve Regurgitation

In the case of regurgitation, the aortic valve does not coapt properly, causing blood to flow retrograde into the left ventricle. The leakage may prevent the heart from efficiently pumping blood to the rest of the body. As a result, the heart has to work harder to compensate for the reduced forward blood flow. This gradually reduces its ability to pump blood and can lead to heart failure (Maganti et al. 2010).

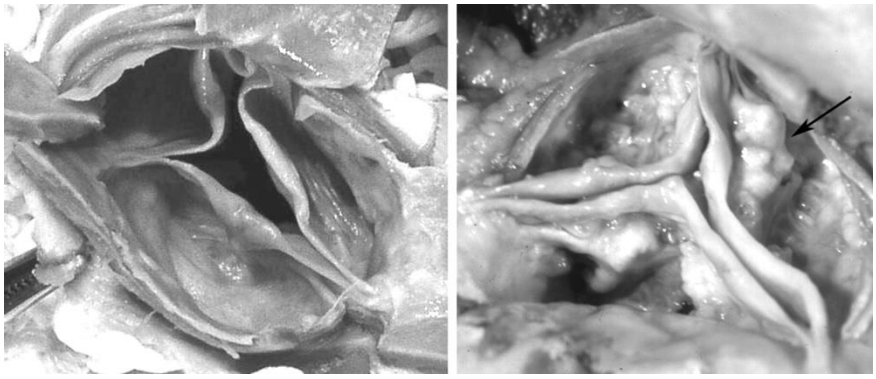

Figure 1.5: Illustration of mild diseased aortic valve (left) and severely stenotic aortic valve (right) (the arrow pointed to prominent lipocalcific changes on aortic side of the valve cusps) (Freeman and Otto 2005).

2.3.2. Treatment Options for Valvular Heart Disease

Treatment for aortic valve disease depends on the type and severity of the pathology. If one experiences mild or no symptoms, lifestyle changes and medications can help to relieve the symptoms and reduce further risk of complications. However, diseased valves will never be restored to their prior function and condition without surgical intervention. Furthermore, there are currently no medications that are FDA-approved to prevent valve disease progression or treat calcified valves, rendering valve replacement as the most common and virtually the only clinical therapy for valve diseases (Maganti et al. 2010; Shipton and Wahba 2001).

The two most commonly used valve replacements are mechanical valves and bioprosthetic valves. Although mechanical valves offer better fluid mechanics and enhanced durability, the risk of infections and thromboembolic complications after implantation is unavoidable due to the presence of foreign materials which are materials from mechanical valves. As a result, patients have to take anticoagulant medication for the entire life. Bioprosthetic valves, on the other hand, are derived from human or animal tissues that are safe to implant and do not require long-term anticoagulant therapy. However, the process of handling of biological tissue can significantly cause structural deterioration and calcification that affect the durability of these heart valve bioprosthetics. This is especially unfavorable for young patients who may need multiple surgeries over the course of their lifetimes. Clearly, an ideal valve substitute has yet to be developed (Zhang et al. 2015; Elhmidi et al. 2013; Godino, Pavon, and Colombo 2013).

2.3.3. Aortic valve mechanics and disease

Physiologically, the aortic valve lives in a harsh and dynamic mechanical environment. It is exposed to pressure, shear stress, bending stress and strain during each cardiac cycle (Figure

1.6). Alteration in any of these major mechanical forces has been showed to associate with aortic valve disease (Arjunon et al. 2013; Sacks, David Merryman, and Schmidt 2009).

Pressure: Under physiological conditions, the closed valve experienced a transvalvular pressure gradient of 80-120 mmHg (Balachandran, Sucosky, and Yoganathan 2011). The pressure generates tensile stress on the leaflets which is endured by the lamina fibrosa layer due to the presence of enrich load-bearing collagen fibers. The change in mean pressure gradient is one of the criteria used to categorize the severity of aortic stenosis. Particularly, mild stenosis has mean pressure gradient lower than 20 mmHg while that of severe stenosis is higher than 40 mmHg (Otto 2006). The effects of dynamic pressure as isolated pressure or combination of pressure and other mechanical forces on aortic valve mechanobiology have been investigated *in vitro.* Increase in pressure alone caused increase in expression of ECM proteins (including collagen, sGAG and MMP-2,9) and inflammation markers (VCAM-1, pentraxin-3, TNF-α and IL-6) while decreased the α-SMA expression. This decrease in α-SMA expression appeared more significant at elevated stretch compared to at physiological 10% stretch. In addition, without pressure, α-SMA expression significantly increased at increasing stretch, while application of pressure seemed to suppress the effect of cyclic stretch on cell phenotype (Xing, He, et al. 2004; Xing, Warnock, et al. 2004; Thayer et al. 2011). Although these studies have clearly showed the mechanobiological effects of transvalvular pressure in valve cell activation and disease initiation, its exact mechanism is still unclear.

Shear stress: The aortic valve leaflets experience shear stress when blood flows in and out the heart during a cardiac cycle. Both sides of the AV are exposed to different fluid shear stress (FSS) due to the different flow environments, which is unidirectional and pulsatile on the ventricularis and bidirectional and oscillatory on the fibrosa (Sun, Rajamannan, and Sucosky

2013). Physiologic FSS contributes to valvular homeostasis by regulating valvular biosynthetic activity and endothelial alignment (Platt et al. 2006; Weston and Yoganathan 2001; Butcher et al. 2004; Deck 1986). In contrast, FSS abnormalities have been shown to promote endothelial activation and leaflet inflammation, two precursors events to calcific aortic valve disease (Sucosky et al. 2009).

When it comes to the effect of FSS on aortic valve biology, most studies mainly focus on the valvular endothelial cells because these cells line up the valve surface and in direct contact with the flow. Emerging evidence points to the role of valvular endothelial cells to mediate FSS-mediated responses in aortic VICs (Butcher and Nerem 2006; Mahler et al. 2014). Thus co-culture model in the presence of mechanical forces would be necessary to understand complex biomechanical relationships between cells that interact *in vivo.*

Bending stress: As the aortic valve opens and closes during the course of the cardiac cycle, the valve leaflets undergo cyclic reversal of their curvature in the circumferential direction that gives rise to bending stresses. Valve cells may experience compressive and/or tensile stress during bending, depending on their position within the leaflet (Balachandran, Sucosky, and Yoganathan 2011). Bending also causes deformation in the ventricularis and fibrosa layers which could be minimized by the presence of middle spongiosa layer with lubricated characteristic. Several *in vivo* studies reported AV leaflet strains to be approximately 10 and 40% in the circumferential and radial directions, respectively. This anisotropic characteristic may be because the collagen in the circumferential direction provides greater tensile strength than that in the radial direction (Arjunon et al. 2013). *Ex vivo* results showed comparable measurement in which porcine aortic valve leaflet had strain of about 11% in the circumferential direction and about 28% in the radial direction (Yap et al. 2010). Measurement of bending strain and stress during valve operation of

polyurethane trileaflet heart valves showed maximum strain of 14.5% and stress of 1.22 MPa during the opening phase while that of closing phase were 8.3% and 0.71 MPa, respectively (Corden, David, and Fisher 1995). These values were used as the reference for physiological and pathophysiological conditions of the valve mechanic environment. Although there are various strain magnitudes that have been used in *in vitro* studies, it has been established that non-physiological strain is associated with pathological conditions in AV leaflets with regard to inflammation, activation, remodeling and calcification (Smith, Metzler, and Warnock 2010; Metzler et al. 2008). Cells under pathological (15% and 20%) stretch significantly increased proliferation, apoptosis and MMPs activity, indicating the disruption in normal homeostasis and ECM remodeling (Balachandran et al. 2009). 15% pathological level of stretch has also been showed to induce AV calcification in the BMP-dependent manner. In particular, osteogenic and calcification responses (ALP activity, Runx2 expression, and calcium levels) were reduced in the presence of BMP antagonist noggin. Interestingly, pro-inflammatory protein expression of VECs were increased at 20% biaxial cyclic strains compared to 10% while application of cyclic strain appeared to inhibit the expression of pro-inflammatory genes in aortic VIC (Balachandran et al. 2010).

As evident now, the aortic valve is subjected to multiple mechanical stimuli during the cardiac cycle naturally. Although studies of AV in the presence of isolated mechanical stimuli will help in understanding how each of them plays a role in regulating AV biology and pathology, it does not represent the true native *in vivo* state and does not provide insights into the interplay of each stimulus in regulating AV health. Thus being able to develop an experimental model that could incorporate and control all of these stimuli would be critical not only to the study of AV biology

but also to the development of tissue-engineered AV. However, this task is difficult to achieve due to the complexity of valve anatomy.

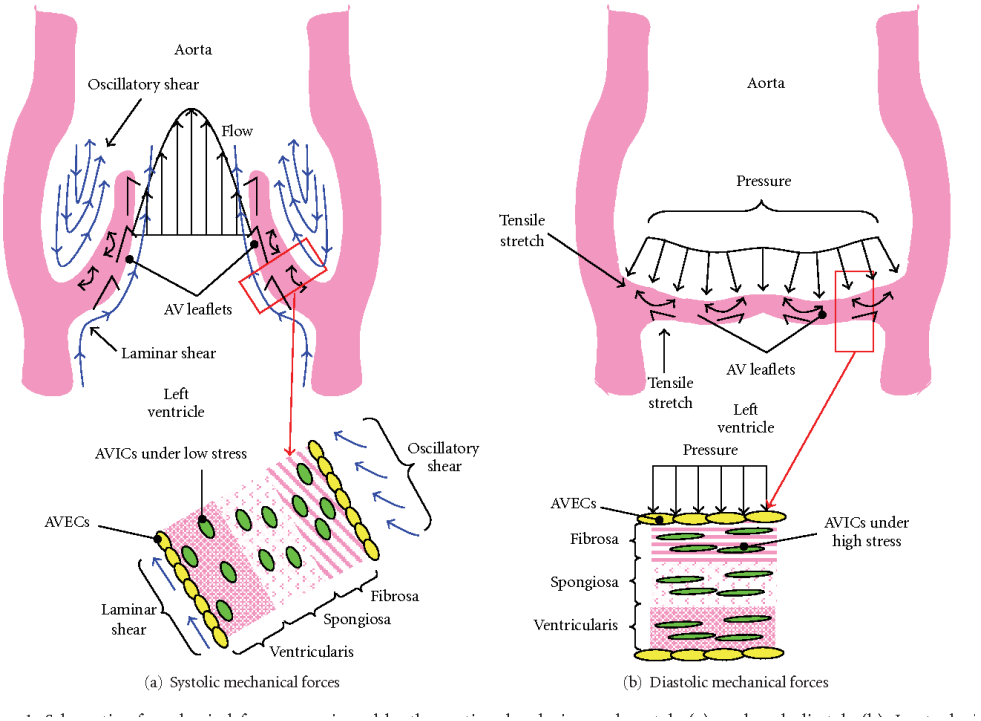

Figure 1.6: Schematic of multiple mechanical forces experienced by the aortic valve during a cardiac cycle (Balachandran, Sucosky, and Yoganathan 2011).

3. OVERVIEW OF THE PATHOPHYSIOLOGICAL ROLES OF FIBROBLAST GROWTH FACTOR SIGNALING IN THE HEART

Due to the many existing challenges in treating valvular heart disease effectively, over the last several years, researchers have focused on the molecular signaling that regulates valve cell response to pathological conditions, with the ultimate goal to identify a therapeutic target to prevent or treat heart valve disease. In the context of this dissertation, the focus is on the role of fibroblast growth factor 1 and fibroblast growth factor 2 (FGF1/FGF2) signaling.

The FGF family is comprised of secreted proteins that signal to receptor tyrosine kinases and intracellular non-signaling proteins that serve as cofactors for voltage gated sodium channels and other molecules. Secreted FGFs are expressed in nearly all tissues and they serve essential roles

in the earliest stages of embryonic development, during organogenesis, and in the adult, where they function as homeostatic factors that are important for tissue maintenance, repair, regeneration, and metabolism (Ornitz and Itoh 2015).

Within the large FGF family of proteins, FGF2 is the most well-studied in the context of the heart and heart valves. FGF2 is one of the most predominantly expressed FGFs in the heart. It is a paracrine FGF molecule that mediates biological responses by binding to and activating FGFRs. Pharmacologic and *in vitro* studies suggest that FGF2 has protective effects on the heart (Detillieux, Cattini, and Kardami 2004; House et al. 2015). In VICs, it has been demonstrated that FGF2 not only inhibits TGF-β-mediated myofibroblast activation but that it also prevents calcified nodule formation and matrix contraction. These pathological VIC phenotypes are both characteristic of end-stage valvular disease, suggesting that the maintenance of FGF2-mediated signaling pathways is integral for the prevention deleterious fibrosis in heart. Treatment with FGF2 was able to repress myofibrolast activation in porcine VICs (Cushing et al. 2008). FGF2 also appears to promote VIC wound repair *in vitro* through activation of Akt and/or TGF-β signaling pathway (Han and Gotlieb 2011, 2012). Because of these positive effects FGF2 has on valve cells, it has been supplemented to cell culture media as a way to maintain and to dedifferentiate the VICs back to a quiescent, fibrolastic phenotype with phenotypic and functional characteristics ascribed to cells in the intact valve (Latif et al. 2015).

Other FGFs such as FGF1, FGF16, FGF21, FGF23 all play roles in cardiac remodeling but their pathophysiological role in the context of heart valve disease is not well-studied (Itoh and Ohta 2013). Because both FGF1 and FGF2 belong to the FGF1 subfamily and FGF1 has been demonstrated to be able to improve cardiac functional recovery and enhance cell survival after ischemia and reperfusion (Palmen et al. 2004; Garbayo et al. 2016), it would be significantly

meaningful for heart valve field to investigate and elucidate the pathophysiological role of FGF1 in valve cells in comparison with FGF2.

There have been numerous studies in other fields that suggested the involvement of Akt as a mediator of FGF signaling in many biological processes (Forough et al. 2005; Priore, Dailey, and Basilico 2006; Mavila et al. 2012; Brewer, Mazot, and Soriano 2016). PI3K/AKT/mTOR pathway is an important pathway in regulating the cell cycle and is directly associated with cell survival, proliferation, metabolism, angiogenesis, among other biological processes (Ersahin, Tuncbag, and Cetin-Atalay 2015). Taken into account that VICs displayed increased proliferation, metabolism and ECM remodeling upon activation, we postulated that there might be a link between FGF1/FGF2 and Akt pathway that contributed to the way VICs responded to external stimulation.

REFERENCES

Arjunon, S., S. Rathan, H. Jo, and A. P. Yoganathan. 2013. Aortic valve: mechanical environment and mechanobiology. *Ann Biomed Eng* 41 (7):1331-46.

Balachandran, K., P. Sucosky, H. Jo, and A. P. Yoganathan. 2009. Elevated cyclic stretch alters matrix remodeling in aortic valve cusps: implications for degenerative aortic valve disease. *Am J Physiol Heart Circ Physiol* 296 (3):H756-64.

Balachandran, K., P. Sucosky, H. Jo, and A. P. Yoganathan. 2010. Elevated cyclic stretch induces aortic valve calcification in a bone morphogenic protein-dependent manner. *Am J Pathol* 177 (1):49-57.

Balachandran, K., P. Sucosky, and A. P. Yoganathan. 2011. Hemodynamics and mechanobiology of aortic valve inflammation and calcification. *Int J Inflam* 2011:263870.

Brewer, J. R., P. Mazot, and P. Soriano. 2016. Genetic insights into the mechanisms of Fgf signaling. *Genes Dev* 30 (7):751-71.

Butcher, J. T., and R. M. Nerem. 2006. Valvular endothelial cells regulate the phenotype of interstitial cells in co-culture: effects of steady shear stress. *Tissue Eng* 12 (4):905-15.

Butcher, J. T., and R. M. Nerem. 2007. Valvular endothelial cells and the mechanoregulation of valvular pathology. *Philos Trans R Soc Lond B Biol Sci* 362 (1484):1445-57.

Butcher, J. T., A. M. Penrod, A. J. Garcia, and R. M. Nerem. 2004. Unique morphology and focal adhesion development of valvular endothelial cells in static and fluid flow environments. *Arterioscler Thromb Vasc Biol* 24 (8):1429-34.

Charitos, E. I., and H. H. Sievers. 2013. Anatomy of the aortic root: implications for valve-sparing surgery. *Ann Cardiothorac Surg* 2 (1):53-6.

Christoffels, V. M., and A. F. Moorman. 2009. Development of the cardiac conduction system: why are some regions of the heart more arrhythmogenic than others? *Circ Arrhythm Electrophysiol* 2 (2):195-207.

Corden, J., T. David, and J. Fisher. 1995. In vitro determination of the curvatures and bending strains acting on the leaflets of polyurethane trileaflet heart valves during leaflet motion. *Proc Inst Mech Eng H* 209 (4):243-53.

Cushing, M. C., J. T. Liao, and K. S. Anseth. 2005. Activation of valvular interstitial cells is mediated by transforming growth factor-beta1 interactions with matrix molecules. *Matrix Biol* 24 (6):428-37.

Cushing, M. C., P. D. Mariner, J. T. Liao, E. A. Sims, and K. S. Anseth. 2008. Fibroblast growth factor represses Smad-mediated myofibroblast activation in aortic valvular interstitial cells. *FASEB J* 22 (6):1769-77.

Deck, J. D. 1986. Endothelial cell orientation on aortic valve leaflets. *Cardiovasc Res* 20 (10):760-7.

Detillieux, K. A., P. A. Cattini, and E. Kardami. 2004. Beyond angiogenesis: the cardioprotective potential of fibroblast growth factor-2. *Can J Physiol Pharmacol* 82 (12):1044-52.

Duan, B., Z. Yin, L. Hockaday Kang, R. L. Magin, and J. T. Butcher. 2016. Active tissue stiffness modulation controls valve interstitial cell phenotype and osteogenic potential in 3D culture. *Acta Biomater* 36:42-54.

Elhmidi, Y., S. Bleiziffer, N. Piazza, B. Voss, M. Krane, M. A. Deutsch, and R. Lange. 2013. Long-term results after transcatheter aortic valve implantation: what do we know today? *Curr Cardiol Rev* 9 (4):295-8.

Ersahin, T., N. Tuncbag, and R. Cetin-Atalay. 2015. The PI3K/AKT/mTOR interactive pathway. *Mol Biosyst* 11 (7):1946-54.

Forough, R., B. Weylie, C. Patel, S. Ambrus, U. S. Singh, and J. Zhu. 2005. Role of AKT/PKB signaling in fibroblast growth factor-1 (FGF-1)-induced angiogenesis in the chicken chorioallantoic membrane (CAM). *J Cell Biochem* 94 (1):109-16.

Freeman, R. V., G. Crittenden, and C. Otto. 2004. Acquired aortic stenosis. *Expert Rev Cardiovasc Ther* 2 (1):107-16.

Freeman, R. V., and C. M. Otto. 2005. Spectrum of calcific aortic valve disease: pathogenesis, disease progression, and treatment strategies. *Circulation* 111 (24):3316-26.

Fukuta, H., and W. C. Little. 2008. The cardiac cycle and the physiologic basis of left ventricular contraction, ejection, relaxation, and filling. *Heart Fail Clin* 4 (1):1-11.

Garbayo, E., J. J. Gavira, M. G. de Yebenes, B. Pelacho, G. Abizanda, H. Lana, M. J. Blanco-Prieto, and F. Prosper. 2016. Catheter-based Intramyocardial Injection of FGF1 or NRG1-loaded MPs Improves Cardiac Function in a Preclinical Model of Ischemia-Reperfusion. *Sci Rep* 6:25932.

Godino, C., A. G. Pavon, and A. Colombo. 2013. Long-term results after transcatheter aortic valve implantation: positive and side effects. *Minerva Cardioangiol* 61 (4):377-91.

Gould, R. A., and J. T. Butcher. 2010. Isolation of valvular endothelial cells. *J Vis Exp* (46).

Gould, S. T., E. E. Matherly, J. N. Smith, D. D. Heistad, and K. S. Anseth. 2014. The role of valvular endothelial cell paracrine signaling and matrix elasticity on valvular interstitial cell activation. *Biomaterials* 35 (11):3596-606.

Han, L., and A. I. Gotlieb. 2011. Fibroblast growth factor-2 promotes in vitro mitral valve interstitial cell repair through transforming growth factor-beta/Smad signaling. *Am J Pathol* 178 (1):119-27.

Han, L., and A. I. Gotlieb. 2012. Fibroblast growth factor-2 promotes in vitro heart valve interstitial cell repair through the Akt1 pathway. *Cardiovasc Pathol* 21 (5):382-9.

Hinton, R. B., and K. E. Yutzey. 2011. Heart valve structure and function in development and disease. *Annu Rev Physiol* 73:29-46.

Hjortnaes, J., K. Shapero, C. Goettsch, J. D. Hutcheson, J. Keegan, J. Kluin, J. E. Mayer, J. Bischoff, and E. Aikawa. 2015. Valvular interstitial cells suppress calcification of valvular endothelial cells. *Atherosclerosis* 242 (1):251-60.

Holliday, C. J., R. F. Ankeny, H. Jo, and R. M. Nerem. 2011. Discovery of shear- and side-specific mRNAs and miRNAs in human aortic valvular endothelial cells. *Am J Physiol Heart Circ Physiol* 301 (3):H856-67.

House, S. L., J. Wang, A. M. Castro, C. Weinheimer, A. Kovacs, and D. M. Ornitz. 2015. Fibroblast growth factor 2 is an essential cardioprotective factor in a closed-chest model of cardiac ischemia-reperfusion injury. *Physiol Rep* 3 (1).

Itoh, N., and H. Ohta. 2013. Pathophysiological roles of FGF signaling in the heart. *Front Physiol* 4:247.

Latif, N., A. Quillon, P. Sarathchandra, A. McCormack, A. Lozanoski, M. H. Yacoub, and A. H. Chester. 2015. Modulation of human valve interstitial cell phenotype and function using a fibroblast growth factor 2 formulation. *PLoS One* 10 (6):e0127844.

Leask, R. L., N. Jain, and J. Butany. 2003. Endothelium and valvular diseases of the heart. *Microsc Res Tech* 60 (2):129-37.

Leopold, J. A. 2012. Cellular mechanisms of aortic valve calcification. *Circ Cardiovasc Interv* 5 (4):605-14.

Liu, A. C., and A. I. Gotlieb. 2008. Transforming growth factor-beta regulates in vitro heart valve repair by activated valve interstitial cells. *Am J Pathol* 173 (5):1275-85.

Liu, A. C., V. R. Joag, and A. I. Gotlieb. 2007. The emerging role of valve interstitial cell phenotypes in regulating heart valve pathobiology. *Am J Pathol* 171 (5):1407-18.

Maganti, K., V. H. Rigolin, M. E. Sarano, and R. O. Bonow. 2010. Valvular heart disease: diagnosis and management. *Mayo Clin Proc* 85 (5):483-500.

Mahler, G. J., C. M. Frendl, Q. Cao, and J. T. Butcher. 2014. Effects of shear stress pattern and magnitude on mesenchymal transformation and invasion of aortic valve endothelial cells. *Biotechnol Bioeng* 111 (11):2326-37.

Mavila, N., D. James, S. Utley, N. Cu, O. Coblens, K. Mak, C. B. Rountree, M. Kahn, and K. S. Wang. 2012. Fibroblast growth factor receptor-mediated activation of AKT-beta-catenin-CBP pathway regulates survival and proliferation of murine hepatoblasts and hepatic tumor initiating stem cells. *PLoS One* 7 (11):e50401.

Merryman, W. D., H. D. Lukoff, R. A. Long, G. C. Engelmayr, Jr., R. A. Hopkins, and M. S. Sacks. 2007. Synergistic effects of cyclic tension and transforming growth factor-beta1 on the aortic valve myofibroblast. *Cardiovasc Pathol* 16 (5):268-76.

Merryman, W. D., and F. J. Schoen. 2013. Mechanisms of calcification in aortic valve disease: role of mechanokinetics and mechanodynamics. *Curr Cardiol Rep* 15 (5):355.

Metzler, S. A., C. A. Pregonero, J. T. Butcher, S. C. Burgess, and J. N. Warnock. 2008. Cyclic strain regulates pro-inflammatory protein expression in porcine aortic valve endothelial cells. *J Heart Valve Dis* 17 (5):571-7; discussion 578.

Ornitz, D. M., and N. Itoh. 2015. The Fibroblast Growth Factor signaling pathway. *Wiley Interdiscip Rev Dev Biol* 4 (3):215-66.

Otto, C. M. 2006. Valvular aortic stenosis: disease severity and timing of intervention. *J Am Coll Cardiol* 47 (11):2141-51.

Palmen, M., M. J. Daemen, L. J. De Windt, J. Willems, W. R. Dassen, S. Heeneman, R. Zimmermann, M. Van Bilsen, and P. A. Doevendans. 2004. Fibroblast growth factor-1 improves cardiac functional recovery and enhances cell survival after ischemia and reperfusion: a fibroblast growth factor receptor, protein kinase C, and tyrosine kinase-dependent mechanism. *J Am Coll Cardiol* 44 (5):1113-23.

Parvin Nejad, S., M. C. Blaser, J. P. Santerre, C. A. Caldarone, and C. A. Simmons. 2016. Biomechanical conditioning of tissue engineered heart valves: Too much of a good thing? *Adv Drug Deliv Rev* 96:161-75.

Platt, M. O., Y. Xing, H. Jo, and A. P. Yoganathan. 2006. Cyclic pressure and shear stress regulate matrix metalloproteinases and cathepsin activity in porcine aortic valves. *J Heart Valve Dis* 15 (5):622-9.

Porras, A. M., N. C. van Engeland, E. Marchbanks, A. McCormack, C. V. Bouten, M. H. Yacoub, N. Latif, and K. S. Masters. 2017. Robust Generation of Quiescent Porcine Valvular Interstitial Cell Cultures. *J Am Heart Assoc* 6 (3).

Priore, R., L. Dailey, and C. Basilico. 2006. Downregulation of Akt activity contributes to the growth arrest induced by FGF in chondrocytes. *J Cell Physiol* 207 (3):800-8.

Quinlan, A. M., and K. L. Billiar. 2012. Investigating the role of substrate stiffness in the persistence of valvular interstitial cell activation. *J Biomed Mater Res A* 100 (9):2474-82.

Rajamannan, N. M., F. J. Evans, E. Aikawa, K. J. Grande-Allen, L. L. Demer, D. D. Heistad, C. A. Simmons, K. S. Masters, P. Mathieu, K. D. O'Brien, F. J. Schoen, D. A. Towler, A. P. Yoganathan, and C. M. Otto. 2011. Calcific aortic valve disease: not simply a degenerative process: A review and agenda for research from the National Heart and Lung and Blood Institute Aortic Stenosis Working Group. Executive summary: Calcific aortic valve disease-2011 update. *Circulation* 124 (16):1783-91.

Richards, J., I. El-Hamamsy, S. Chen, Z. Sarang, P. Sarathchandra, M. H. Yacoub, A. H. Chester, and J. T. Butcher. 2013. Side-specific endothelial-dependent regulation of aortic valve

calcification: interplay of hemodynamics and nitric oxide signaling. *Am J Pathol* 182 (5):1922-31.

Sacks, M. S., W. David Merryman, and D. E. Schmidt. 2009. On the biomechanics of heart valve function. *J Biomech* 42 (12):1804-24.

Shipton, B., and H. Wahba. 2001. Valvular heart disease: review and update. *Am Fam Physician* 63 (11):2201-8.

Smith, K. E., S. A. Metzler, and J. N. Warnock. 2010. Cyclic strain inhibits acute pro-inflammatory gene expression in aortic valve interstitial cells. *Biomech Model Mechanobiol* 9 (1):117-25.

Sucosky, P., K. Balachandran, A. Elhammali, H. Jo, and A. P. Yoganathan. 2009. Altered shear stress stimulates upregulation of endothelial VCAM-1 and ICAM-1 in a BMP-4- and TGF-beta1-dependent pathway. *Arterioscler Thromb Vasc Biol* 29 (2):254-60.

Sun, L., N. M. Rajamannan, and P. Sucosky. 2013. Defining the role of fluid shear stress in the expression of early signaling markers for calcific aortic valve disease. *PLoS One* 8 (12):e84433.

Taylor, P. M., P. Batten, N. J. Brand, P. S. Thomas, and M. H. Yacoub. 2003. The cardiac valve interstitial cell. *Int J Biochem Cell Biol* 35 (2):113-8.

Thayer, P., K. Balachandran, S. Rathan, C. H. Yap, S. Arjunon, H. Jo, and A. P. Yoganathan. 2011. The effects of combined cyclic stretch and pressure on the aortic valve interstitial cell phenotype. *Ann Biomed Eng* 39 (6):1654-67.

Tseng, H., L. R. Balaoing, B. Grigoryan, R. M. Raphael, T. C. Killian, G. R. Souza, and K. J. Grande-Allen. 2014. A three-dimensional co-culture model of the aortic valve using magnetic levitation. *Acta Biomater* 10 (1):173-82.

van der Wall, E. E. 2015. Bicuspid aortic valve; optimal diagnosis and latest interventional treatment. *Neth Heart J* 23 (3):149-50.

van Weerd, J. H., and V. M. Christoffels. 2016. The formation and function of the cardiac conduction system. *Development* 143 (2):197-210.

Walker, G. A., K. S. Masters, D. N. Shah, K. S. Anseth, and L. A. Leinwand. 2004. Valvular myofibroblast activation by transforming growth factor-beta: implications for pathological extracellular matrix remodeling in heart valve disease. *Circ Res* 95 (3):253-60.

Wang, H., L. A. Leinwand, and K. S. Anseth. 2014. Cardiac valve cells and their microenvironment--insights from in vitro studies. *Nat Rev Cardiol* 11 (12):715-27.

Weston, M. W., and A. P. Yoganathan. 2001. Biosynthetic activity in heart valve leaflets in response to in vitro flow environments. *Ann Biomed Eng* 29 (9):752-63.

Xing, Y., Z. He, J. N. Warnock, S. L. Hilbert, and A. P. Yoganathan. 2004. Effects of constant static pressure on the biological properties of porcine aortic valve leaflets. *Ann Biomed Eng* 32 (4):555-62.

Xing, Y., J. N. Warnock, Z. He, S. L. Hilbert, and A. P. Yoganathan. 2004. Cyclic pressure affects the biological properties of porcine aortic valve leaflets in a magnitude and frequency dependent manner. *Ann Biomed Eng* 32 (11):1461-70.

Yap, C. H., H. S. Kim, K. Balachandran, M. Weiler, R. Haj-Ali, and A. P. Yoganathan. 2010. Dynamic deformation characteristics of porcine aortic valve leaflet under normal and hypertensive conditions. *American journal of physiology. Heart and circulatory physiology* 298 (2):H395-405.

Yip, C. Y., J. H. Chen, R. Zhao, and C. A. Simmons. 2009. Calcification by valve interstitial cells is regulated by the stiffness of the extracellular matrix. *Arterioscler Thromb Vasc Biol* 29 (6):936-42.

Zhang, X., B. Xu, D. S. Puperi, Y. Wu, J. L. West, and K. J. Grande-Allen. 2015. Application of hydrogels in heart valve tissue engineering. *J Long Term Eff Med Implants* 25 (1-2):105-34.

CHAPTER 2

Rational for Dissertation research

1. RATIONAL FOR DISSERTATION RESEARCH

In order to identify candidate therapeutic treatment targets for valvular heart disease, it is important to understand how resident cells in the valve behave in physiological versus pathological environment and a possible signaling pathway that regulates these responses. As mentioned earlier, many previous studies were performed either on excised leaflets (tissue scale) or on cell models (cell scale) that lack appropriate mechanical stimulation or appropriate extracellular matrix cues. Hence, in this dissertation project, a multiscale approach is used to study VIC behavior at both the single cell and the 3D cell-ECM level in the presence of mechanical stimulation. It is hoped that the information gained from this study together with information from other models published in the literature will give us a more complete picture of VIC pathophysiological behavior, and potential signaling pathways that could be targeted for therapeutic benefit.

2. HYPOTHESIS AND SPECIFIC AIMS

The overall hypothesis of this dissertation is that VICs become more prone to pathological activation and dramatically alter their cellular activities, such as proliferation and metabolism in response to abnormal mechanical stimulation, including abnormal shape and stretch. Additionally, it is postulated that the Akt/mTOR pathway plays a role in FGF1/FGF2-mediated cellular responses to abnormal mechanical stimulation.

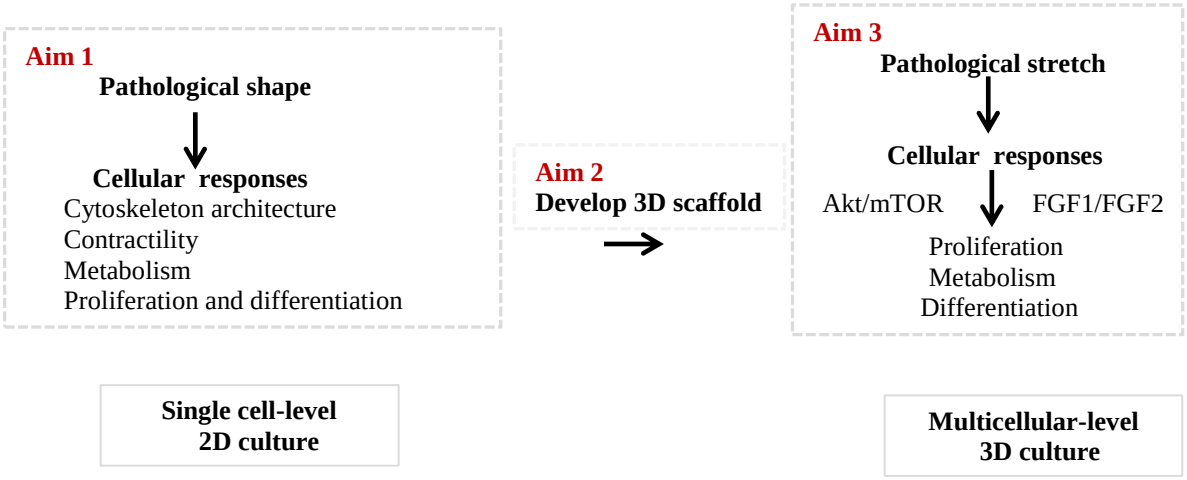

Figure 2.1: Schematic summarized all 3 aims in the project.

The above hypothesis is tested via the following specific aims:

In aim 1, the role of abnormal cell shape on VIC biological response was studied at the single cell level. Single VICs were controlled to adopt the *in vivo* cell shapes that were observed when AV leaflets were stretched at normal and pathological magnitudes. Inhibitor of actin filaments was added to further tease out the role of cytoskeletal architecture on shape-mediated cellular responses. In order to see how single VICs responded to different shapes, we examined their actin cytoskeletal and nuclear structure using Phalloidin and DAPI staining. Cell contractility and metabolism were studied via traction force microscopy and redox imaging technique. Cell proliferation and differentiation potentials were assessed through the expression of proliferation marker Ki67 and activated marker of VIC, α-Smooth muscle actin. We found that upon experiencing pathological shape, VICs started to re-organize and align their actin filaments along the longitudinal direction of the cells. Cell nuclei were also deformed as a function of altered shape. VICs significantly increased contractility, metabolism and proliferation. They also expressed higher level of activated marker of VICs, suggesting they were more prone to activation.

To extend the findings from aim 1 to a larger scale 3D VIC model, in **aim 2**, we developed a stretchable hydrogel scaffold that contained major natural ECMs found within heart valves to serve as a 3D model for culture of VICs in the presence of physiological and pathological cyclic stretching. Matrigel and Collagen I were mixed at different concentration ratios and a thorough characterization process was performed. For physical characterization, we used scanning electron microscope to examine hydrogel structure and instron tester to assess hydrogel mechanical properties. For biocompatibility, VICs were cultured into these hydrogels. Live/Dead assay and MTT assay were performed to evaluable cell proliferation and viability. Western blot was used to detect expression of common phenotypic markers of VICs to confirm the biocompatibility of matrigel. Finally, these hydrogels were subjected to cyclic stretching for 48 hours and their sizes were measured every 24 hours to examine their mechanical strength. We found that all the mixed matrigel-collagen hydrogel was scaffold with enhanced mechanical stiffness compared to collagen-only hydrogel. The presence of matrigel improved hydrogel mechanical properties while collagen was essential for VIC's growth as demonstrated in Live/dead and MTT assays. Since matrigel was not a naturally occurring matrix compound found in heart valves, we verified that its presence did not induce valve cell pathological activation compared to collagen-only hydrogels. Importantly, mixed matrigel-collagen hydrogel was able to maintain its structural integrity over the course of 48 hours under cyclic stretching conditions. Taken together, this composite scaffold appeared to have potential for use in culturing heart valve cells in the presence of cyclic stretch.

Aim 3 focused on studying the role of FGF1/2 in regulating VIC response to normal and pathological mechanical stimulation with regard to Akt/mTOR pathway using the 3D model developed in aim 2. FGFR1 inhibitor was used to tease out the role of FGF1 versus FGF2.

Encapsulated cells were subjected to 10% and 20% cyclic stretch in the presence/absence of FGF1/FGF2 and FGFR1 inhibitor. First, the involvement of Akt/mTOR pathway was tested using western blot. Cells were stretched at 10% and 20% and lysed at different time points to detect phosphorylation of Akt/mTOR. Then western blot was used to determine FGFR1 inhibitor dosage. Next the effect of FGF1/2 on stretch-mediated cellular response via Akt/mTOR pathway was tested by the treatment of FGFR1 inhibitor, FGF1/FGF2 to the stretched VICs. All samples were lysed and western blot was performed. Cell metabolism, proliferation and differentiation potentials were all examined using redox imaging and western blot technique. We reported that Akt/mTOR phosphorylation was up-regulated in pathological stretch compared to 10% physiological stretch. This upregulation was correlated with increased metabolism, proliferation and expression of activated markers observed in cells under 20% stretch. Addition of FGF1/FGF2 appeared to reverse all of these responses in 20% stretched cells, suggesting possible protective role of FGF1/FGF2 on valve cells. At 10% stretch we reported opposite observations. FGF1/FGF2 aided in cell metabolism and proliferation while did not seem to modulate their phenotype. Treatment with FGFR1 inhibitor mitigated all above-mentioned cellular responses. Overall, these data clearly highlighted the possible drug-based therapeutic potential of FGF1/FGF2.

Lam, N. T., T. J. Muldoon, K. P. Quinn, N. Rajaram, and K. Balachandran. 2016. Valve interstitial cell contractile strength and metabolic state are dependent on its shape. *Integr Biol (Camb)* 8 (10):1079-1089.

CHAPTER 3

Valve interstitial cell contractile strength and metabolic state are dependent on its shape

ABSTRACT

The role of valvular interstitial cell (VIC) architecture in regulating cardiac valve function and pathology is not well understood. VICs are known to be more elongated in a hypertensive environment compared to those in a normotensive environment. We have previously reported that valve tissues cultured under hypertensive conditions are prone to acute pathological alterations in cell phenotype and contractility. We therefore aimed to rigorously study the relationship between VIC shape, contractile output and other functional indicators of VIC pathology. We developed an *in vitro* model to engineer VICs to take on the same shapes as those seen in normal and hypertensive conditions. VICs with longer cellular and nuclear shapes, as seen in hypertensive conditions, had greater contractile response to endothelin-1 that correlated with increased anisotropy of the actin architecture. These elongated VICs also demonstrated altered cell metabolism through a decreased optical redox ratio, which coincided with increased cellular proliferation. In the presence of actin polymerization inhibitor, however, these functional responses were significantly reduced, suggesting the important role of cytoskeletal actin organization in regulating cellular responses to abnormal shape. Overall, these results demonstrate the relationship between cell shape, cytoskeletal and nuclear organization, with functional output including contractility, metabolism, and proliferation.

1. INTRODUCTION

Valvular heart disease accounts for approximately 3% of all cardiovascular pathologies and is associated with abnormal valve structure and function (Maganti et al. 2010). *In vivo*, the valves maintain their integrity and functionality by a complex interaction between the valve cusps, cells, their relative structures and the surrounding hemodynamic and mechanical environment (Balachandran, Sucosky, and Yoganathan 2011; Gould et al. 2013). Significant prior work has focused on the role of the mechanical environment in potentiating cellular alterations and subsequent progression toward disease (Balachandran et al. 2009, 2010; Warnock et al. 2006; Merryman et al. 2006; Yip et al. 2009). However, the role of cellular shape and architecture in regulating the overall balance between health and disease in the context of the valve is not well understood.

The cells and nuclei of the valve interstitial cells (VICs) within aortic valve cusps respond very rapidly to mechanical stimuli by dynamic elongation and deformation. For instance, VIC nuclear width-to-length aspect ratio (AR) almost instantaneously increased from 1:2 to 1:5 when transvalvular pressure was increased from 0 to 90 mmHg (Huang, Liao, and Sacks 2007). This elongation was correlated with significant alterations in collagen fiber architecture (Huang, Liao, and Sacks 2007). Similarly, cell and nuclear ARs significantly increased from 1:5 to 1:7 and 1:6 to 1:9, respectively, when aortic leaflet tissues were subjected to increasing strains from 10 to 20 % (Sacks, David Merryman, and Schmidt 2009). These aforementioned strains represented a transition from normotension to hypertension (Yap et al. 2010). Furthermore, transition from the systolic tension-free state to fully-closed diastolic tension resulted in a 1.5-fold increase in nuclear elongation of the VICs within the mitral valve (Lee, Carruthers, et al. 2015). These

observations thus suggest the possibility for a role for altered VIC shape and architecture in directly modulating cellular biology and function.

Although studies on the role of cell shape in modulating VIC behavior are few in number, there are several reports in the literature on the effects of constraining cell shape in influencing function and biology in other cell types. The AR of ventricular myocytes decreased from 1:7 to 1:5 during concentric hypertrophy, while it increased up to 1:11 in eccentric hypertrophy (McCain and Parker 2011). These alterations impaired cytoskeletal contractility and were therefore associated with heart failure (McCain and Parker 2011). Human mesenchymal stem cells differentiated into chondrocytes when they were cultured on micropatterned substrates and exposed to TGF-β, while they became smooth muscle cells if they were unpatterned and exposed to TGF-β (Gao, McBeath, and Chen 2010; Kilian et al. 2010). Additionally, the orientation of smooth muscle cell F-actin as well as nuclear elongation and chromatin density was found to be significantly altered as cell AR increased (Harkness et al. 2015). Elongated smooth muscle cells also showed higher contractile strength in relation to its basal tone after stimulation with ET-1 (Thakar et al. 2009; Alford et al. 2011; Win et al. 2014). These studies clearly demonstrated that changes in cell shape can potentiate functional changes.

We hypothesized that by engineering the shape of single VICs to acquire the AR of cells seen in normal and pathological conditions, we could induce changes in cell architecture, subsequently potentiating acute alterations in cell function, specifically cell contractility, metabolism, proliferation and activation. Our hypothesis was rigorously tested using an engineered single VIC model with cells forced to adopt shape of 1:3, 1:5 and 1:7 aspect ratios with the surface area of the patterns maintained constant. We demonstrate that these aspect ratios correspond to the steady-state shapes adopted by VICs when cyclically strained to 0%, 10% and 20%, respectively.

Cytochalasin D, an inhibitor of actin polymerization, was used to study the causal relationship between changes in cell shape and changes in intracellular structure/function. Cytoskeletal and nuclear architecture were quantified and correlated with contraction measured via traction force microscopy, metabolic cofactor autofluorescence imaging, immunostaining and western blotting for detection of cellular proliferation and activation. We report here that cell shape significantly influenced cytoskeletal and nuclear architecture. Elongated cells generated greater active traction stresses, suggesting a greater capacity for mobility. These elongated cells also had a lower redox ratio, higher expression of activation marker α-SMA and proliferation markers Ki-67. These responses were significantly decreased with the addition of cytochalasin D. These results suggested that altered actin cytoskeletal architecture as a result of altered cell shape caused significant changes in cell function. These cells appeared more primed for increased contractility, proliferation and pathological activation.

2. MATERIALS AND METHODS

2.1. Valve interstitial cell isolation

Fresh porcine hearts (3-6 months old) were obtained from Cockrum's Custom Meat Processing (Rudy, AR) and transported to our laboratory in cold Dulbecco's Phosphate Buffered Saline (dPBS; ThermoFisher, Waltham MA) supplemented with 1% antibiotic/antimycotic solution. Hearts were immediately dissected aseptically to reveal the aortic valve leaflets. Left, right and non-coronary leaflets were pooled and washed 2 times in Hank's Balanced Salt Solution (HBSS; ThermoFisher). Cells were isolated using collagenase digestion as described in previous protocols (Butcher and Nerem 2004; Gould and Butcher 2010). Briefly, valve endothelial cells (VECs) were removed by incubating the leaflets in collagenase solution (60U/ml) for 30 minutes and discarding the digestate. Valve interstitial cells (VICs) were then isolated by incubation the

leaflets in collagenase solution (60U/ml) at 37°C for 2 hours with frequent agitation. The digestate was spun down in centrifuge at 250g for 5 minutes at 4°C and resuspended and cultured in Dulbecco's Modified Eagle Medium (DMEM) supplemented with 10% fetal bovine serum (FBS), 50U/mL penicillin, 50U/mL streptomycin, and 10mM HEPES (all ThermoFisher). Fresh DMEM was exchanged every two to three days. Cells from passages 2-7 were used in all subsequent experiments.

2.2. Parameters for single cell model

2.2.1. Surface area of spreading and thickness of valve interstitial cell *in vitro*

We first measured the natural area of spreading of valve interstitial cells (VICs) in sparse *in vitro* culture conditions on different substrates, to determine the surface area of spreading of VICs as a function of substrate stiffness. These results were then used to design rectangular templates for subsequent soft lithography and microcontact printing experiments. Briefly, VICs were sparsely seeded onto collagen gels, polydimethylsiloxane (PDMS; Sylgard 184, Dow Corning, Midland MI) coated coverslip and tissue culture plastic at a density of 3000 cells/cm^2. After 24 and 48 hours, phase contrast images of at least 50 single VICs per substrate were captured using a regular phase contrast microscope. Surface area of spreading of the VICs was then computed using Image J software (National Institutes of Health, Bethesda MD). Unconfined compressive stiffnesses of the seeding substrates were measured using an Instron 5944 uniaxial apparatus (Instron Corp, Norwood MA) using standard testing protocols (Badrossamay et al. 2014).

2.2.2. Verification of valve interstitial cell aspect ratio as a function of imposed mechanical strain

As we mentioned previously, we chose three width-to-length aspect ratios (ARs; 1:3, 1:5, 1:7) for the current study based on previously published data on cell shape in normotensive and

hypertensive strain and pressure conditions (Huang, Liao, and Sacks 2007; Sacks, David Merryman, and Schmidt 2009). In order to independently confirm this, we seeded VICs at a confluent density within chambers on a stretchable polydimethylsiloxane (PDMS) membrane imposed external cyclical strain at 0%, 10% and 20% for 48 hours (Balachandran et al. 2011). Phase contrast images of cells were taken using an upright microscope and the cellular AR was measured by manual tracing using ImageJ software.

2.2.3. Determination of optimum culture conditions to maintain single cell culture

VICs in suspension are significantly smaller in projected area than adhered cells (142.6±3.26μm vs. 944.59±3.26μm based on our measurements, $n>50$, $p<0.05$; Figure 3.1 D). There is therefore a high possibility that more than one cell can adhere onto a rectangular fibronectin feature during initial seeding. In addition, cells can also divide while on a rectangular feature. Our first objective was therefore to determine the optimum culture conditions that would result in the highest yield of single cells on the coverslip, both on first seeding and over the course of the 24 to 48 hour experiment. We hypothesized that (I) feature surface area; (II) cell seeding density and (III) FBS concentration would have the highest effects on single cell yield, and tested these factors as follows.

(I) Effect of feature surface area. As mentioned earlier, cells are significantly smaller in suspension than when adhered. We therefore first tested single cell yield on a range of island surface areas based on the spread of VICs on PDMS. We hypothesized that the larger the surface area, the lower the single cell yield as a larger number of cells might fall on larger fibronectin features. Briefly, based on the surface area of spread of VICs (Figure 3.1 A), cells were seeded on 1500, 1700, 1900 and 2000μm^2 features. After 48 hours, cells were fixed with 4% paraformaldehyde (PFA; Electron Microscopy Sciences, Hatfield PA) and fluorescently stained

with 4',6-diamidino-2-phenylindole (DAPI; Life Technologies, ThermoFisher, Waltham MA). Images were then obtained at more than 20 image fields of the coverslips. Percentage of single cells was quantified by dividing the number of counted single cells by the total number of cells in that specific image field.

(II) Effect of seeding density. As mentioned earlier, each substrate coverslip had approximately 12,500 single cell island features. We thus hypothesized that the closer the seeding density was to this number of features, the higher the yield of single cells. We further postulated that a seeding number lower than the total number of features would increase the chance of single cell islands on the coverslip. We therefore tested seeding densities from 5,000 – 15,000 cells per coverslip (corresponding to approximately 500 - 1500 cells/cm^2 seeding density). After 48 hours, cells were fixed with 4% PFA and fluorescently stained with DAPI and quantified as before.

(III) Effect of FBS concentration. As increasing FBS concentration has a strong proliferative effect on cells (Shodell and Rubin 1970), we hypothesized that lowering the concentration of FBS during the course of culture would prevent VICs from dividing while on a rectangle. Three concentrations of FBS (0%, 2% and 10%) were tested by exchanging the culture media at 4 hours and 24 hours after seeding. All other components of the media remained unchanged. After 48 hours, cells were fixed with 4% PFA and fluorescently stained with DAPI and quantified as before.

2.3. Photolithography

Photolithographic transparency masks were designed in AutoCAD (Autodesk Inc., San Rafael CA) and fabricated by CAD/Art Services Inc. (Bandon, OR). The design of the masks for the single cell studies consisted of rectangular features of constant surface area spaced 50μm apart, with variable width-to-length aspect ratios (1:3 [23.80 x 71.41μm]; 1:5 [18.43 x 92.19μm]; 1:7

[15.58 x 109.09μm] in rectangular grids. These aspect ratios represented the AR of cells that underwent 0% (undeformed), 10% (normal physiological stretch), and 20% (elevated) stretch, respectively (Sacks, David Merryman, and Schmidt 2009). Each grid contained 12,500 single cell features. Silicon wafers (Wafer World, West Palm Beach FL) were then spin coated with Su-8 2005 negative photoresist (MicroChem Corp, Westborough MA) and exposed to ultraviolet light through the photomask and developed using standard photolithography protocols (Kane et al. 1999; Qin, Xia, and Whitesides 2010). Silicon wafers were then subsequently silanized with tridecafluoro-1,1,2,2-tetrahydrooctyl-1-trichlorosilane (United Chemical Corp, Filmore CA) overnight in a vacuum dessicator.

2.4. Microcontact printing and cell culture

Polydimethylsiloxane (PDMS; Dow Corning, Midland MI) was poured over the above silicon wafer and allowed to cure for 3 hours at 70°C. PDMS stamps with the desired features were then cut out. 50μg/mL Fibronectin (Corning, Corning NY) was incubated on the PDMS stamps with aforementioned microscale raised rectangular features for 1 hour at room temperature and blown dry gently. The stamp was then placed in contact with Ultraviolet-Ozone treated PDMS-coated coverslips for 5 minutes, thereby transferring the pattern. Coverslips were then blocked for 10 minutes with 1% Pluronics F-127 (Sigma) to prevent non-specific cell binding onto the PDMS substrate. The coverslips were washed three times with dPBS and VICs were seeded at 1000 cells per cm^2 coverslip area and cultured at 37°C, 5% CO_2. For samples that were treated with cytochalasin D, 0.1μM of the drug was added to the cell 24 hours before terminating for sample processing.

2.5. Fluorescent staining of actin and nucleus

After 48 hours of culture, cells were fixed with 4% paraformaldehyde (PFA), permeabilized using 0.5% Triton X-100 and stained for F-actin using Alexa Fluor 488 phalloidin (1:100; ThermoFisher) and for nuclei using 25µg/mL 4',6-diamidino-2-phenylindole (DAPI; ThermoFisher) for 1 hour at room temperature. Samples were then mounted onto a glass slide using Prolong Gold mounting medium (ThermoFisher), allowed to dry overnight and imaged using a Nikon Ti epifluorescence microscope.

2.6. Analysis of actin and nuclear architecture

Actin alignment was quantified using a custom-written MATLAB script, and reported using the Orientation parameter (OP), where an OP of 1 indicated perfect anisotropy and an OP of zero indicated isotropy of the actin filaments (Balachandran et al. 2011). To characterize the 3D nuclear size and morphology, image volumes of DAPI-stained samples were acquired using a commercial multiphoton microscope (Ultima Investigator, Bruker Corp.) with a water immersion 20X objective (1.0 NA). The two-photon excitation wavelength was 755nm, and emission was collected by a non-descanned detector with a 460(±20) nm bandpass emission filter. Digital voxel resolution was 0.5µm in the axial and lateral resolution. Laser power and detector gain were initially optimized to prevent photobleaching and pixel saturation and remained consistent throughout the experiment. Using MATLAB, an intensity threshold of 250 was applied to the 13-bit intensity images to produce a nuclear mask from each image volume. Individual nuclei were identified based on pixel connectivity, and nuclear volume as well as average intensity within each nucleus were computed. Finally, a maximum intensity z-projection of the image volume was obtained and the aspect ratio was computed from the major and minor axes of an ellipse fit to each nucleus using the regionprops.m function.

2.7. Traction force microscopy and analysis

VICs were seeded on 9kPa polyacrylamide gels for traction force microscopy (TFM) using methods published by others (Versaevel, Grevesse, and Gabriele 2012; Versaevel et al. 2014). Polyacrylamide gels were prepared by mixing 40% acrylamide and 2% bis-acrylamide stock solutions with 2% v/v N-hydroxyethylacrylamide and 4% v/v Alexa Fluore 488-conjugated fluorescent beads (0.2µm fluorospheres, ThermoFisher) in 50mM HEPES. This mixture was sonicated for 20 minutes, followed by the addition of ammonium persulfate and tetramethylethylenediamine (TEMED) to allow polymerization. 15µL of this mixture was pipetted onto silane-activated 35mm coverslips (Versaevel et al. 2014). A clean 18mm coverslip was put on top of the droplet to create a flat gel. This gel-coverslip was UV-O treated for 10 minutes before microcontact printing and cell seeding was performed as outlined earlier. Samples treated with cytochalasin D were cultured as mentioned earlier. At the end of the culture period, the sample was transferred to a heated imaging chamber (Warner Instruments, Hamden CT) and incubated in Tyrode's buffer (Sigma). Fluorescent images of the beads immediately beneath the patterned cells were recorded using the previously mentioned two-photon microscope with a 960nm excitation wavelength and a 525nm/45nm emission filter. The change in the position of the fluorescent beads was quantified using a MATLAB script using an algorithm described by others (Versaevel, Grevesse, and Gabriele 2012; Ye et al. 2014; Butler et al. 2002). Cell contractility was quantified by VIC response to 50nM ET-1 (Sigma) after 5 minutes. VIC basal tone was quantified by VIC response to a 100µM saturating dose of the rho-activated kinase inhibitor and vasodilator HA-1077 after 5 minutes. Tractions were calculated from the displacement field using a Fourier Transform method with mechanical properties of the gel assumed to be known (Young's Modulus = 9kPa; Poisson's ratio = 0.5) (Butler et al. 2002).

As the traction stresses are mostly confined to the ends of the cell, each cell was then longitudinally divided into five equal sections and the mean traction stresses within the sections at the ends of the cell were calculated and reported.

2.8. Two-photon redox imaging

For redox imaging, VIC samples were placed in a heated imaging chamber as before and imaged using a custom-built resonant-scanning multiphoton microscopy platform with a 40X, 0.8 NA water immersion objective (Nikon, Japan) and a MaiTai ultrafast Ti:Sapphire tunable laser source (Spectra-Physics, Santa Clara CA). The laser excitation source was tuned to 755nm (NADH fluorescence) or 860nm (FAD fluorescence) and images were acquired via non-descanned detectors with 460nm/40nm (NADH) or 525nm/45nm (FAD) bandpass filters, respectively. Laser power was kept constant at 30mW at the sample plane and photomultiplier tube (PMT) gain was fixed at 90%. Images of a cuvette filled with 4ng/mL Rhodamine B (Sigma) were acquired via a 607nm/70nm bandpass filter, under identical conditions for both NADH and FAD acquisitions, to account for possible day-to-day variation in laser intensity. Images were analyzed using a custom MATLAB script and redox ratio was calculated using the following equation on a per pixel basis (Skala and Ramanujam 2010):

$$\text{Redox ratio} = \frac{[FAD]}{[NADH]+[FAD]}$$

[FAD] represents intensity of the FAD image normalized by the corresponding rhodamine intensity. [NADH] represents intensity of the NADH image normalized by the corresponding rhodamine intensity.

2.9. Immunofluorescence and western blotting for proliferation/activation markers

For Ki-67 immunostaining, cells were fixed and permeabilized with 4% PFA and 0.5% Triton-X100 for 10 minutes. An equal mixture of 5% bovine serum albumin (BSA; Sigma) and goat

serum (Abcam, Cambridge United Kingdom) were used to block non-specific binding for 2 hours at room temperature. The cells were then incubated with Ki-67 antibody (Abcam) at a dilution of 1:500 and kept at 4°C overnight. Alexa Fluor 488-conjugated goat-anti-rabbit antibody (1:200; ThermoFisher) and 50µg/mL DAPI were applied to the cells and incubated for 1 hour before mounting the coverslips onto a glass slide using Prolong Gold antifade reagent for imaging.

For western blotting, cells were lysed with urea lysis buffer (Balachandran et al. 2011). Cell lysate was centrifuged at 10,000 rpm at 4°C and the supernatant was collected and quantified by BCA assay. 10µg of total protein was loaded onto each well of a 4-15% polyacrylamide gel (Bio-Rad, Hercules CA) and separated by electrophoresis at 150V. Proteins were then transferred to a polyvinyldifluoride (PVDF, EMD Millipore, Billerica MA) membrane, blocked in blocking buffer (Li-Cor, Lincoln NE) for 2 hours before probing with rabbit total ERK1/2 antibody (Cell Signaling Technology, Danvers MA; 1:50) and mouse phosphorylated ERK1/2 (Cell Signaling Technology; 1:500), rabbit anti-α-SMA (Abcam, 1:200), mouse anti-vimentin (Abcam, 1:1000), mouse anti-SM-MHC (Millipore, 1:20) or mouse β-actin (Abcam, 1:500). The membranes were kept at 4°C overnight. Appropriate secondary antibodies (Li-Cor; 1:15,000) were subsequently added to the membranes and incubated for 1 hour with gentle shaking, followed by washing with dPBS and distilled-deionized water. Membranes were then scanned using a Licor Odyssey scanner. Protein expression was quantified by obtaining the band intensity for the α-SMA protein and normalizing it with the intensity obtained for β-actin protein.

2.10. Statistical Analysis

All data were first analyzed for normality using the Anderson–Darling method. All normally distributed data were subsequently analyzed by one- or two-way ANOVA followed by Holm-

Sidak multiple pairwise comparisons. Data not normally distributed were analyzed using Mann-Whitney non-parametric methods. Unless otherwise specified, a p-value of less than 0.05 was used to indicate statistical significance. Data was plotted as mean with standard error bars. All results were from a sample size of at least 4 or more separate experiments.

3. RESULTS

3.1. Verification of single cell model

With regard to cell spreading area, we recorded an average cell spreading areas of single VIC ranged from 600-1800um^2 after 48 hours culture as a function of substrate stiffness (Figure 3.1 A). Specifically, VIC surface area measurements were consistently about 1700μm^2 for a wide range of substrate moduli from 10kPa to 1MPa, 48 hours after seeding (Figure 3.1 A). VIC thickness was statistically similar for the three aspect ratios (Figure 3.1 B). Additionally, AR measurement from our monolayer stretching experiment further supported the notion that our chosen three ARs (1:3, 1:5, 1:7) were a reasonable representation of cells under 0%, 10% and 20% cyclic strain, respectively. In order to achieve high yield of single cell, the following parameters also mattered: surface area of features, seeding density and the amount of FBS in culture media. Particularly, our results indicated that single cell yield was significantly higher for 1500, 1700 and 1900μm^2 patterns compared to 2000μm^2 patterns (Figure 3.2 A). Within these three surface areas, 1700μm^2 patterns tended to reliably yield the largest numbers of single cells. We thus proceeded to use a pattern surface area of 1700μm^2 for all subsequent experiments.

Seeding densities from 500 to 1000 cells/cm^2 consistently produced approximately 80% of single cell yield. We observed that the number of multiple cells per feature increased if we increased the seeding density as seen in the density of 1200-1500 cells/cm^2. Therefore, we used a seeding density of 1000 cells/cm^2 for the remaining experiments reported in this paper (Figure 3.2 B).

Our results indicated that low FBS-containing media produced high number of single cells (Figure 3.2 C-E). The best culture condition was to feed cells with 0% FBS-containing medium for the first 4 hours. This condition was postulated to restrict cells to attach solely to fibronectin patterns. After 4 hours, 2% FBS-containing medium was exchanged to both remove non-adhered cells and provide enough nutrients for cells to grow. 24 hours later, cells were fed with 0% FBS-containing medium for growth arrest. From this point, we kept using 1700 μm^2 patterns as well as the seeding density of 1000 cells/cm^2. Taken together, we consistently obtained an average of 80% single cells per coverslip. This result was especially significant as it was currently the only study that reported the specific yield of single cells and the methodology to achieve it. Other studies on single cells *in vitro* either did not report the exact number of single cell that they achieved or reported very low numbers of approximately smaller than 10% (Ye et al. 2014; McCain et al. 2012; Cheng, Komvopoulos, and Li 2011).

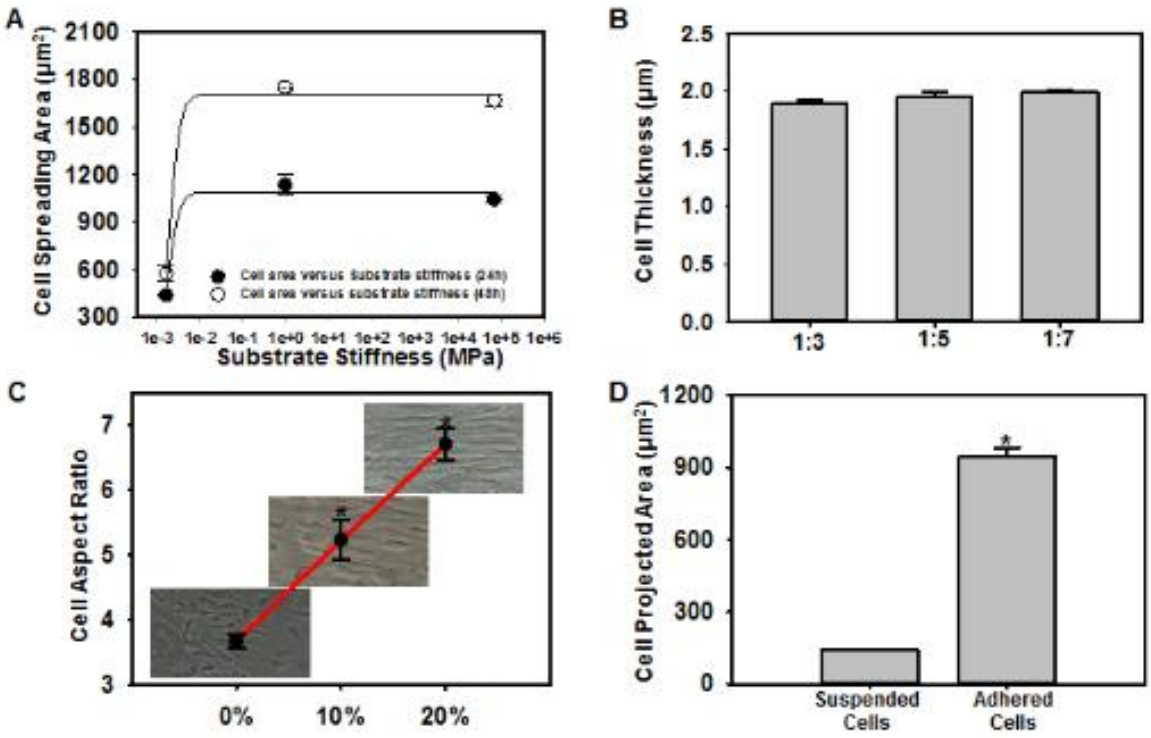

Figure 3.1: (A) Variation of VIC spreading area as a function of substrate stiffness measured after 24 and 48 hours post-seeding of cells. (B) VIC cell thickness data. (C) VIC AR measured on cyclically stretched cells. (D) Projected area of cells in suspension and adherent cells, *$p<0.05$.

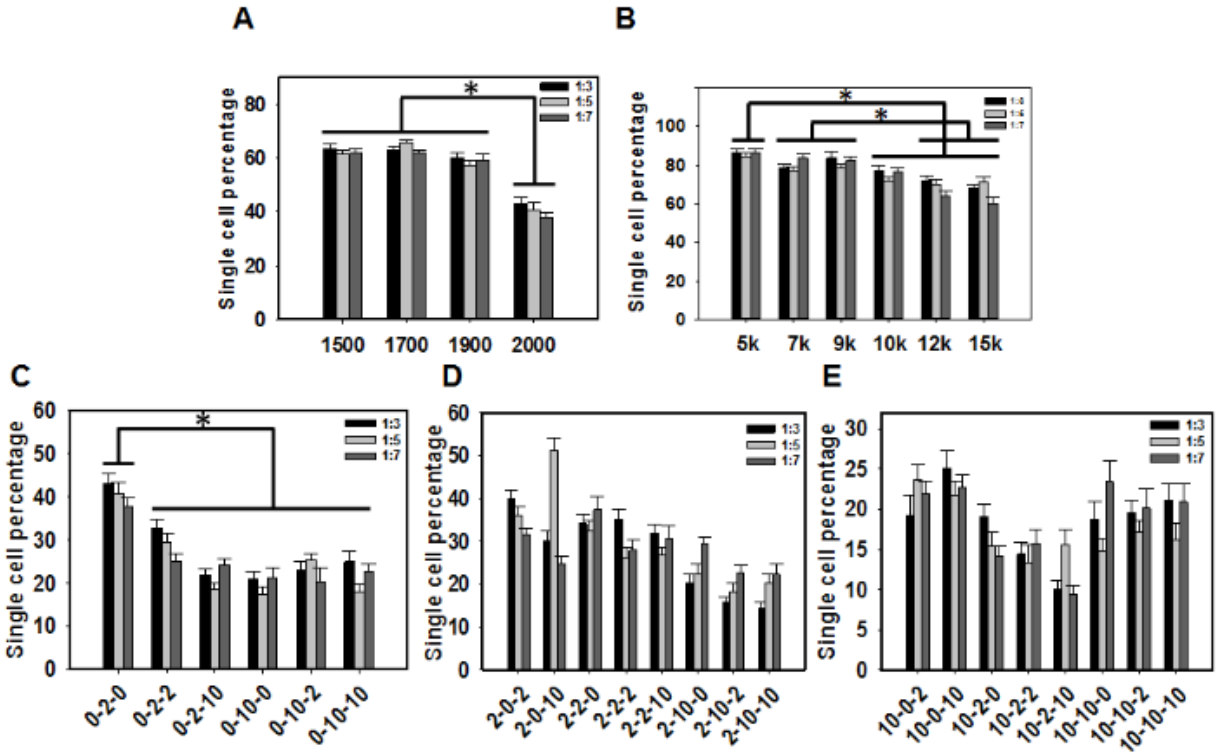

Figure 3.2: Factors affected single cell yield. (A) Percentage of single cells as a function of patterned fibronectin surface area. (B) Percentage of single cells at different seeding densities. (C-E) Percentage of single cells as a function of FBS percentage in media grouped according to concentration at seeding, n>50 individual cells, * $p<0.05$.

3.2. Engineering valve interstitial cell shape

Previous studies revealed that cells adopt different spreading areas depending on the stiffness of the underlying substrate (Yeung et al. 2005; Chaudhuri et al. 2015). We therefore first quantified the average spreading area of isolated VICs on polydimethylsiloxane (PDMS) coated coverslips (Figure 3.3 A), and show that the cell spreading area had a mean of 1700μm^2. Reports in the literature have indicated that VICs can adopt a wide variety of morphological shapes (Liu and Gotlieb 2007), but are typically confined to aspect ratios (AR) of 1:3 to 1:7 depending on the magnitude of cyclic hemodynamic pressure (Sacks, David Merryman, and Schmidt 2009). We validated this same range of ARs in an *in vitro* VIC monolayer cyclic strain model (Figure 3.3 C) and selected width-to-length ARs of 1:3 (23.8 x 71.4 μm), 1:5 (18.4 x 92.2 μm) and 1:7 (15.58 x

109.09 μm), representing the mechanical strain experienced during static, healthy and hypertensive hemodynamic conditions, respectively (Sacks, David Merryman, and Schmidt 2009). Fibronectin was microcontact printed on PDMS-coated coverslips at these same aspect ratios and VICs were seeded at 1000 cells per cm^2 coverslip area. Cells self-assembled and assumed the rectangular shape of these three aspect ratios (Figure 3.3 A-C).

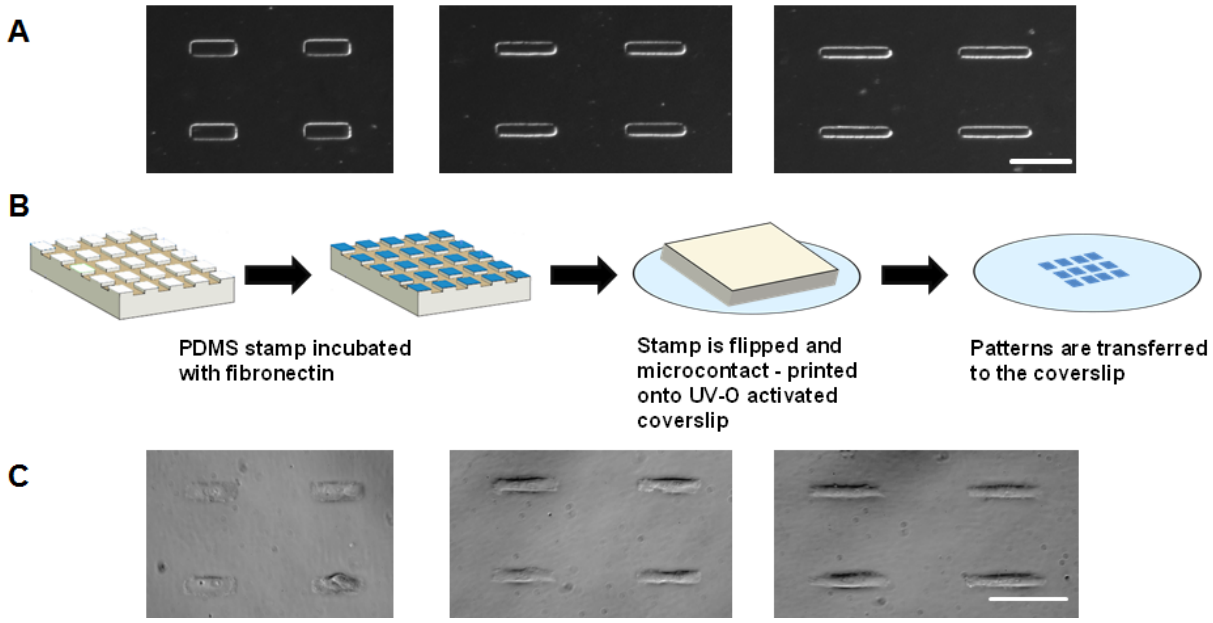

Figure 3.3: Single-cell culture model. (A) Photomasks of single-cell grid arrays with differing width-length aspect ratios, scale bar = 100μm, (B) Schematic depicting microcontact printing protocol. (C) Single cell culture images, scale bar = 100μm.

3.3. Actin and nuclear architecture and orientation varied as a function of cellular shape

Previous studies have reported that cellular structure was altered due to changes in the external mechanical boundary conditions (Balachandran et al. 2011; Ye et al. 2014). We therefore evaluated whether altered VIC shape resulted in changes in cytoskeletal and nuclear architecture. Phalloidin staining of F-actin, showed that the filaments became more prominent and aligned along the longitudinal direction of the cell as AR increased (Figure 3.4 A). Quantification of actin alignment using a previously developed technique (Balachandran et al. 2011) revealed that alignment to be statistically higher ($p<0.05$) at an AR of 1:7 compared to 1:5 and 1:3 (Figure 3.4

C). In the presence of cytochalasin D, cells did not exhibit prominent actin stress fibers (Figure 3.4 A). Cells treated with cytochalasin D at 1:7 had significantly ($p<0.05$) more aligned actin filaments compared to 1:3 and 1:5 cells. Overall, the actin orientation parameter was significantly reduced ($p<0.05$) when the cells were treated with cytochalasin D.

The actin cytoskeleton is thought to be stress-sensitive, allowing the cytoskeleton to detect extrinsic mechanical stimuli and dynamically remodel itself to accommodate the mechanical load (McCain and Parker 2011; Versaevel, Grevesse, and Gabriele 2012). It has been suggested that extracellular forces are transmitted to the cell nucleus via the cytoskeleton causing substantial deformation in the nucleus which could contribute to changes in chromatin structure and later on transcriptional regulation (Dahl, Ribeiro, and Lammerding 2008; Versaevel, Grevesse, and Gabriele 2012). Nuclear staining using DAPI (Figure 3.4 B) indeed did indicate significantly increased nuclear elongation ($p<0.05$) with increasing cellular AR (Figure 3.4 D). VIC nuclear ARs ranged from 1.7 to 2.2 for cell AR from 1:3 to 1:7, suggesting that the nucleus did not elongate to the same extent as the cell, probably due its higher mechanical rigidity (Lee, Adams, et al. 2015). Analysis of nuclear 3D volume (Figure 3.4 E) showed that as cell AR increased, 3D volume was not significantly altered, suggesting that actin cytoskeletal modulation of nuclear AR occurred without any alteration of the nuclear volume. Average intensity of chromatin was also analyzed from DAPI stained images and revealed significant higher chromatin intensity in the presence of cytochalasin D ($p < 0.05$) (Figure 3.4 F).

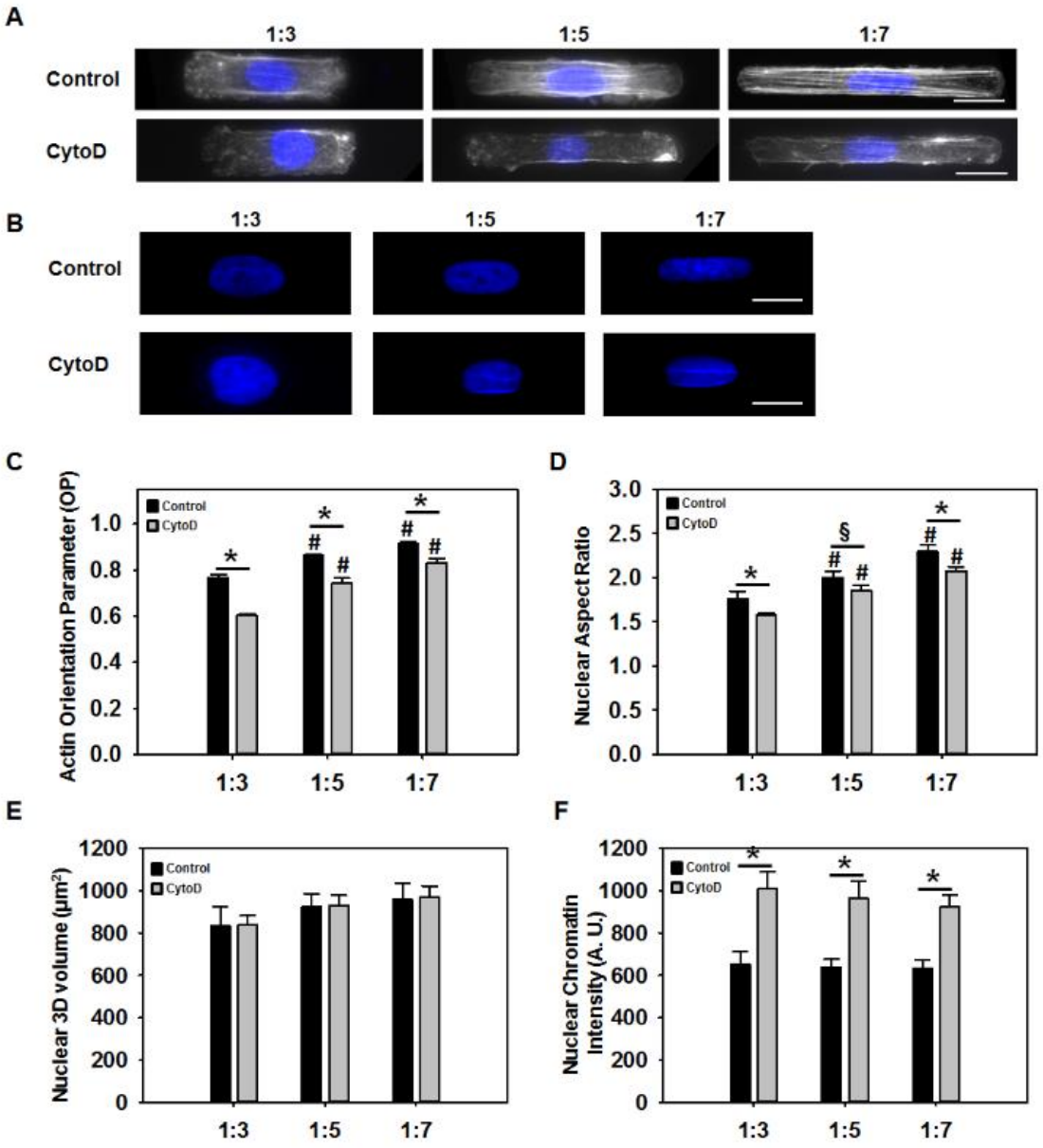

Figure 3.4: Actin orientation and nuclear morphology analysis of single cells. (A) Single VICs fluorescently stained with Phalloidin (white) and DAPI (blue), scale bar = 10μm. (B) Higher magnification DAPI images utilized for nuclear morphology analysis, scale bar = 5μm. (C) Actin orientation parameter data. (D) Nuclear aspect ratio data. (E) Nuclear 3D volume data. (F) Nuclear chromatin density data, * $p<0.05$; # $p<0.05$ with respect to 1:3.

3.4. Elongated VICs generated greater contractile traction

Cells generate tractions on their underlying substrate, that are thought to control cell shape and maintain cellular homeostasis, regulating diverse processes such as motility, differentiation and proliferation (DuFort, Paszek, and Weaver 2011; Oakes et al. 2014; Parsons, Horwitz, and Schwartz 2010). As elongated VICs were typically found in higher and elevated mechanical stress environments (Sacks, David Merryman, and Schmidt 2009), we hypothesized that VIC elongation would induce a greater capacity for contractile stress generation, that would be dependent on actin organization. This hypothesis was tested via traction force microscopy (TFM), wherein VICs with varying ARs, without and with cytochalasin D, were seeded on polyacrylamide substrates doped with fluorescent beads. Samples were first imaged prior to stimulation and sequentially stimulated with 50nM of the vasoconstrictor endothelin-1 (ET-1) and a saturating dose of 100μM of the vasodilator HA-1077 for 5 minutes each. Samples were imaged after each treatment, and traction stresses were calculated from the bead displacement images using the unstimulated image as the reference state (Ye et al. 2014). As expected, the highest VIC contractile (Figure 3.5 B) and relaxation (Figure 3.5 C) tractions were primarily localized to the longitudinal ends of the cells (Figure 3.5 A). VIC contractile strength, as computed by the traction stress applied by the cell on its substrate due to ET-1, significantly increased with increasing cellular elongation (Figure 3.5 B). Basal tone, as quantified from the response to HA-1077, was low at 1:3 AR and significantly higher at 1:5 AR (Figure 3.5 C). However there was no significant difference in basal tone between 1:5 and 1:7 ARs. When the actin filaments were disrupted with cytochalasin D, significantly reduced contractility and basal tone were observed ($p<0.05$) (Figure 3.5 B-C). Taken as a whole, these results suggested that higher alignment and prominence of F-actin stress fibers potentiated by cellular elongation

increased the ability of the VICs to generate an active contraction and maintain its basal cellular tone.

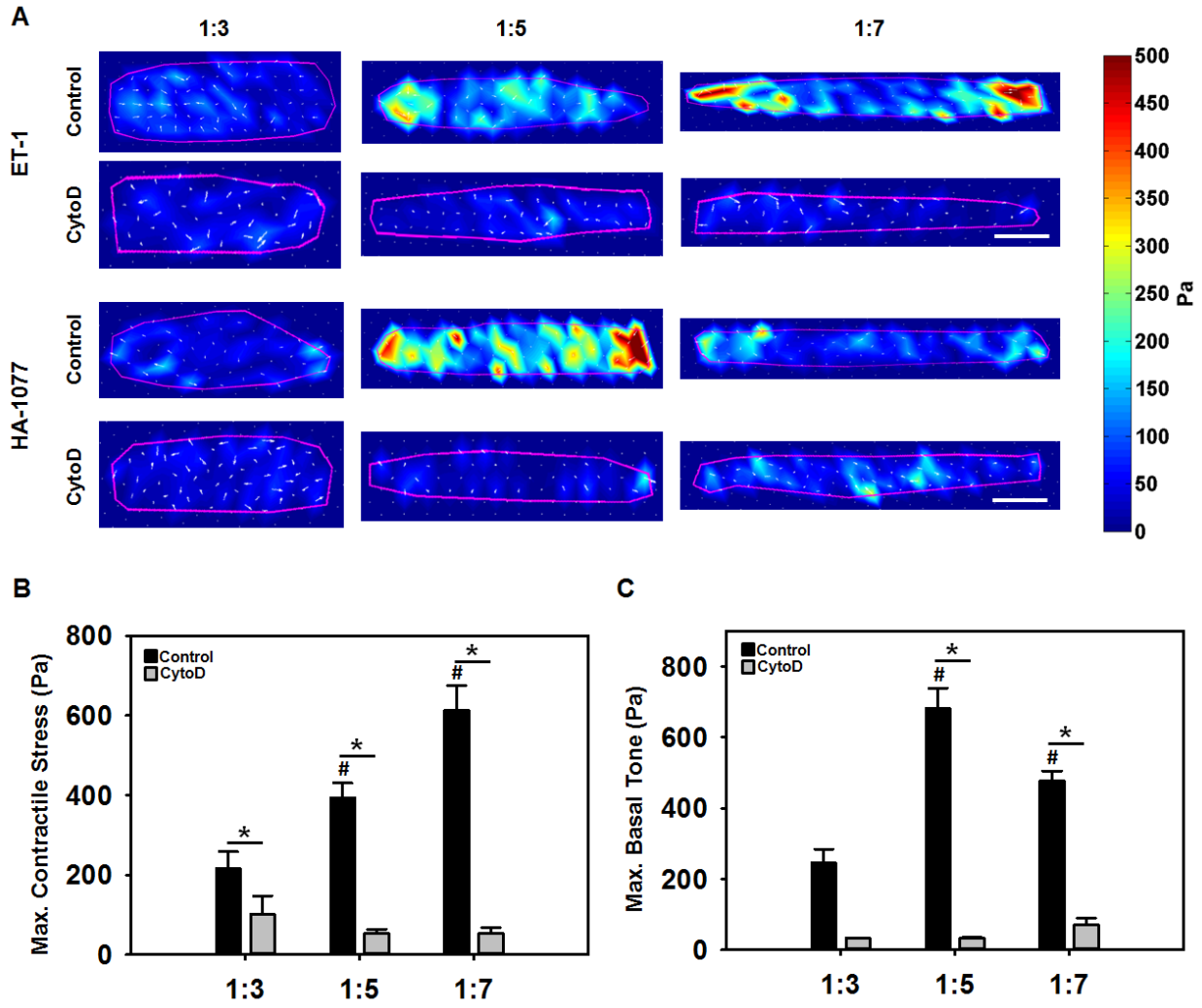

Figure 3.5: Traction force microscopy data. Representative constrained traction stress color maps representing (A) peak contractile stress generation due to ET-1 and peak relaxation due to HA-1077, scale bar = 10μm. (B) Mean contractile traction due to ET-1. (C) Mean relaxation traction/basal tone due to HA-1077, * $p<0.05$; # $p<0.05$ with respect to 1:3.

3.5. Elongated VICs exhibited reduced metabolic redox ratio

Reduced nicotinamide adenine dinucleotide (NADH) and flavin adenine dinucleotide (FAD) are coenzymes and electron carriers associated with metabolism in all eukaryotic cells. Many studies have demonstrated the potential of using the endogenous fluorescence of NADH and FAD as an indicator of cell metabolism (Georgakoudi and Quinn 2012). We evaluated whether an optical

redox ratio of FAD/(NADH+FAD) fluorescence was altered as a function of cellular AR elongation and whether the presence of an intact actin cytoskeleton affected these responses. To address this question, we collected NADH and FAD fluorescence images and computed optical redox ratios from cells in each of the three (1:3, 1:5 and 1:7) ARs without and with cytochalasin D (Figure 3.6 A-C).

Our results show that as VIC AR increased, there was a significant decrease ($p<0.05$) in redox ratio (Figure 3.6 B). In the presence of cytochalasin D, redox ratio was significantly higher than VICs without cytochalasin D, and there was no significant difference as a function of cellular AR ($p<0.05$). A decrease in the optical redox ratio was observed in mesenchymal stem cells undergoing osteogenic differentiation (Quinn et al. 2013). Additionally, decreased redox ratios have been observed upon an increase in the proliferation of keratinocytes (Quinn et al. 2016). In the context of the current study, our results thus suggest the possibilities that (I) Elongated VICs with prominent actin fibers were more likely to be at the onset of the pathologic de-differentiation process, or that (II) elongated VICs are more proliferative, or both.

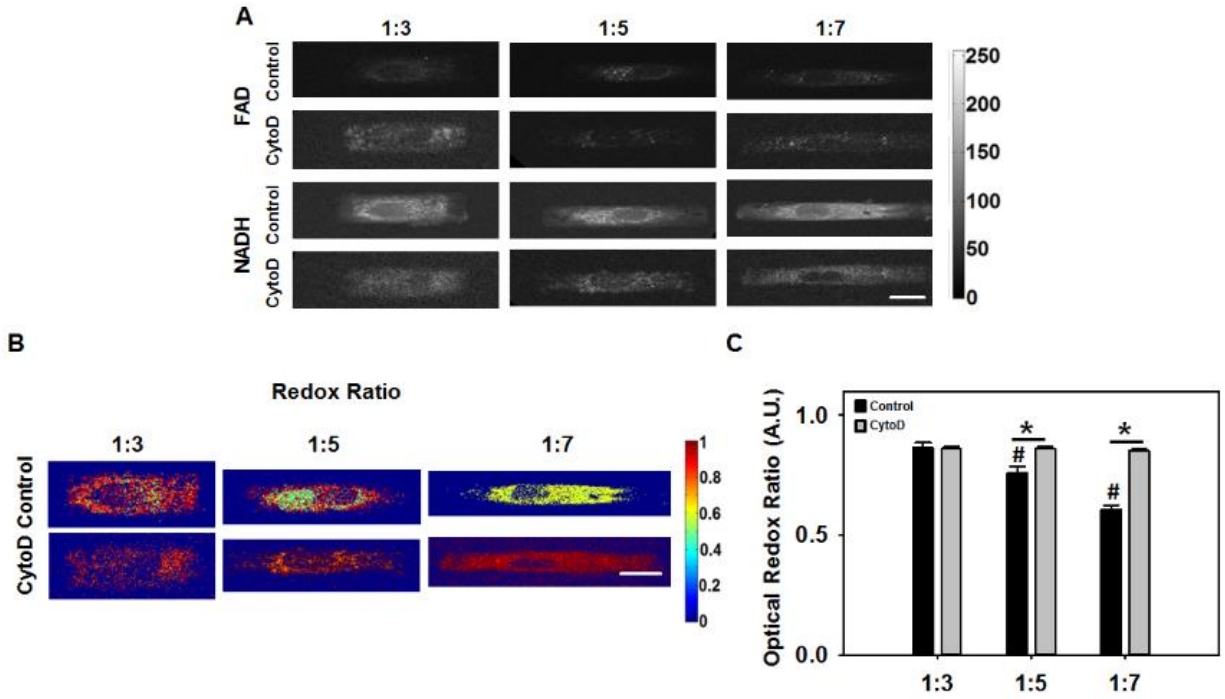

Figure 3.6: Redox imaging of single cell (A) Representative FAD and NADH fluorescence images, scale bar = 10µm. (B) Representative color maps of VIC optical redox ratios, scale bar = 10µm. (C) Mean redox ratio data for all VICs, * $p<0.05$; # $p<0.05$ with respect to 1:3.

3.6. Elongated cells exhibited higher proliferation capability and were prone to pathological activation

We considered the hypothesis that VICs with longer ARs and lower redox ratios had a higher cell proliferation and activation potential. First, VICs at the three ARs (1:3, 1:5, 1:7) were analyzed using a known indicator of cellular proliferation. Ki-67 expression, as determined via immunostaining (Figure 3.8 A) and semi-quantitation (Figure 3.8 B), significantly increased as cell AR increased. Additionally, ERK-1/2 phosphorylation was also increased as cell AR increased (Figure 3.7). Addition of cytochalasin D significantly reduced the expression of Ki67 in all cases although higher expression was still found at increased ARs. Ki-67 is a nuclear protein that is associated with cell proliferation and these results suggested that VICs possess higher proliferation capability with increasing elongation only if the actin cytoskeleton was intact.

Next, we performed western blotting to detect the expression of VIC phenotype markers α-smooth muscle actin (α-SMA), smooth muscle myosin heavy chain (SM-MHC) and vimentin. α-SMA is a cytoskeletal isoform of actin which is usually found in activated VICs, SM-MHC is a smooth muscle-specific marker, and vimentin is typically an indicator of quiescent, non-activated VICs (Rabkin et al. 2002). Additionally, α-SMA-positive activated cells typically display features of myofibroblasts such as increased contraction and prominent stress fibers (Balachandran et al. 2011). As expected, cells at the longest ARs had significantly increased α-SMA expression while adding cytochalasin D reduced its expression (Figure 3.8 C-D). This particular reduction was statistically significant only at the 1:7 aspect ratio (Figure 3.8 D). There was no significant difference in expression of SM-MHC and vimentin (Figure 3.8 C). Overall, these results suggested that VIC elongation potentiated stronger proliferative responses than differentiation ones. VICs did demonstrate moderately increased activated myofibroblast phenotype at the highest level of cell elongation, and these responses were more pronounced in the presence of actin cytoskeletal stress fibers.

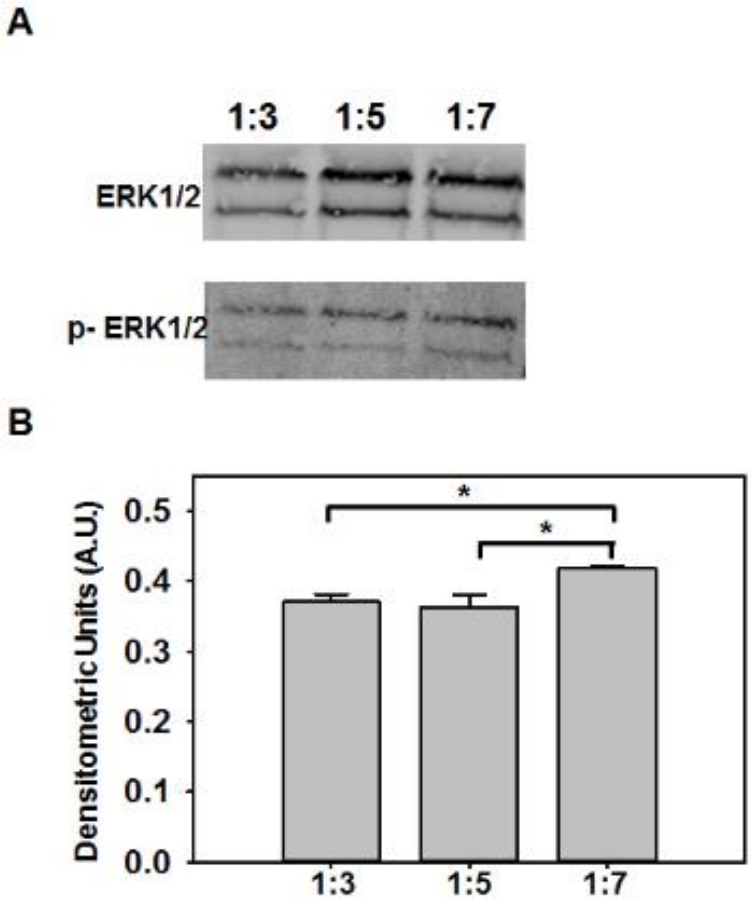

Figure 3.7: (A) Representative western blot scan for ERK1/2 phosphorylation analysis. (B) Densitometric analysis of ERK1/2 phosphorylation western blots,* $p<0.05$.

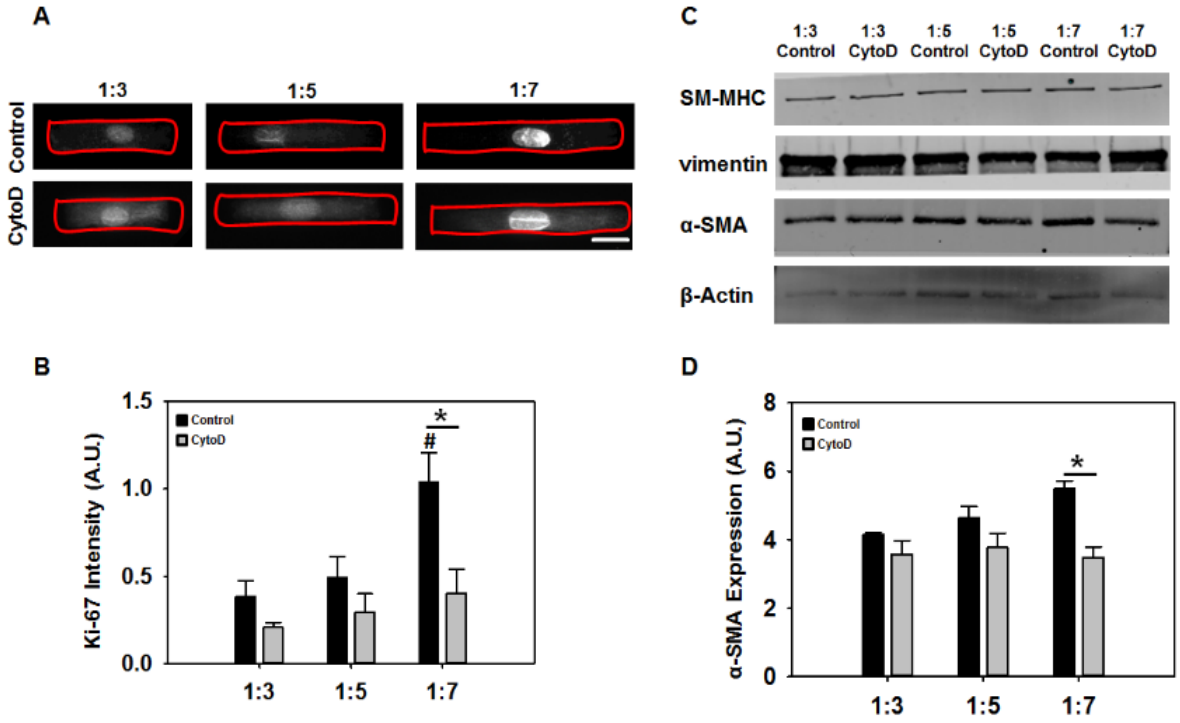

Figure 3.8: Immunofluorescent and western blotting data showing the proliferation and pathological activation of VICs. (A) Representative immunofluorescently stained VICs for Ki-67 (white), scale bar = 10μm. (B) Semi-quantitation of Ki-67 immunostains. (C) Representative western blot scan for VIC phenotype markers. (D) Densitometric analysis of α-SMA western blots, * $p<0.05$; # $p<0.05$ with respect to 1:3.

4. DISCUSSION

We show in this work that altered actin cytoskeletal organization due to elongated VIC shape was an important factor in regulating VIC acute contractile function, metabolism, proliferation and phenotypic activation. While several other methods exist wherein cellular shape and structure could be modulated while maintaining cell-cell contact (Chaterji et al. 2014; Alford et al. 2011; Win et al. 2014), our single cell model represents the smallest functional unit of the VIC and thus an important first step in understanding the role of VIC shape on its biology and function. Shorter and wider VICs generated less contractile stress and were at a less biosynthetic and proliferative state, while elongated narrower VICs had greater contractile stress generation, more biosynthesis, increased proliferation and α-SMA activation, correlating with greater

organization of the actin cytoskeleton. Our results suggest that VICs in a higher pressure environment *in vivo*, which are more elongated with typical ARs of 1:7 (Sacks, David Merryman, and Schmidt 2009; Huang, Liao, and Sacks 2007), have a greater potential for increased cellular activity, proliferation and myofibroblast differentiation.

Since the actin cytoskeletal, was responsible for maintaining the cell shape and mechanical resistance to deformation, any change in cell shape was expected to change the actin organization and subsequent modulation of nuclear shape (Vishavkarma et al. 2014). Our results supported the notion that as the VIC elongated, cytoskeletal actin and cell nuclear significantly altered their organization and shape, respectively. Specifically, actin filaments became more prominent with increased anisotropy, while cell nuclei elongated and increased 2D area and AR, while conserving nuclear volume. Others have demonstrated that forces transduced to altered cell architecture could result in significant nuclear deformations (Guilak, Tedrow, and Burgkart 2000; Guilak 1995). The primary mediator for these structural alterations is thought to be the actin filament (Maniotis, Chen, and Ingber 1997). Previous work had demonstrated that vascular smooth muscle cells (vSMC) became more elongated and expressed higher α-SMA as well as more aligned stress fibers on engineered nanogrooves compared to unpatterned substrates (Chaterji et al. 2014). This altered F-actin cytoskeleton remodeling was known to significantly affect vSMC proliferation and migration ability (Kim et al. 2008). The increase in alignment and organization of actin that we observed in elongated VICs was thus thought to allow for generation of extra tension that might be needed for a functional response or migration (Oakes et al. 2014). The causal relationship between cell shape, actin and nuclear shape was demonstrated when the addition of cytochalasin D to the single cell culture significantly mitigated changes in actin and nuclear structure. Our TFM results further supported our above-mentioned conclusion

as elongated 1:7 AR cells which had more prominent actin filaments, generated greater contractile response to ET-1. It should be noted that the increased contractile strength did not result in a significant change in the basal tone of the 1:7 AR cells compared to the 1:5 cells, suggesting that the basal tension in these elongated cells was not increased as a result of shape elongation, but its active contractility was. When the actin filament network was disrupted, cells were no longer able to potently respond to ET-1 as well as HA1077.

The decrease in the optical redox ratio has been used previously to monitor precancerous transformations (Skala et al. 2007; Varone et al. 2014), cell proliferation during wound healing (Quinn et al. 2016), and as an early indicator of cellular differentiation in mesenchymal stem cells (Quinn et al. 2013). Our results show that the redox ratio can serve as an indicator of VIC proliferation and to a lesser extent, phenotypic activation. Redox ratio was significantly lowered in the 1:7 AR cells, which were also contractile and proliferative. Hence, an overall decrease in redox ratio could also be an indicator of increased macro molecule synthesis for proliferation (Quinn et al. 2013). The clear correlation between reduced redox ratio and increased contractility and proliferative potential in elongated VICs suggests that the redox ratio might be an early indicator of dysfunction in the VIC, and merits future study.

We also observed altered Ki-67 and α-SMA protein expression as a result of the altered actin architecture potentiated by VIC shape change. A number of studies have reported that large scale changes in cell shape increased force transduction and affected nuclear chromatin condensation and subsequent gene expression (Versaevel, Grevesse, and Gabriele 2012; Zink, Fischer, and Nickerson 2004). We observed similar responses in our current work. Chromatin density was statistically similar for all ARs. In the presence of actin inhibitor, chromatin density was significantly increased. A recent report on cancer cells did report highest levels of chromatin

density in cells undergoing normal growth, while activated cancer cells showed lower levels of chromatin density (Oh, Gertych, and Tajbakhsh 2013). This same study reported that senescent cells, where there was no proliferation, had the lowest levels of chromatin density (Oh, Gertych, and Tajbakhsh 2013). Our results thus possibly suggest that elongated cells with more aligned actin filaments were likely to experience pathological activation (i.e the cell differentiation process in which quiescent VIC exhibited features of myofibroblast). This notion was further supported by our western blot which showed the increased expression of α-SMA marker as ARs increased. When the cytoskeleton was disrupted, its expression was reduced. Overall, our results underlined the potential role of the cytoskeleton, and the actin network in particular, in acting as an 'antenna' for the VIC mechanobiological response - receiving external signals, processing and transducing downstream signals to the cell nucleus to exert appropriate responses.

The following limitations are to be noted. We have subjected a single VIC to different width-to-length ARs to study the correlation between cell elongation and its function. Our model does not recapitulate cell-cell contact, or the three-dimensional environment that exists within the valve interstitial milieu. However, as mentioned previously, being able to comprehend VIC behavior at its fundamental, functional, single-cell unit is an important first step toward understanding valve physiology as well as pathology. Our model also does not directly apply mechanical forces onto the VICs. However, we demonstrate (Figure 3.1) that the ARs employed in our study (1:3, 1:5, 1:7) are a reasonable approximation of the steady-state shape achieved by VICs that are cyclically stretched to 0%, 10% and 20%, respectively.

In summary, we demonstrate the strong correlation between VIC shape and its contractile and metabolic function. VIC shape change could be thus seen as an indication of potential changes in

the cell activity and vice versa. We also propose the possibility of using redox ratio as one of the tools for early detection of the pathological state of VICs.

5. CONCLUSIONS

In this study, we reported a development of a single cell model to study how valve cells responded to alteration in cell shape. Single valve interstitial cells were engineered to adopt varying width-to-length ratios and their contractility as well as metabolic activity were quantified. We observed an increase in contractile strength and decrease in metabolic redox ratio as cells became more elongated and their actin architecture became more aligned. These results suggested that valve interstitial cells modulated their contractile and metabolic function depending on their shape and arrangement of cytoskeletal elements.

These promising results motivated us to explore further valve interstitial cell pathophysiology in a more complex model. Based on current limitations of the single cell model, we set out our next aim to develop a 3D cell culture platform where mechanical force was present. We hoped that the 3D model would be a better representative of *in vivo* condition and gave us more insight into the influence of microenvironment signaling on valve cell functional behavior.

REFERENCES

Alford, P. W., A. P. Nesmith, J. N. Seywerd, A. Grosberg, and K. K. Parker. 2011. Vascular smooth muscle contractility depends on cell shape. *Integr Biol (Camb)* 3 (11):1063-70.

Badrossamay, M. R., K. Balachandran, A. K. Capulli, H. M. Golecki, A. Agarwal, J. A. Goss, H. Kim, K. Shin, and K. K. Parker. 2014. Engineering hybrid polymer-protein super-aligned nanofibers via rotary jet spinning. *Biomaterials* 35 (10):3188-97.

Balachandran, K., P. W. Alford, J. Wylie-Sears, J. A. Goss, A. Grosberg, J. Bischoff, E. Aikawa, R. A. Levine, and K. K. Parker. 2011. Cyclic strain induces dual-mode endothelial-mesenchymal transformation of the cardiac valve. *Proceedings of the National Academy of Sciences of the United States of America* 108 (50):19943-8.

Balachandran, K., P. Sucosky, H. Jo, and A. P. Yoganathan. 2009. Elevated cyclic stretch alters matrix remodeling in aortic valve cusps: implications for degenerative aortic valve disease. *American journal of physiology. Heart and circulatory physiology* 296 (3):H756-64.

Balachandran, K., P. Sucosky, H. Jo, and A. P. Yoganathan. 2010. Elevated cyclic stretch induces aortic valve calcification in a bone morphogenic protein-dependent manner. *Am J Pathol* 177 (1):49-57.

Balachandran, K., P. Sucosky, and A. P. Yoganathan. 2011. Hemodynamics and mechanobiology of aortic valve inflammation and calcification. *Int J Inflam* 2011:263870.

Butcher, J. T., and R. M. Nerem. 2004. Porcine aortic valve interstitial cells in three-dimensional culture: comparison of phenotype with aortic smooth muscle cells. *The Journal of heart valve disease* 13 (3):478-85; discussion 485-6.

Butler, J. P., I. M. Tolic-Norrelykke, B. Fabry, and J. J. Fredberg. 2002. Traction fields, moments, and strain energy that cells exert on their surroundings. *American journal of physiology. Cell physiology* 282 (3):C595-605.

Chaterji, S., P. Kim, S. H. Choe, J. H. Tsui, C. H. Lam, D. S. Ho, A. B. Baker, and D. H. Kim. 2014. Synergistic effects of matrix nanotopography and stiffness on vascular smooth muscle cell function. *Tissue engineering. Part A* 20 (15-16):2115-26.

Chaudhuri, O., L. Gu, M. Darnell, D. Klumpers, S. A. Bencherif, J. C. Weaver, N. Huebsch, and D. J. Mooney. 2015. Substrate stress relaxation regulates cell spreading. *Nat Commun* 6:6364.

Cheng, Q., K. Komvopoulos, and S. Li. 2011. Surface chemical patterning for long-term single-cell culture. *Journal of biomedical materials research. Part A* 96 (3):507-12.

Dahl, K. N., A. J. Ribeiro, and J. Lammerding. 2008. Nuclear shape, mechanics, and mechanotransduction. *Circulation research* 102 (11):1307-18.

DuFort, C. C., M. J. Paszek, and V. M. Weaver. 2011. Balancing forces: architectural control of mechanotransduction. *Nat Rev Mol Cell Biol* 12 (5):308-19.

Gao, L., R. McBeath, and C. S. Chen. 2010. Stem cell shape regulates a chondrogenic versus myogenic fate through Rac1 and N-cadherin. *Stem cells* 28 (3):564-72.

Georgakoudi, I., and K. P. Quinn. 2012. Optical imaging using endogenous contrast to assess metabolic state. *Annual review of biomedical engineering* 14:351-67.

Gould, R. A., and J. T. Butcher. 2010. Isolation of valvular endothelial cells. *Journal of visualized experiments : JoVE* (46).

Gould, S. T., S. Srigunapalan, C. A. Simmons, and K. S. Anseth. 2013. Hemodynamic and cellular response feedback in calcific aortic valve disease. *Circulation research* 113 (2):186-97.

Guilak, F. 1995. Compression-induced changes in the shape and volume of the chondrocyte nucleus. *J Biomech* 28 (12):1529-41.

Guilak, F., J. R. Tedrow, and R. Burgkart. 2000. Viscoelastic properties of the cell nucleus. *Biochemical and biophysical research communications* 269 (3):781-6.

Harkness, T., J. D. McNulty, R. Prestil, S. K. Seymour, T. Klann, M. Murrell, R. S. Ashton, and K. Saha. 2015. High-content imaging with micropatterned multiwell plates reveals influence of cell geometry and cytoskeleton on chromatin dynamics. *Biotechnology journal* 10 (10):1555-67.

Huang, H. Y., J. Liao, and M. S. Sacks. 2007. In-situ deformation of the aortic valve interstitial cell nucleus under diastolic loading. *J Biomech Eng* 129 (6):880-89.

Kane, R. S., S. Takayama, E. Ostuni, D. E. Ingber, and G. M. Whitesides. 1999. Patterning proteins and cells using soft lithography. *Biomaterials* 20 (23-24):2363-76.

Kilian, K. A., B. Bugarija, B. T. Lahn, and M. Mrksich. 2010. Geometric cues for directing the differentiation of mesenchymal stem cells. *Proceedings of the National Academy of Sciences of the United States of America* 107 (11):4872-7.

Kim, H. R., C. Gallant, P. C. Leavis, S. J. Gunst, and K. G. Morgan. 2008. Cytoskeletal remodeling in differentiated vascular smooth muscle is actin isoform dependent and stimulus dependent. *American journal of physiology. Cell physiology* 295 (3):C768-78.

Lee, C. H., C. A. Carruthers, S. Ayoub, R. C. Gorman, J. H. Gorman, 3rd, and M. S. Sacks. 2015. Quantification and simulation of layer-specific mitral valve interstitial cells deformation under physiological loading. *Journal of theoretical biology* 373:26-39.

Lee, H., W. J. Adams, P. W. Alford, M. L. McCain, A. W. Feinberg, S. P. Sheehy, J. A. Goss, and K. K. Parker. 2015. Cytoskeletal prestress regulates nuclear shape and stiffness in cardiac myocytes. *Experimental biology and medicine*.

Liu, A. C., and A. I. Gotlieb. 2007. Characterization of cell motility in single heart valve interstitial cells in vitro. *Histol Histopathol* 22 (8):873-82.

Maganti, K., V. H. Rigolin, M. E. Sarano, and R. O. Bonow. 2010. Valvular heart disease: diagnosis and management. *Mayo Clin Proc* 85 (5):483-500.

Maniotis, A. J., C. S. Chen, and D. E. Ingber. 1997. Demonstration of mechanical connections between integrins, cytoskeletal filaments, and nucleoplasm that stabilize nuclear structure. *Proceedings of the National Academy of Sciences of the United States of America* 94 (3):849-54.

McCain, M. L., T. Desplantez, N. A. Geisse, B. Rothen-Rutishauser, H. Oberer, K. K. Parker, and A. G. Kleber. 2012. Cell-to-cell coupling in engineered pairs of rat ventricular cardiomyocytes: relation between Cx43 immunofluorescence and intercellular electrical conductance. *American journal of physiology. Heart and circulatory physiology* 302 (2):H443-50.

McCain, M. L., and K. K. Parker. 2011. Mechanotransduction: the role of mechanical stress, myocyte shape, and cytoskeletal architecture on cardiac function. *Pflugers Arch* 462 (1):89-104.

Merryman, W. D., I. Youn, H. D. Lukoff, P. M. Krueger, F. Guilak, R. A. Hopkins, and M. S. Sacks. 2006. Correlation between heart valve interstitial cell stiffness and transvalvular pressure: implications for collagen biosynthesis. *American journal of physiology. Heart and circulatory physiology* 290 (1):H224-31.

Oakes, P. W., S. Banerjee, M. C. Marchetti, and M. L. Gardel. 2014. Geometry regulates traction stresses in adherent cells. *Biophysical journal* 107 (4):825-33.

Oh, J. H., A. Gertych, and J. Tajbakhsh. 2013. Nuclear DNA methylation and chromatin condensation phenotypes are distinct between normally proliferating/aging, rapidly growing/immortal, and senescent cells. *Oncotarget* 4 (3):474-93.

Parsons, J. T., A. R. Horwitz, and M. A. Schwartz. 2010. Cell adhesion: integrating cytoskeletal dynamics and cellular tension. *Nat Rev Mol Cell Biol* 11 (9):633-43.

Qin, D., Y. Xia, and G. M. Whitesides. 2010. Soft lithography for micro- and nanoscale patterning. *Nat Protoc* 5 (3):491-502.

Quinn, K. P., E. C. Leal, A. Tellechea, A. Kafanas, M. E. Auster, A. Veves, and I. Georgakoudi. 2016. Diabetic Wounds Exhibit Distinct Microstructural and Metabolic Heterogeneity through Label-Free Multiphoton Microscopy. *J Invest Dermatol* 136 (1):342-4.

Quinn, K. P., G. V. Sridharan, R. S. Hayden, D. L. Kaplan, K. Lee, and I. Georgakoudi. 2013. Quantitative metabolic imaging using endogenous fluorescence to detect stem cell differentiation. *Scientific reports* 3:3432.

Rabkin, E., S. P. Hoerstrup, M. Aikawa, J. E. Mayer, Jr., and F. J. Schoen. 2002. Evolution of cell phenotype and extracellular matrix in tissue-engineered heart valves during in-vitro maturation and in-vivo remodeling. *The Journal of heart valve disease* 11 (3):308-14; discussion 314.

Sacks, M. S., W. David Merryman, and D. E. Schmidt. 2009. On the biomechanics of heart valve function. *J Biomech* 42 (12):1804-24.

Shodell, M., and H. Rubin. 1970. Studies on the nature of serum stimulation of proliferation in cell culture. *In vitro* 6 (1):66-74.

Skala, M. C., K. M. Riching, A. Gendron-Fitzpatrick, J. Eickhoff, K. W. Eliceiri, J. G. White, and N. Ramanujam. 2007. In vivo multiphoton microscopy of NADH and FAD redox states,

fluorescence lifetimes, and cellular morphology in precancerous epithelia. *Proceedings of the National Academy of Sciences of the United States of America* 104 (49):19494-9.

Skala, M., and N. Ramanujam. 2010. Multiphoton redox ratio imaging for metabolic monitoring in vivo. *Methods in molecular biology* 594:155-62.

Thakar, R. G., Q. Cheng, S. Patel, J. Chu, M. Nasir, D. Liepmann, K. Komvopoulos, and S. Li. 2009. Cell-shape regulation of smooth muscle cell proliferation. *Biophysical journal* 96 (8):3423-32.

Varone, A., J. Xylas, K. P. Quinn, D. Pouli, G. Sridharan, M. E. McLaughlin-Drubin, C. Alonzo, K. Lee, K. Munger, and I. Georgakoudi. 2014. Endogenous two-photon fluorescence imaging elucidates metabolic changes related to enhanced glycolysis and glutamine consumption in precancerous epithelial tissues. *Cancer research* 74 (11):3067-75.

Versaevel, M., T. Grevesse, and S. Gabriele. 2012. Spatial coordination between cell and nuclear shape within micropatterned endothelial cells. *Nat Commun* 3:671.

Versaevel, M., T. Grevesse, M. Riaz, J. Lantoine, and S. Gabriele. 2014. Micropatterning hydroxy-PAAm hydrogels and Sylgard 184 silicone elastomers with tunable elastic moduli. *Methods in cell biology* 121:33-48.

Vishavkarma, R., S. Raghavan, C. Kuyyamudi, A. Majumder, J. Dhawan, and P. A. Pullarkat. 2014. Role of actin filaments in correlating nuclear shape and cell spreading. *PLoS One* 9 (9):e107895.

Warnock, J. N., S. C. Burgess, A. Shack, and A. P. Yoganathan. 2006. Differential immediate-early gene responses to elevated pressure in porcine aortic valve interstitial cells. *The Journal of heart valve disease* 15 (1):34-41; discussion 42.

Win, Z., G. D. Vrla, K. E. Steucke, E. N. Sevcik, E. S. Hald, and P. W. Alford. 2014. Smooth muscle architecture within cell-dense vascular tissues influences functional contractility. *Integr Biol (Camb)* 6 (12):1201-10.

Yap, C. H., H. S. Kim, K. Balachandran, M. Weiler, R. Haj-Ali, and A. P. Yoganathan. 2010. Dynamic deformation characteristics of porcine aortic valve leaflet under normal and hypertensive conditions. *American journal of physiology. Heart and circulatory physiology* 298 (2):H395-405.

Ye, G. J., Y. Aratyn-Schaus, A. P. Nesmith, F. S. Pasqualini, P. W. Alford, and K. K. Parker. 2014. The contractile strength of vascular smooth muscle myocytes is shape dependent. *Integr Biol (Camb)* 6 (2):152-63.

Yeung, T., P. C. Georges, L. A. Flanagan, B. Marg, M. Ortiz, M. Funaki, N. Zahir, W. Ming, V. Weaver, and P. A. Janmey. 2005. Effects of substrate stiffness on cell morphology, cytoskeletal structure, and adhesion. *Cell motility and the cytoskeleton* 60 (1):24-34.

Yip, C. Y., J. H. Chen, R. Zhao, and C. A. Simmons. 2009. Calcification by Valve Interstitial Cells Is Regulated by the Stiffness of the Extracellular Matrix. *Arterioscler Thromb Vasc Biol*.

Zink, D., A. H. Fischer, and J. A. Nickerson. 2004. Nuclear structure in cancer cells. *Nat Rev Cancer* 4 (9):677-87.

Lam, N. T., H. Lam, N. M. Sturdivant, and K. Balachandran. 2017. Fabrication of a matrigel-collagen semi-interpenetrating scaffold for use in dynamic valve interstitial cell culture. *Biomed Mater* 12 (4):045013.

CHAPTER 4

Fabrication of a matrigel-collagen semi-interpenetrating scaffold for use in dynamic valve interstitial cell culture

ABSTRACT

The previous study provides us with valuable information regarding heart valve cell behavior in response to abnormal alteration in shape at single cell level. The results encourage us to look further into the underlying mechanism that regulates these responses. In order to do that, we need to have a culture model that is more closely mimic the natural heart valve environment because virtually the study of heart valve homeostatic and disease mechanisms are limited by the challenges in simulating the *in vivo* milieu, where valve cells are surrounded by the extracellular matrix in a three dimensional environment and experience multiple dynamic mechanical forces. Type I collagen is typically the most common three dimensional matrix used to culture valve cells *in vitro*. Unfortunately, this material has poor mechanical behavior due to an inherent propensity to compact significantly, unlike native valve leaflets. We hypothesized that incorporation of matrigel, which contains other heart valve-relevant matrix components such as type IV collagen and sulfated proteoglycans, to type I collagen would provide an appropriate physiological milieu for *in vitro* valve interstitial cell culture. Different semi-interpenetrating mixtures of collagen type I and matrigel were prepared and a thorough characterization of their physical, mechanical and biocompatibility properties was performed. We observed that the matrigel-collagen hydrogel was porous and degradable with tunable swelling behavior. Incorporation of matrigel not only enhanced the mechanical behavior of the composite hydrogel but also presented the cultured valve interstitial cells with a more enriched extracellular matrix network for *in vitro* culture. We showed that cells cultured in the composite hydrogel had comparable viability, proliferation and cell phenotype as compared with those in a collagen only gel. Importantly, the composite hydrogel also was amenable to *in vitro* cyclic stretching culture for 48 hours. Overall, we report here the potential use of the matrigel-collagen hydrogel as a

three dimensional scaffold for the dynamic mechanical culture of valve interstitial cells *in vitro* as well as a possible culture platform for signaling study.

1. INTRODUCTION

Valvular heart disease (VHD) affects approximately 3% of the population, with surgical replacement as the only viable treatment option (Rajamannan et al. 2011). For years, researchers have focused on deciphering the specific molecular mechanisms for VHD pathogenesis and progression *in vitro*, in order to find a better, non-surgical treatment. Most early *in vitro* studies were carried out in a traditional two-dimensional (2D) cell culture platform that did not effectively mimic the complex hemodynamic *in vivo* environment (Osman et al. 2006; Fisher, Chen, and Merryman 2013; Hjortnaes et al. 2015; Jian et al. 2002). Recently, three-dimensional (3D) scaffolds have come to the fore as being superior to the 2D format by providing a more physiological framework to support cell growth, and presenting the cells with similar physiochemical profiles as the native valve extracellular matrix (ECM) (Zhang et al. 2015; Geckil et al. 2010). Type I collagen-based hydrogels are one of the most common scaffolds that have been used for culturing heart valve cells, especially valve interstitial cells (VICs) as this isoform of collagen is the most prevalent and also acts as the load-bearing ECM protein in native heart valves (Butcher and Nerem 2004; Gupta et al. 2007). However, a disadvantage of type I collagen gels is its propensity to significantly compact *in vitro*. Other natural hydrogels such as hyaluronic acid, gelatin, alginate have also been widely used in many applications, either alone or in combination with other materials (Masters et al. 2005; Duan et al. 2013). The concern associated with natural hydrogels is that while they show good bioactivity, they are mechanically weak (Zhu and Marchant 2011). Synthetic hydrogels, in contrast, show tunable mechanical performances and have more reproducible physical and chemical properties. However, their biocompatibility and potential cytotoxicity are a major concern. In fact, only few of them have been approved by the FDA for clinical applications, such as poly(ethylene glycol) (PEG),

polylactic acid (PLA) and poly(lactic-co-glycolic acid) (PLGA) (Lam and Wu 2012; Zhang et al. 2015; Young, Poole-Warren, and Martens 2012; Shin, Nichol, and Khademhosseini 2011). Indeed, the ideal 3D scaffolding material for the *in vitro* culture of heart valve cells as well as the *in vitro* study of valve mechanobiology is still open to debate in the field.

In the context of understanding valve biology and pathology *in vitro*, it is of utmost importance to incorporate mechanical stimulation in the cell culture system to better simulate the *in vivo* hemodynamic milieu of the heart valves. Heart valves, specifically the aortic valve, experience multiple types of mechanical forces (i.e. shear stress, pressure, tensile stretch) during a cardiac cycle (Balachandran, Sucosky, and Yoganathan 2011). There have been several efforts toward applying one to two forces *in vitro* to study relevant cellular responses (Balachandran et al. 2009, 2010; Balachandran, Alford, et al. 2011; Thayer et al. 2011; Xing et al. 2004; Sacks, David Merryman, and Schmidt 2009). It should be noted that most of those experiments were done at the tissue level on the *ex vivo* leaflet explants, but not at the cellular scale, simply because of the lack of an appropriate 3D culture model that could sustain the cyclic mechanical stimulation. Accordingly, our goal for this study was to create a collagen-based hydrogel scaffold that could serve as a 3D matrix for regular VIC culture and be amenable to dynamic mechanical stimulation.

We hypothesized that addition of matrigel, thus supplementing the matrix with valve-relevant ECM components, such as laminin, proteoglycan and collagen type IV, would enhance the overall mechanical performance of the scaffold without affecting cell viability and health. It is worth noting that a similar matrigel-collagen semi-interpenetrating hydrogel has been studied by others for different cell types. For instance, when collagen was mixed with matrigel and cultured with cardiac myocytes, it was observed that the "engineered heart tissue" displayed functional

and morphological properties of differentiated heart muscle (Zimmermann, Schneiderbanger, et al. 2002; Zimmermann, Melnychenko, and Eschenhagen 2004). This construct was also implanted into syngeneic rats and showed positive outcomes which included vascularization and acquisition of a highly differentiated cardiac phenotype 14 days after transplantation (Zimmermann, Didie, et al. 2002). Mixture of matrigel and collagen was also used to successfully culture cardiomyocyte progenitor cells, without mitigating their viability and proliferation while promoting cell differentiation and ECM remodeling capacity compared to 2D culture (van Marion et al. 2015). Similarly, this hydrogel was also reported to promote survival and morphology of Schwann cells *in vitro* (Dewitt et al. 2009). Despite these precedent studies, the potential use of the matrigel-collagen hydrogel has not yet been thoroughly investigated in the heart valve field. Matrigel alone has been used for valve interstitial cell-valve endothelial cell (VEC) co-culture model, but in the absence of mechanical stimulation (Arevalos et al. 2016). Our results demonstrated that VICs cultured in a matrigel-collagen semi-interpenetrating hydrogel had comparable viability, proliferation and cell phenotype as compared with those cultured in a pure collagen gel. Importantly, the composite hydrogel was amenable to *in vitro* cyclic stretching culture for 48 hours, without spontaneous gel compaction. It is hoped that this composite scaffolding material will have potential applications for the study of valve cell mechanobiology.

2. MATERIALS AND METHODS

2.1. Fabrication of the matrigel-collagen hydrogel

Rat tail collagen type I and reduced growth factor matrigel were both purchased from Corning, NY. Collagen was diluted in phosphate-buffered saline (PBS) to appropriate final concentrations and neutralized with 1M sodium hydroxide (NaOH). The collagen-only and matrigel-only

hydrogels served as the controls. Collagen type I is the main constituent of the heart valve ECM and is commonly used as an *in vitro* 3D matrix for culturing heart valve cells at the concentration of 1-2mg/ml (Gould et al. 2012; Kamel et al. 2014; Sapp et al. 2015). Hence, we chose 1mg/ml and 2mg/ml working concentrations of collagen to use as the controls. Four different semi-interpenetrating combinations of matrigel and collagen (M-C) were made by incorporating of 80%, 65%, 55% and 45% matrigel by volume to the collagen solutions at concentration of 0.5 mg/ml, 1 mg/ml, 1.5 mg/ml and 2 mg/ml, respectively, and mixing gently via pipetting. During the preparation process, all reagents were kept on ice. The hydrogels were then allowed to polymerize at 37°C for at least 30 minutes. A total of seven samples were made and denoted as in table 4.1.

Table 4.1: Summary of the samples used in the study

	Matrigel	Collagen 1 mg/ml	Collagen 2 mg/ml	M-C 0.5 mg/ml	M-C 1mg/ml	M-C 1.5 mg/ml	M-C 2 mg/ml
Matrigel (v/v)	100%	None	None	80%	65%	55%	45%
Collagen	None	1mg/ml	2mg/ml	0.5mg/ml	1mg/ml	1.5mg/ml	2mg/ml
NaOH	None	Yes	Yes	Yes	Yes	Yes	Yes

2.2. Characterization of the matrigel-collagen hydrogel

2.2.1. Scanning electron microscopy (SEM)

After the hydrogels (Table 4.1) were prepared as described above, they were first processed for SEM imaging to analyze their morphology and structure. The gels were fixed with glutaraldehyde for 3 hours at 4°C followed by dehydration via a series of ethanol exchanges (50%, 75%, 90% and 100%). These samples were left overnight in hexamethyldisilazane (HMDS) to ensure complete dehydration. Dry hydrogels were sputtered coated with gold for 2 minutes and imaged with a FEI Nova Nanolab 200 Dual-Beam (FEI, OR) at magnification of

10,000X. At least 10 fields were taken per sample and ImageJ was used to measure the pore diameter. Cross-sectional SEM images were also taken to visualize the distribution of the pores throughout the scaffold structure.

2.2.2. Swelling and degradation studies

For the swelling assay, the hydrogel samples (Table 4.1) were prepared as described previously and then lyophilized overnight using a Freezone 4.5 system (Labconco, MO). The gels were weighed one by one and the dry weight of each gel was noted as W0. They were then transferred to 1.5ml microcentrifuge tubes, and immersed in 1X PBS and stored at 37°C. At 1, 6, 12, 24 and 48 hour time points, the PBS solution was carefully removed; the gels were weighed again and the wet weights were noted as W1. The swelling ratio for each sample was calculated as in equation 1:

$$Equation\ 1: Swelling\ ratio = \frac{W1 - W0}{WO} * 100$$

For the degradation study, the hydrogels (Table 4.1) were prepared and weighed right after gelation, without the lyophilization step. Initial wet weight of each sample was noted as W0. 1mg/ml lysozyme (Worthington, NJ) was dissolved in 1X PBS before adding to the samples and keeping at 37°C to mimic *in vivo* enzymatic degradation (Tan, Rubin, and Marra 2010; Babu et al. 2011). At 1, 2, 5, 7, 14, 21, and 28 days, the lysozyme solution was removed carefully; the gels were weighed and the final wet weights were noted as W1. Degradation ratio for each sample was calculated as in equation 2:

$$Equation\ 2: Degradation\ ratio = W0 - \frac{W1}{W0} * 100$$

2.2.3. Mechanical testing

An Instron™ 5900 Series (Canton, MA) mechanical tester was used to measure the mechanical properties of seven samples. Gels with a 13 mm diameter and 2-3 mm height were tested in

unconfined compression. The gel was compressed at a rate of 1 mm/min and the test was ended once the gel was compressed to 1/10 of its original height. The compressive extension and the compressive load were recorded every 0.05 seconds. Using a custom MATLAB code, the slope of the stress versus strain curve was calculated between each time point and the average slope was reported as the Young's modulus.

2.3. Biocompatibility of the matrigel-collagen hydrogel

2.3.1. Cell isolation and culture

Valve interstitial cells (VICs) were isolated and cultured as described elsewhere (Butcher and Nerem 2004; Lam et al. 2016; Tandon et al. 2016). Briefly, porcine hearts obtained from local abattoir (Cockrum's Custom Meat Processing and Taxidermy, AR) were dissected aseptically and the aortic valve leaflets were collected. 1mg/ml collagenase solution (Worthington, NJ) was added to the leaflets for 3 hours at 37°C with frequent agitation. Cold 10% fetal bovine serum (FBS)-containing Dulbecco's Modified Eagle Medium (DMEM) was added to quench enzymatic activity. The solution was allowed to flow through the cell strainer (Corning, NY) to remove any remained tissue debris before centrifuging for 5 minutes at 4°C. The cell pellet was resuspended in the cell culture media, plated in a flask in a 37°C incubator. Fresh media was changed every 3 days. Cells from passage 1-7 were used in all subsequent experiments.

2.3.2. 3-(4,5-dimethylthiazol-2-yl)-2,5-diphenyltetrazolium bromide (MTT) assay

For the cell proliferation assessment, VICs were trypsinized and mixed with the ice-cold hydrogel solutions. All samples (Table 4.1) had equal amounts of starting cells (10^6 cells). The gel constructs were allowed to polymerize for 30 minutes in a 37°C incubator. Cell culture media was then added on top of the gels and the constructs kept in culture for a subsequent 48 hours. After culture, samples were rinsed twice with PBS before 5mg/ml MTT reagent (Life

technologies, CA) was added onto the hydrogels and incubated at 37°C for 4 hours. DMEM only samples served as the blank/negative control. The positive control was VICs cultured in regular 2D cell culture plastic. After 4 hours, MTT solution was carefully removed and dimethyl sulfoxide (DMSO) was added for 15 minutes to solubilize the formazan – the end-product of the MTT reduction due to intracellular enzyme activity. Solutions on top of the gels were transferred to a 96 well-plate and the absorbance was read at 570nm. These absorbance values were used to directly assess cell proliferation.

2.3.3. Live/dead assay

The hydrogels encapsulated with cells were prepared as described above. Live/Dead assay kit reagents (Life technologies, CA) were thawed at room temperature and mixed with 1X PBS to obtain the working concentrations of 10μM Calcein AM and 10μM Ethidium-1. This mixture was added to the hydrogel samples and incubated in the dark at room temperature for 45 minutes. Live cells interacted with Calcein AM dye and stained green while dead cells interacted with Ethidium-1 dye and stained red. Labeled cells were visualized under an epifluorescent microscope. At least 10 fields per channel were imaged per sample at the same intensity and acquisition integration time. Based on visual inspection, a threshold was defined for each channel and kept consistent through samples. Live and dead cells were manually counted in every image and the percentage of live cells was calculated as the number of live cells over the total number of cells (i.e. live and dead cells) in that image field.

2.4. ECM remodeling and differentiation potential of VIC in matrigel-collagen hydrogels

To be used as a 3D substrate for *in vitro* cell culture, it was important to ensure that the scaffolding material of this composite hydrogel did not detrimentally alter the normal

homeostatic behavior of the cell as in other standard *in vitro* culture techniques. To evaluate this, we performed two sets of experiments as described below:

2.4.1. MMP-2 and -9 proteolytic activity

VICs were cultured in the composite and control hydrogels for 2 days before their proteolytic activities were detected via gelatin zymography. Cells were lysed with RIPA buffer (Santa Cruz Biotechnology, CA), followed by protein collection and quantification via a bicinchoninic acid (BCA) assay (Life technologies, CA). Cell lysate was mixed with 4X Laemmli sample buffer. 10% of resolving gel and 4% of stacking gel were prepared as described elsewhere (Balachandran et al. 2009). Equal amounts of lysate were loaded to each lane and electrophoresis was run for 3 hours at 4^0C, 80V under non-reducing conditions. The gels were then washed sequentially in 2.5% triton X-100 and development buffer (50mM Tris-HCl, pH 7.5, 200mM NaCl, 5mM $CaCl_2$), followed by an overnight incubation at 37^0C. The next day, samples were stained with 0.5% Coomassie brilliant blue for 2 hours and destained until the bands were resolved. Visualization of the proteolytic activity appeared as white bands over a dark background. Intensity of the bands was quantified using imageJ.

2.4.2. VIC phenotype in matrigel-collagen hydrogels

We asked if VICs cultured in the matrigel-collagen composite hydrogel were able to maintain their normal phenotypic profile compared to those cultured in the collagen-only hydrogels. Cell lysates were prepared as for zymography but with the presence of the reducing agent - β-mercaptoethanol. Western blotting was performed using previously published methods (Lam et al. 2016) to detect the expression of the following markers: α-SMA (Abcam, 1:200), calponin (Abcam, 1:1000), fibronectin (Abcam, 1:500) and vimentin (Abcam, 1:1500) with β-actin (Abcam, 1:200) as the loading control.

2.5. Matrigel-collagen hydrogel mechanical behavior

2.5.1. Gel compaction study

2.5.1.1. Compaction characteristic of native valve leaflets

In order to study the compaction nature of native valve leaflets, we collected aortic valve leaflets from porcine heart as described in cell isolation section. After dissection, these valves were kept in DMEM medium for 2 days at 37^0C, 5% CO_2. Images were taken every 24 hours to measure changes in size of these leaflets.

2.5.1.2. Hydrogel compaction study

Since excised aortic leaflets showed no change in size for at least two days in culture (Figure 4.10), we postulated that the addition of matrigel would reduce the spontaneous compacting behavior observed in collagen-only hydrogels and make the composite one to behave in a similar manner as native aortic valve leaflets. The hydrogels (Table 4.1) were subjected to uniaxial cyclic stretching and changes in gel contraction were measured over the period of 2 days. Specifically, a small silicone ring (diameter = 1.5 inches) was attached to a 0.01 inch elastomeric membrane (Specialty Manufacturing, Inc.) to create a chamber for cell culture. The two ends of the membrane were constrained by a set of clamps so that the whole setup could be mounted onto a custom-built cyclic biostretcher device (Figure 4.1 A-C). VICs were mixed with the ice-cold hydrogel solution and pipetted into the ring. Cell culture media were added 30 minutes after gelation. Uniaxial stretching was initiated to 20% strain magnitude, 1 Hz and kept running for 48 hours. Strain on the gel was validated using marker tracking experiments (Figure 4.2). The samples were imaged at 24 and 48 hours after initiation of stretching and ImageJ was used to track changes in gel size from these images. The chosen strain magnitude was based on prior

publications and represented the higher end of mechanical stimulation that valve cells might experience *in vivo* (Yap et al. 2010).

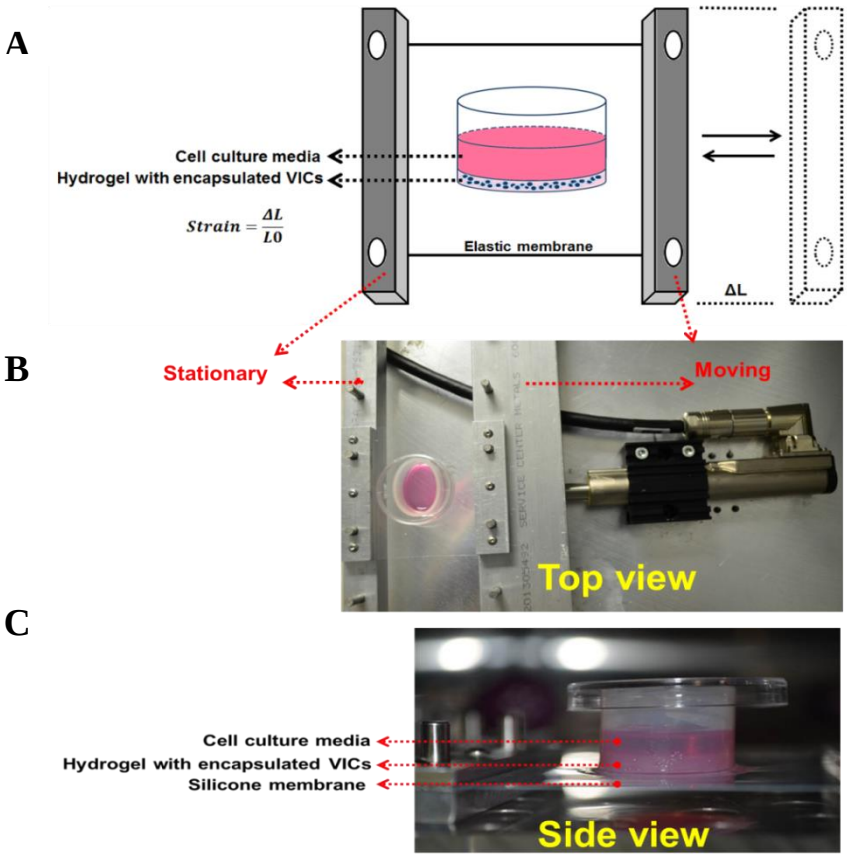

Figure 4.1: (A) Schematic of custom-designed culture chamber with silicone ring attached to a silicone membrane. The two ends of the membrane were constrained by a clamping system. One end was coupled to a linear actuator and would stretch, while the other end stayed stationary. ΔL was calculated to give a desired strain magnitude. Representative images of the culture chamber that was inserted onto the biostretcher, provided with (B) top view and (C) side view.

Figure 4.2: Representative images showing marker grid used to validate strain on Matrigel-Collagen hydrogel.

2.5.2. Changes in morphology of encapsulated VICs as the effect of cyclic stretch

To assess acute changes in cell morphology under cyclic stretch, VICs were cultured in the matrigel-collagen composite gel that demonstrated the least contraction and delamination in the previous study, and cyclically stretch for 48 hours. The control sample was VICs cultured in the composite gel without cyclic mechanical stimulation. At the end of the experiment, the hydrogels (stretched and static) were fixed with PFA for 15 minutes before they were incubated with DAPI (Life technologies, 1:100) and phalloidin (Life technologies, 1:100) for 1 hour at room temperature. These samples were then visualized under an epifluorescent microscope with appropriate channels (i.e. blue channel for DAPI and green channel for phalloidin). At least 10 fields per channel were imaged per sample. Using phalloidin staining images, actin alignment was analyzed with a previously published MATLAB code (Lam et al. 2016).

We also took z-stack images of a representative sample stained with Phalloidin to look into cell distribution through the scaffold.

2.6. Statistical methods

All quantitative data were first analyzed for normality using the Anderson-Darling method. All normally distributed data were subsequently analyzed by one-way ANOVA followed by Holm-Sidak multiple pairwise comparisons. A p-value of less than 0.05 was used to indicate statistical significance differences between samples. Data was plotted as mean with standard error bars.

3. RESULTS

3.1. The matrigel-collagen hydrogel was porous, degradable, with tunable swelling and mechanical properties

SEM images revealed different morphologies and porosities among seven hydrogel samples (Figure 4.3 A-B). Specifically, the matrigel-only and all four composite hydrogels were porous scaffolds, with pore size between 1.13-1.57 μm (Figure 4.3 A1, A4-A7). No fiber-like structures were readily visible in these scaffolds. In contrast, the collagen-only samples had clearly visible fiber-like structures with some porosity between their fibers (Figure 4.3 A2-A3). With increasing concentrations of collagen in the composite hydrogels, the pores tended to become larger with greater diameter (1.13 -1.57 μm) compared to the matrigel-only (0.59 μm) ($p=0.09$). Cross-sectional images (Figure 4.4) indicated the porosity characteristics of these scaffolds were consistent within the thickness of the gel structure, with highest porosity observed in the M-C 2mg/ml samples.

The matrigel-collagen hydrogel showed variable swelling and degradation behavior compared to the controls, depending on matrigel concentration. The collagen-only hydrogels (both 1mg/ml and 2mg/ml) showed minimal swelling (Figure 4.5 A). The matrigel-only hydrogels, on the other hand, gradually increased fluid uptake from the 0 to 24 hour time point, then followed by a drop in swelling after 48 hours. The matrigel-collagen composite hydrogels shared similar behavior with the matrigel-only hydrogel with slight difference in the final swelling ratio. The speed of swelling in these samples appeared to inversely correlate with the amount of collagen.

Collagen-only hydrogels were enzymatically degraded to undetectable levels within the first day of the assay while the matrigel-only hydrogel demonstrated comparable degradation only after the third week (Figure 4.5 B). The matrigel-collagen composite hydrogels demonstrated variable

degradation depending on the amount of matrigel and collagen present in each sample. Particularly, the matrigel-collagen 0.5mg/ml, 1mg/ml and 1.5mg/ml samples started to degrade at the 5^{th} day of the experiment whereas the matrigel-collagen 2mg/ml showed an acute drop in weight after 24 hours and was completely degraded after 4 weeks. Similar to the swelling studies, the presence of matrigel appeared to significantly improve the degradation properties of the composite scaffold for longer durations than the collagen-only hydrogel samples. We also analyzed the mechanical stiffness of these hydrogel samples (Figure 4.5 C-D). The matrigel-only hydrogel had Young's modulus between that of the collagen 1mg/ml and collagen 2mg/ml samples. Incorporation of matrigel into collagen 1mg/ml and 2mg/ml significantly increased the gel mechanical stiffnesses (from 13.4 to 21.7 kPa, and 19.2 to 39.1 kPa, respectively) ($p<0.05$). Overall, all four composite hydrogels had equal to higher Young's moduli compared to the controls, suggesting that the combination of matrigel and collagen in a semi-penetrating network improved the mechanical strength of the overall hydrogel compared to when the components were separate.

A

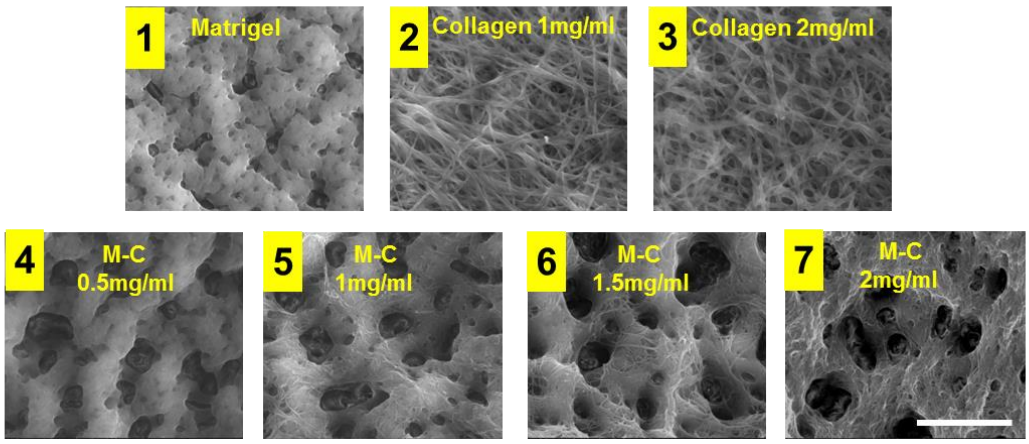

B

Samples	Matrigel	Collagen 1mg/ml	Collagen 2mg/ml	M-C 0.5mg/ml	M-C 1mg/ml	M-C 1.5mg/ml	M-C 2mg/ml
Pore diameter (µm)	**0.59** +/- 0.095	N/A	N/A	**1.13** +/- 0.019	**1.45** +/- 0.052	**1.51** +/- 0.059	**1.57** +/- 0.003

Figure 4.3: Representative SEM images of seven samples. (A) All samples showed some levels of porosity but (A1) and (A4-7) were considered as porous scaffolds; (A2 and A3) were more fibrous , scale bar = 5µm, n=2. (B) Mean scaffold pore diameter data.

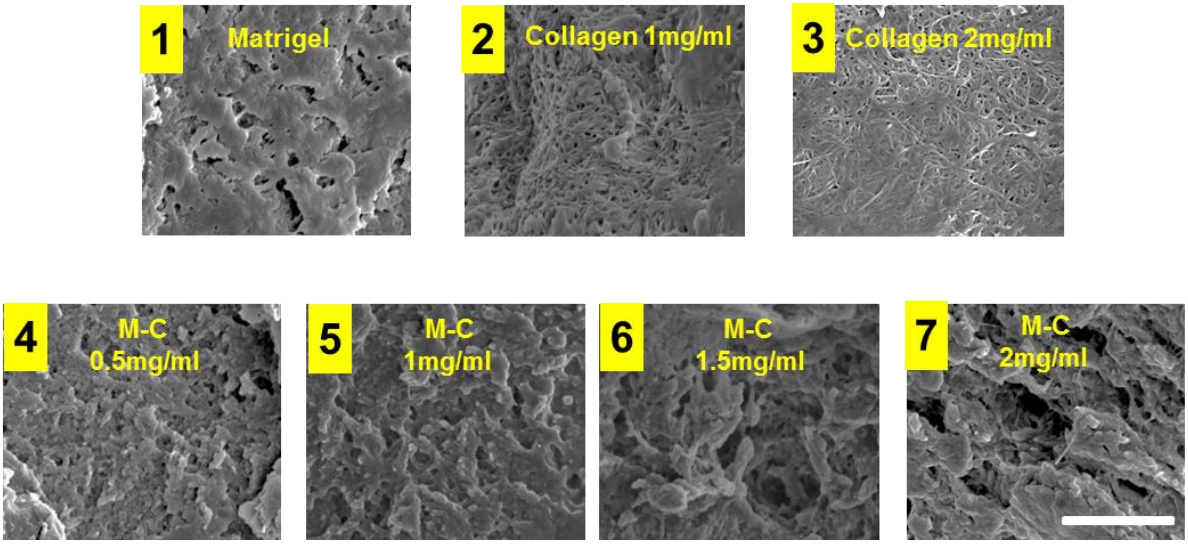

Figure 4.4: Cross-sectional scanning electron microscopy images showed evidence of the pores throughout the structure of the matrigel and matrigel-collagen scaffolds, scale bar = 5µm.

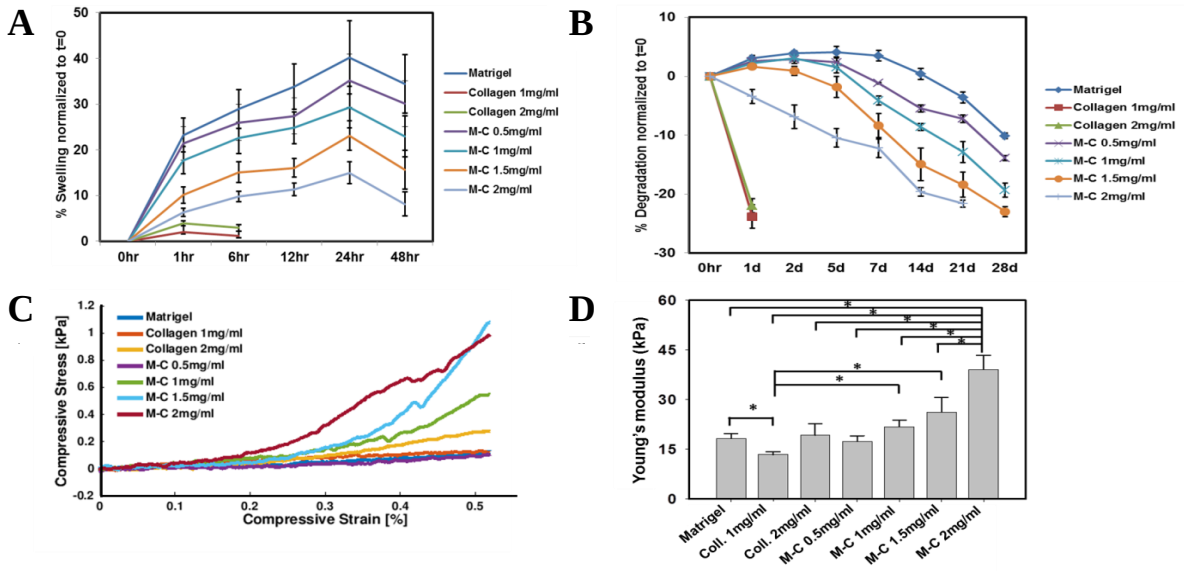

Figure 4.5: (A) swelling ratio, (B) degradation ratio, (C) representative stress versus strain curves and (D) Young's modulus of the hydrogels, n=5, * $p<0.05$.

3.2. Collagen increased cell viability and proliferation

Cell viability and proliferation were assessed across the seven hydrogel samples after two days in culture using Live/Dead and MTT assays. As shown in figure 4.6 A, cells tended to be more clustered with numerous small branches in samples that had lower amounts of collagen, including the matrigel, matrigel-collagen 0.5mg/ml, matrigel-collagen 1mg/ml and matrigel-collagen 1.5mg/ml. In contrast, they were more separate, and spread-out in samples that had pure collagen or high concentrations of collagen, including the collagen 1mg/ml, 2 mg/ml, and matrigel-collagen 2mg/ml. Significantly higher cell viability was also observed in these samples (Figure 4.6 B, Figure 4.7, $p<0.05$) that was thought to be due to the fact that the VICs were surrounded by collagen, as it is *in vivo.* Consistently, the presence of collagen in the composite hydrogel was the determining factor for improved cell viability as VICs in samples with higher proportion of matrigel (i.e. matrigel-collagen 0.5mg/ml and matrigel-collagen 1mg/ml) had significantly lower viability than in samples with higher proportion of collagen (i.e. collagen-

only hydrogels, matrigel-collagen 2mg/ml) (Figure 4.6 B, Figure 4.7). Live/Dead results were further supported by the MTT assay (Figure 4.6 C). The collagen 1mg/ml sample had the highest level of viable metabolically active cells, even significantly higher than in the collagen 2mg/ml sample ($p<0.05$). In all other samples, incorporation of matrigel did not cause significant change in cell proliferation ($p>0.05$) although there was a clear increasing trend with increasing concentrations of collagen.

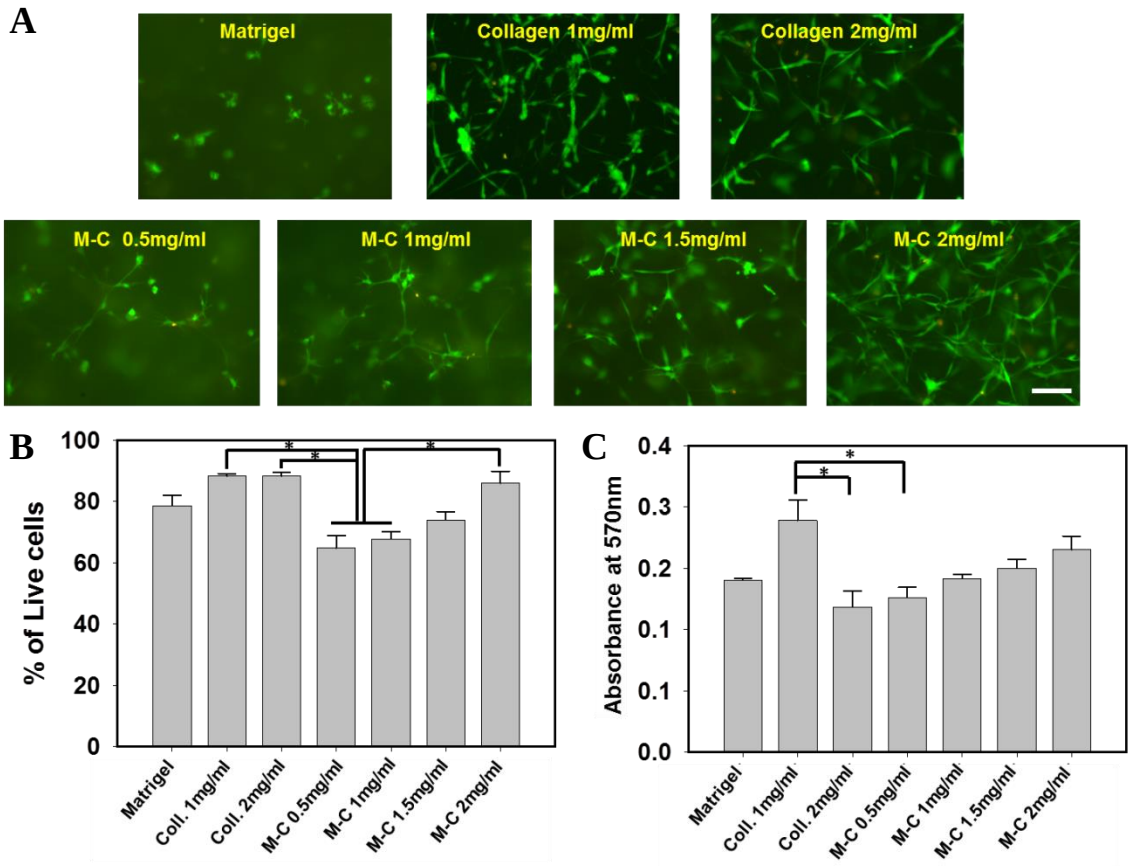

Figure 4.6: (A) Representative merged Live/Dead images. Live cells appear green; dead cells appear red, scale bar = 100µm (B) Quantitative analysis of cell viability which was calculated as the number of live cells over the total number of cells. (C) Absorbance reading for MTT assay at 570nm, corresponding to the proliferation state of VICs across samples, n=3 for Live/Dead assay, n=4 for MTT assay, * $p<0.05$.

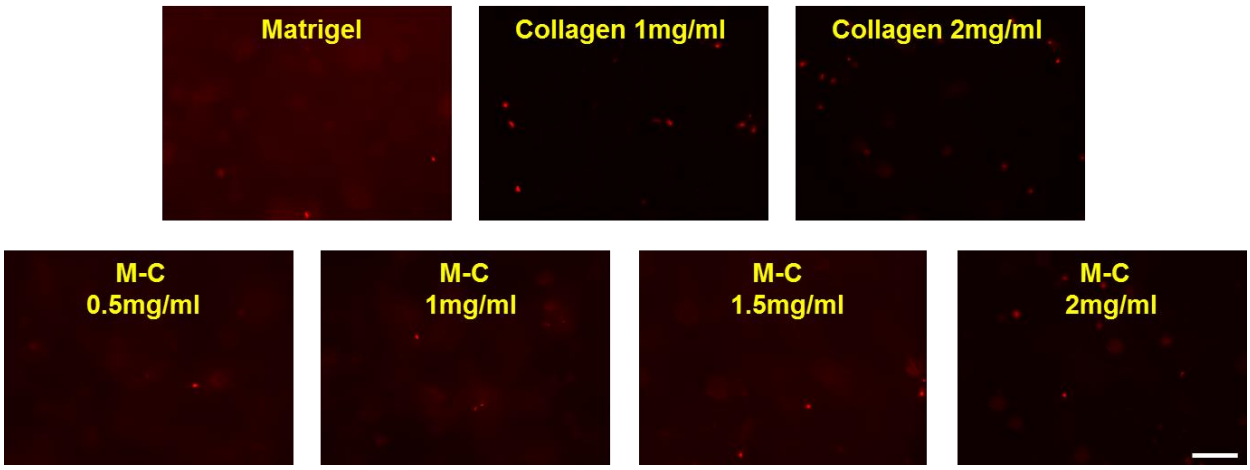

Figure 4.7: Representative dead stained cells, scale bar = 100µm.

3.3. Matrigel did not induce altered ECM remodeling activity or differentiation in VICs

We first evaluated changes in the proteolytic activity of MMP-2 and -9 in cultured VICs as these enzymes play important roles in maintaining ECM homeostasis (Cox and Erler 2011). As shown in figure 4.7 A, pro-MMP2 and active MMP-2 were seen at 72kDa and 66kDa regions while triple gelatinolytic bands of MMP-9 migrated at the region of 90kDa. Whereas pro-MMP9 and active MMP9 were usually seen at 92kDa and 82kDa, respectively, the identity of the third band could be a partially glycosylated MMP9 at around 83-85kDa (Toth and Fridman 2001). Using imageJ, we quantified the integrative intensity of these gelatinase bands (i.e. double bands of MMP-2 and triple bands of MMP-9). As shown in figure 4.8 B-C, the proteolytic activity of MMP-2 and -9 was not altered by the matrix materials that were used in the composite hydrogel scaffold as no statistically significant difference was found between the samples for both MMP-2 ($p=0.8$) and MMP-9 ($p=0.6$).

In addition to zymography, western blotting was performed to examine the phenotypic profile of VICs (Figure 4.9 A-E). The expression of vimentin is commonly an indicator of a quiescent VIC phenotype, while the expression of fibronectin, smooth muscle actin (SMA) and calponin is associated with activated VICs (Liu, Joag, and Gotlieb 2007). Our western blotting reported

similar observations as in the zymography results. Although we observed a pretty consistent pattern of expression in which the four markers of interest had equal to higher level of expression in the collagen-only samples as compared to the matrigel-only hydrogel and their expression was up-regulated with increasing concentrations of collagen, we found no statistically significant difference in the expression profile of these phenotypic markers among the seven hydrogel samples (vimentin ($p=0.9$), α-SMA ($p=0.2$), calponin ($p=0.7$) and fibronectin ($p=0.09$)).

Taken as a whole, these results suggest that cells in the matrigel-collagen composite hydrogel behaved similarly to those in the control samples. Incorporation of matrigel did not result in significant changes in cellular activity (i.e. ECM remodeling activity and differentiation capacity), at least over the course of 48 hours as shown in our experiment.

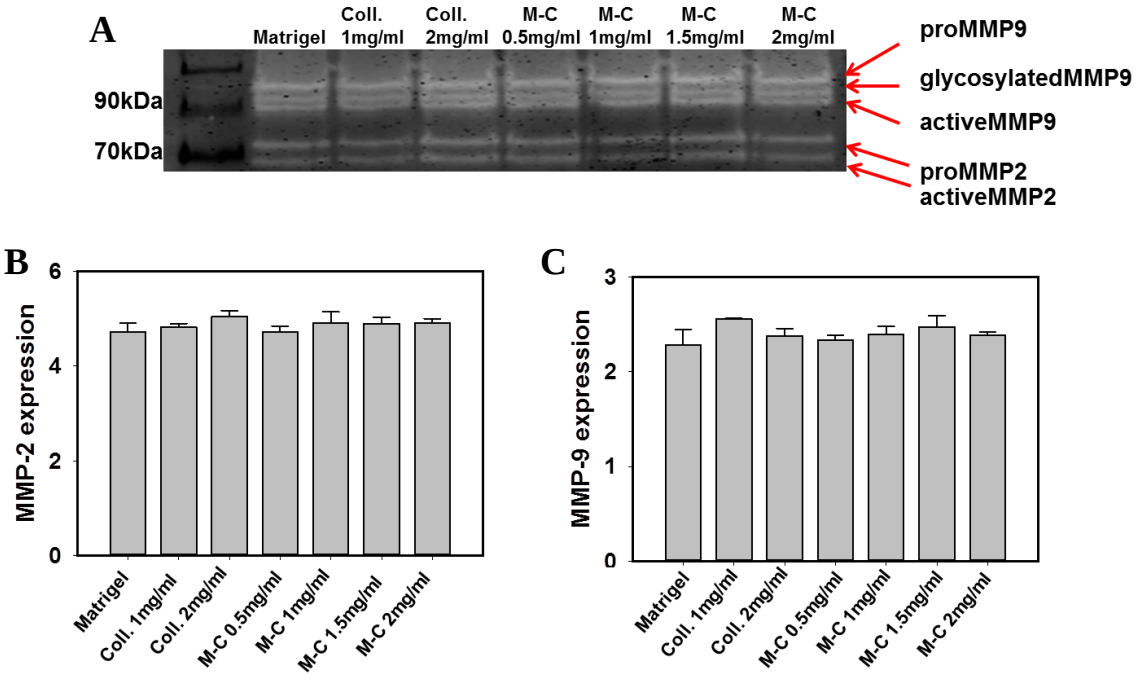

Figure 4.8: (A) Gel zymogram depicting expressions of MMP-2 and MMP-9 among seven hydrogel samples. Quantitative analysis of band intensity for (B) MMP-2 and (C) MMP-9, n=3.

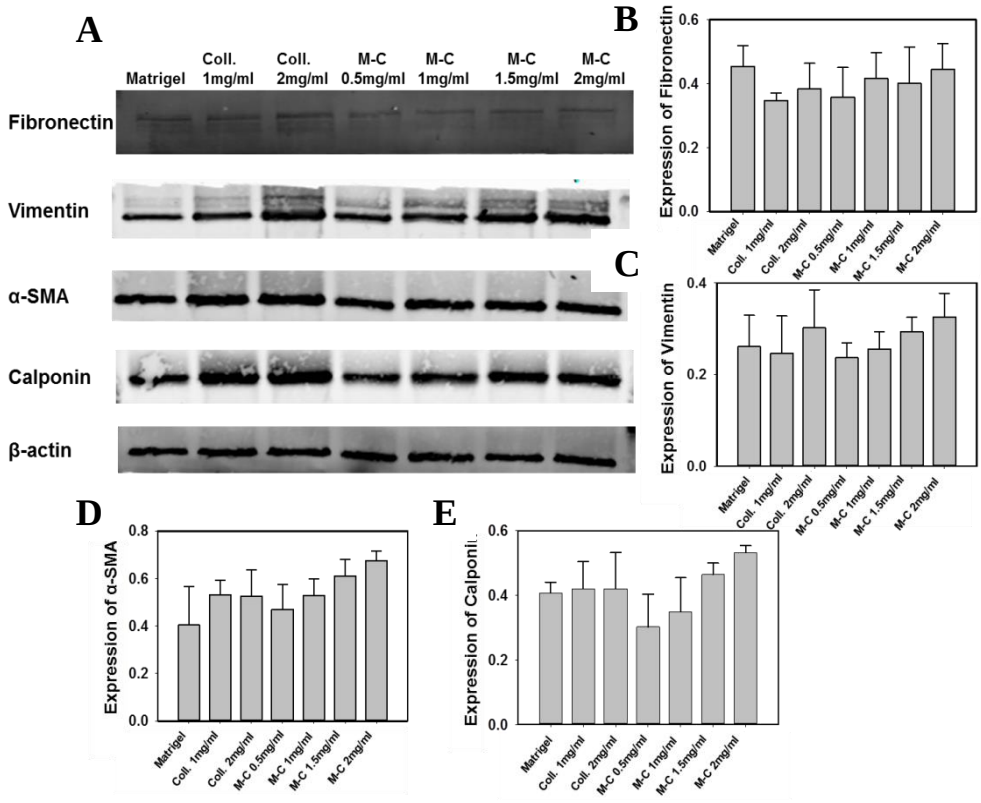

Figure 4.9: (A) Representative western blot images for four proteins of interest (fibronectin, vimentin, α-SMA and calponin) and loading control β-actin. Semi-quantitative analysis of band intensity for (B) fibronectin, (C) vimentin, (D) α-SMA, and (E) calponin, n=3.

3.4. Matrigel enhanced mechanical performance of the composite hydrogel scaffold

Due to the tendency of the collagen hydrogel to spontaneously compact, it is typically challenging to use in studies that require dynamic cyclic mechanical stimulation. Additionally, this behavior does not mimic that of native valve leaflets (Figure 4.10). We hypothesized that incorporation of matrigel, with its sulfated proteoglycan and collagen type IV content, might reduce substrate compaction. As shown in figure 4.11 A-B, samples with high amounts of matrigel, including the matrigel-only, matrigel-collagen 0.5mg/ml matrigel-collagen 1mg/ml and matrigel-collagen 1.5mg/ml, successfully remained intact during the course of 48 hours while the collagen 1mg/ml and 2 mg/ml significantly compacted after the first 24 hours. The matrigel-collagen 2mg/ml, due to the presence of high amount of collagen, behaved similarly to the

collagen-only hydrogels in which they became significantly contracted at the end of the experimental duration. We observed that while the collagen gels initially adhered to the silicone chamber, they slowly detached and started to shrink when the stretch was initiated. In the case of the matrigel-collagen 2mg/ml, while the gels did compact, they did not lose their attachment to the underlying silicone membrane.

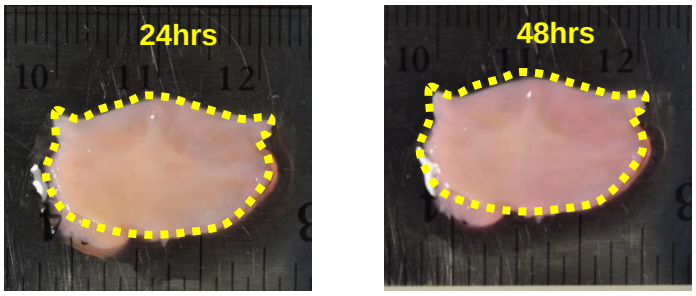

Figure 4.10: Representative images showing no compaction and thus no change in size of the native excised aortic leaflets after 48 hours in culture (dashed lines showed how we tracked the leaflet size overtime).

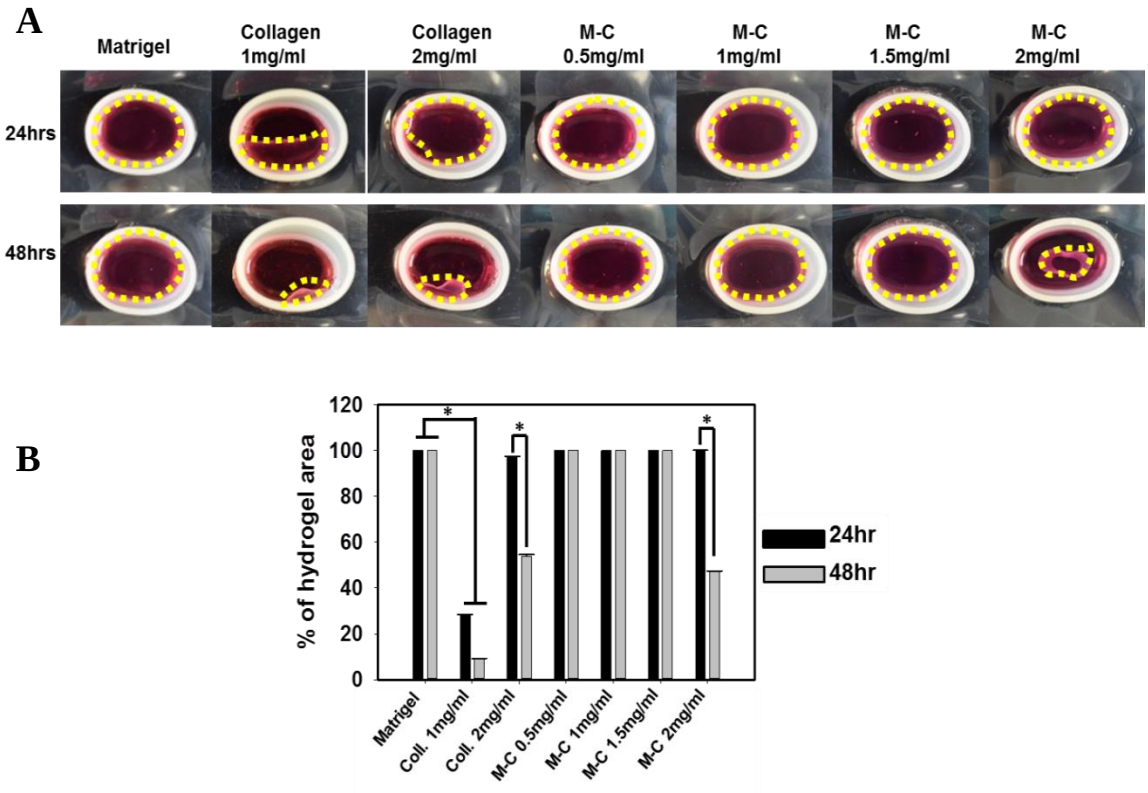

Figure 4.11: (A) Changes in the morphology of seven hydrogels over 48 hours and (B) quantification of gel compaction, n=3, * $p<0.05$. Dashed lines depict gel size.

3.5. Encapsulated cells became more aligned under cyclic stretch

We asked if the encapsulated VICs were able to sense and respond to the applied stretch from the matrigel-collagen scaffold. Among three composite hydrogels that did not show contraction in previous study, we picked the matrigel-collagen 1mg/ml to use for this specific experiment. DAPI and Phalloidin staining images showed that the cell cytoskeleton in the stretched sample became aligned with the direction of stretch while that of the control sample was oriented randomly (Figure 4.12 A). Analysis of actin fiber alignment using a previously published orientation parameter technique (Lam et al. 2016) showed significantly reduced actin alignment in the static sample compared to the stretched one (Figure 4.12 B). Together with the contraction study, these data highlight the potential of using this composite hydrogel for the 3D culture of VICs *in vitro*, in the presence of mechanical stimulation.

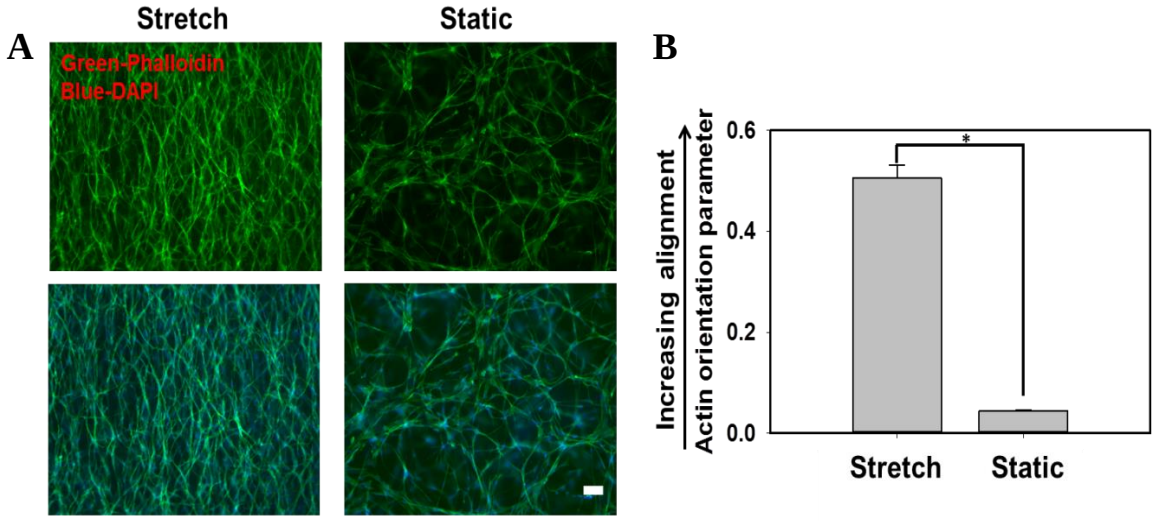

Figure 4.12: (A) Representative phalloidin and merged (with DAPI) images of encapsulated VICs in stretched versus static samples. (B) Analysis of actin orientation, scale bar =100µm, n=4, *p<0.05.

4. DISCUSSION

One of the primary principles of scaffold design for basic science studies, tissue engineering or regenerative medicine, is the provision of temporary structural support for cell attachment, migration and growth, thus facilitating the production of ECM, remodeling and eventual replacement of the scaffold (Zhang et al. 2015). Additionally, in the case of a dynamically deforming *in vivo* tissue such as the heart valve, the scaffold material must be able to deform in a similar manner. Our data suggests that a matrigel-collagen semi-penetrating hydrogel might be superior to collagen-only gels in these regards. In particular, rapid degradation rates as seen in the collagen-only hydrogels could impair the structural and mechanical properties of the scaffolds while the overly slow rates of swelling and degradation of pure matrigel substrates might inhibit cell remodeling and tissue regeneration (Nicodemus and Bryant 2008). In contrast, the matrigel-collagen composite hydrogel at various concentrations showed tunable swelling and degradation behavior. They increased water uptake in the first 24 hours and gradually degraded after 48 hours. Similarly, their degradation rates were in between that of the collagen and

matrigel-only samples. These composite gels also had a porous structure which could potentially aid in exchanging of oxygen, nutrients and cellular metabolic wastes (Dhivya et al. 2015).

We observed a positive correlation between porosity and compressive mechanical properties of the scaffold, wherein the matrigel-collagen hydrogels exhibited greater porosity and increased compressive Young's Moduli. It is possible that the higher porosity, together with the fibrous and hydrated characteristics of the collagen and matrigel, respectively, increased the inter-connectivity of the scaffold network, thus providing greater compressive resistance to these samples via better stress distribution within the scaffold network. Similar improvements in mechanical properties were observed when hydrated polysaccharide networks were combined with fiber-based scaffolds (Roohani-Esfahani, Newman, and Zreiqat 2016). In the context of the cardiac valve, previous studies suggested that substrate stiffness could regulate VIC phenotype such that stiffer matrices would likely induce more α-SMA-positive stress fibers (Quinlan and Billiar 2012) or even calcification (Yip et al. 2009). The moduli across the samples in our experiment ranged from 13.4 to 39.1 kPa which could potentially activate VICs, based on 2D cell culture studies. It should however be noted, as shown by others, that the range of stiffnesses that induce pathogenic differentiation in VICs is significantly different in 3D culture compared to 2D (Yip et al. 2009).

Another important principle of scaffold design for cell culture is the cytocompatibility of the scaffold and its ability to promote interactions between cells and their local environment. The scaffolding material must also provide cells with specific biological cues to direct cell fate and physiological functions (Zhang et al. 2015). According to our MTT and Live/Dead assay, cells in the collagen-only hydrogels, specifically the 1mg/ml composition, displayed the highest levels of cell survival and proliferation. This concentration also appeared to be superior to the 2mg/ml

one, which could suggest that 1mg/ml of collagen gel was sufficient to produce appropriate matrix density and stability for VIC encapsulation, and subsequent proliferation. Overall, survival and proliferation increased with increasing concentrations of collagen clearly highlighting its importance as a scaffolding material for valve cell culture.

Addition of matrigel enriched our composite hydrogel with various valve-relevant ECM proteins, specifically collagen IV, laminin and proteoglycan thus recapitulating, in part, the natural ECM composition found in the heart valve (Rabkin et al. 2001; Aikawa et al. 2006). Interestingly, while matrigel itself contained a variety of matrix proteins and growth factors, its presence did not seem to significantly affect cell survival and proliferation across the samples, at least during the course of 48 hours. In fact, our results showed that incorporation of matrigel significantly aided in improving the dynamic, load-bearing properties of the composite hydrogel. In particular, samples with high amounts of matrigel (i.e. the matrigel-only hydrogel, matrigel-collagen 0.5mg/ml, matrigel-collagen 1mg/ml and matrigel-collagen 1.5mg/ml) successfully remained intact after 48 hours of uniaxial stretching, without significant compaction, mimicking a native excised valve leaflet (Figure 4.10). Encapsulated VICs also became significantly aligned to the direction of applied stretch as observed in other 3D culture systems (Farrar et al. 2016; Bono et al. 2016; Heher et al. 2015), while unstretched samples showed randomly oriented cells. The ability of these composite hydrogels to remain structurally undamaged indeed opens up the opportunity to utilize this 3D culture model to study valve cell mechanobiology in the future. Additionally, we observed that encapsulated VICs were distributed throughout the scaffold, and not concentrated at the surfaces (Figure 4.13).

The commercially available matrigel that was used in our study is derived from mouse tumor ECM. This raises the concern of pathological signaling during cell culture. Our data, however,

demonstrated that matrigel did not cause any significant changes in VIC phenotype as well as the ECM remodeling activity over the course of 48 hours in culture compared to the controls. While longer term studies are needed, our results suggest the applicability of matrigel for use in acute VIC *in vitro* studies.

Our study has the following limitations. We performed our dynamic stimulation experiments under uniaxial stimulation, and not biaxially as observed *in vivo*. However, we do subject the construct to 20% stretch, which is typically close to the upper limit of cyclic stretch that is experienced by valve tissue *in vivo* [20]. We also do acknowledge that our model does not simulate other mechanical forces such as hemodynamic pressures or flow, and that will be the focus of our future studies.

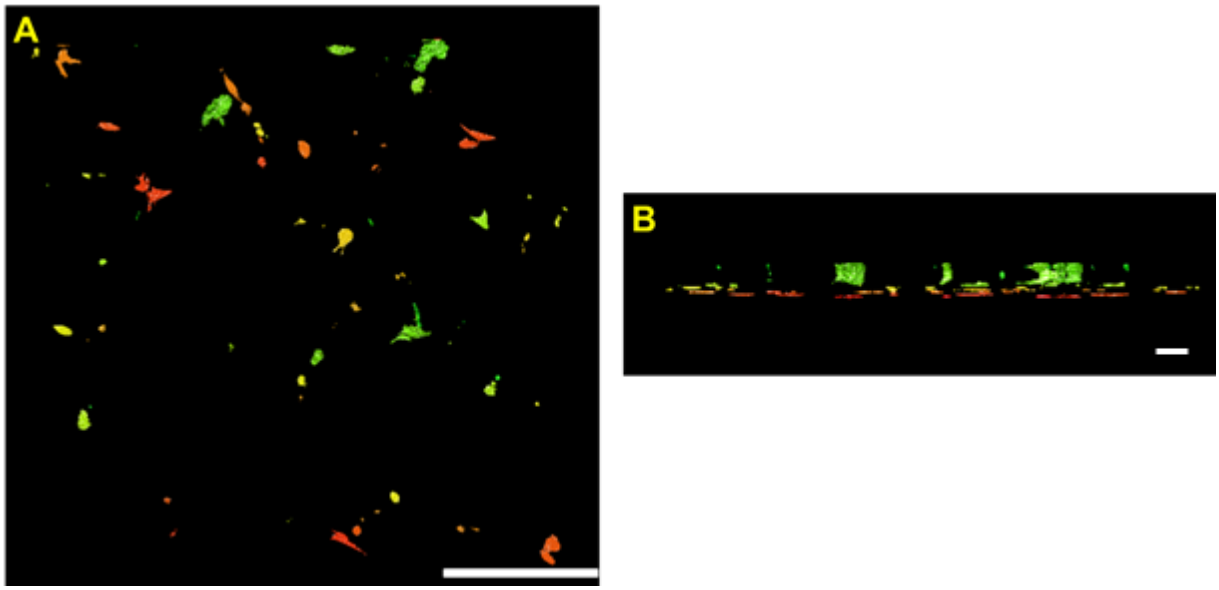

Figure 4.13: Representative 3D visualization of cells in hydrogel, providing with (A) maximum projected top view, scale bar = 30µm, and (B) projected side view, scale bar = 500µm. Cells were seen to distribute throughout the scaffold. Cells at different focal planes were labeled with different colors.

5. CONCLUSIONS

In this study, we presented a detailed characterization of a matrigel-collagen composite hydrogel and proposed this hydrogel as a 3D substrate for acute VIC culture *in vitro*. The combination of matrigel and collagen presented the VICs a porous, degradable and cytocompatible scaffold with an ECM composition that partly mimics the natural valve milieu. The composite hydrogel was amenable to dynamic culture as evidenced by our cyclic stretching experimental results. Further work should be carried out with other types of mechanical forces as well as for longer culture durations. While the idea of combining matrigel and collagen has been reported in few other cell types, this is the first study to consider the use of this type of hydrogel for VICs. More importantly, we have attempted to apply mechanical force (i.e. cyclic stretch) onto this construct and have shown its potential in serving as a load-bearing matrix to culture heart valve cells and hence, as a robust platform to study heart valve cell mechanobiology.

REFERENCES

Aikawa, E., P. Whittaker, M. Farber, K. Mendelson, R. F. Padera, M. Aikawa, and F. J. Schoen. 2006. Human semilunar cardiac valve remodeling by activated cells from fetus to adult: implications for postnatal adaptation, pathology, and tissue engineering. *Circulation* 113 (10):1344-52.

Arevalos, C. A., J. M. Berg, J. M. Nguyen, E. L. Godfrey, C. Iriondo, and K. J. Grande-Allen. 2016. Valve Interstitial Cells Act in a Pericyte Manner Promoting Angiogensis and Invasion by Valve Endothelial Cells. *Ann Biomed Eng* 44 (9):2707-23.

Babu, M., H.K.S. Yadav, A. Moin, and Shivakumar H.G. 2011. *In vitro-in vivo* evaluation of poly(2-hydroxyethyl methacrylate-co-methyl methacrylate) hydrogel implants containing cisplatin. *Acta Pharmaceutica Sinica B* 1 (4):261-7.

Balachandran, K., P. W. Alford, J. Wylie-Sears, J. A. Goss, A. Grosberg, J. Bischoff, E. Aikawa, R. A. Levine, and K. K. Parker. 2011. Cyclic strain induces dual-mode endothelial-mesenchymal transformation of the cardiac valve. *Proc Natl Acad Sci U S A* 108 (50):19943-8.

Balachandran, K., P. Sucosky, H. Jo, and A. P. Yoganathan. 2009. Elevated cyclic stretch alters matrix remodeling in aortic valve cusps: implications for degenerative aortic valve disease. *Am J Physiol Heart Circ Physiol* 296 (3):H756-64.

Balachandran, K., P. Sucosky, H. Jo, and A. P. Yoganathan. 2010. Elevated cyclic stretch induces aortic valve calcification in a bone morphogenic protein-dependent manner. *Am J Pathol* 177 (1):49-57.

Balachandran, K., P. Sucosky, and A. P. Yoganathan. 2011. Hemodynamics and mechanobiology of aortic valve inflammation and calcification. *Int J Inflam* 2011:263870.

Bono, N., D. Pezzoli, L. Levesque, C. Loy, G. Candiani, G. B. Fiore, and D. Mantovani. 2016. Unraveling the role of mechanical stimulation on smooth muscle cells: A comparative study between 2D and 3D models. *Biotechnol Bioeng* 113 (10):2254-63.

Butcher, J. T., and R. M. Nerem. 2004. Porcine aortic valve interstitial cells in three-dimensional culture: comparison of phenotype with aortic smooth muscle cells. *J Heart Valve Dis* 13 (3):478-85; discussion 485-6.

Cox, T. R., and J. T. Erler. 2011. Remodeling and homeostasis of the extracellular matrix: implications for fibrotic diseases and cancer. *Dis Model Mech* 4 (2):165-78.

Dewitt, D. D., S. N. Kaszuba, D. M. Thompson, and J. P. Stegemann. 2009. Collagen I-matrigel scaffolds for enhanced Schwann cell survival and control of three-dimensional cell morphology. *Tissue Eng Part A* 15 (10):2785-93.

Dhivya, S., S. Saravanan, T. P. Sastry, and N. Selvamurugan. 2015. Nanohydroxyapatite-reinforced chitosan composite hydrogel for bone tissue repair in vitro and in vivo. *J Nanobiotechnology* 13:40.

Duan, B., L. A. Hockaday, K. H. Kang, and J. T. Butcher. 2013. 3D bioprinting of heterogeneous aortic valve conduits with alginate/gelatin hydrogels. *J Biomed Mater Res A* 101 (5):1255-64.

Farrar, E. J., V. Pramil, J. M. Richards, C. Z. Mosher, and J. T. Butcher. 2016. Valve interstitial cell tensional homeostasis directs calcification and extracellular matrix remodeling processes via RhoA signaling. *Biomaterials* 105:25-37.

Fisher, C. I., J. Chen, and W. D. Merryman. 2013. Calcific nodule morphogenesis by heart valve interstitial cells is strain dependent. *Biomech Model Mechanobiol* 12 (1):5-17.

Geckil, H., F. Xu, X. Zhang, S. Moon, and U. Demirci. 2010. Engineering hydrogels as extracellular matrix mimics. *Nanomedicine (Lond)* 5 (3):469-84.

Gould, R. A., K. Chin, T. P. Santisakultarm, A. Dropkin, J. M. Richards, C. B. Schaffer, and J. T. Butcher. 2012. Cyclic strain anisotropy regulates valvular interstitial cell phenotype and tissue remodeling in three-dimensional culture. *Acta Biomater* 8 (5):1710-9.

Gupta, V., J. A. Werdenberg, T. L. Blevins, and K. J. Grande-Allen. 2007. Synthesis of glycosaminoglycans in differently loaded regions of collagen gels seeded with valvular interstitial cells. *Tissue Eng* 13 (1):41-9.

Heher, P., B. Maleiner, J. Pruller, A. H. Teuschl, J. Kollmitzer, X. Monforte, S. Wolbank, H. Redl, D. Runzler, and C. Fuchs. 2015. A novel bioreactor for the generation of highly aligned 3D skeletal muscle-like constructs through orientation of fibrin via application of static strain. *Acta Biomater* 24:251-65.

Hjortnaes, J., K. Shapero, C. Goettsch, J. D. Hutcheson, J. Keegan, J. Kluin, J. E. Mayer, J. Bischoff, and E. Aikawa. 2015. Valvular interstitial cells suppress calcification of valvular endothelial cells. *Atherosclerosis* 242 (1):251-60.

Jian, B., J. Xu, J. Connolly, R. C. Savani, N. Narula, B. Liang, and R. J. Levy. 2002. Serotonin mechanisms in heart valve disease I: serotonin-induced up-regulation of transforming growth factor-beta1 via G-protein signal transduction in aortic valve interstitial cells. *Am J Pathol* 161 (6):2111-21.

Kamel, P. I., X. Qu, A. M. Geiszler, D. Nagrath, R. Harmancey, H. Taegtmeyer, and K. J. Grande-Allen. 2014. Metabolic regulation of collagen gel contraction by porcine aortic valvular interstitial cells. *J R Soc Interface* 11 (101):20140852.

Lam, M. T., and J. C. Wu. 2012. Biomaterial applications in cardiovascular tissue repair and regeneration. *Expert Rev Cardiovasc Ther* 10 (8):1039-49.

Lam, N. T., T. J. Muldoon, K. P. Quinn, N. Rajaram, and K. Balachandran. 2016. Valve interstitial cell contractile strength and metabolic state are dependent on its shape. *Integr Biol (Camb)* 8 (10):1079-1089.

Liu, A. C., V. R. Joag, and A. I. Gotlieb. 2007. The emerging role of valve interstitial cell phenotypes in regulating heart valve pathobiology. *Am J Pathol* 171 (5):1407-18.

Masters, K. S., D. N. Shah, L. A. Leinwand, and K. S. Anseth. 2005. Crosslinked hyaluronan scaffolds as a biologically active carrier for valvular interstitial cells. *Biomaterials* 26 (15):2517-25.

Nicodemus, G. D., and S. J. Bryant. 2008. Cell encapsulation in biodegradable hydrogels for tissue engineering applications. *Tissue Eng Part B Rev* 14 (2):149-65.

Osman, L., M. H. Yacoub, N. Latif, M. Amrani, and A. H. Chester. 2006. Role of human valve interstitial cells in valve calcification and their response to atorvastatin. *Circulation* 114 (1 Suppl):I547-52.

Quinlan, A. M., and K. L. Billiar. 2012. Investigating the role of substrate stiffness in the persistence of valvular interstitial cell activation. *J Biomed Mater Res A* 100 (9):2474-82.

Rabkin, E., M. Aikawa, J. R. Stone, Y. Fukumoto, P. Libby, and F. J. Schoen. 2001. Activated interstitial myofibroblasts express catabolic enzymes and mediate matrix remodeling in myxomatous heart valves. *Circulation* 104 (21):2525-32.

Rajamannan, N. M., F. J. Evans, E. Aikawa, K. J. Grande-Allen, L. L. Demer, D. D. Heistad, C. A. Simmons, K. S. Masters, P. Mathieu, K. D. O'Brien, F. J. Schoen, D. A. Towler, A. P.

Yoganathan, and C. M. Otto. 2011. Calcific aortic valve disease: not simply a degenerative process: A review and agenda for research from the National Heart and Lung and Blood Institute Aortic Stenosis Working Group. Executive summary: Calcific aortic valve disease-2011 update. *Circulation* 124 (16):1783-91.

Roohani-Esfahani, S. I., P. Newman, and H. Zreiqat. 2016. Design and Fabrication of 3D printed Scaffolds with a Mechanical Strength Comparable to Cortical Bone to Repair Large Bone Defects. *Scientific reports* 6:19468.

Sacks, M. S., W. David Merryman, and D. E. Schmidt. 2009. On the biomechanics of heart valve function. *J Biomech* 42 (12):1804-24.

Sapp, M. C., H. J. Fares, A. C. Estrada, and K. J. Grande-Allen. 2015. Multilayer three-dimensional filter paper constructs for the culture and analysis of aortic valvular interstitial cells. *Acta Biomater* 13:199-206.

Shin, H., J. W. Nichol, and A. Khademhosseini. 2011. Cell-adhesive and mechanically tunable glucose-based biodegradable hydrogels. *Acta Biomater* 7 (1):106-14.

Tan, H., J. P. Rubin, and K. G. Marra. 2010. Injectable in situ forming biodegradable chitosan-hyaluronic acid based hydrogels for adipose tissue regeneration. *Organogenesis* 6 (3):173-80.

Tandon, I., A. Razavi, P. Ravishankar, A. Walker, N. M. Sturdivant, N. T. Lam, J. C. Wolchok, and K. Balachandran. 2016. Valve interstitial cell shape modulates cell contractility independent of cell phenotype. *J Biomech* 49 (14):3289-3297.

Thayer, P., K. Balachandran, S. Rathan, C. H. Yap, S. Arjunon, H. Jo, and A. P. Yoganathan. 2011. The effects of combined cyclic stretch and pressure on the aortic valve interstitial cell phenotype. *Ann Biomed Eng* 39 (6):1654-67.

Toth, M., and R. Fridman. 2001. Assessment of Gelatinases (MMP-2 and MMP-9 by Gelatin Zymography. *Methods Mol Med* 57:163-74.

van Marion, M. H., N. A. Bax, M. C. van Turnhout, A. Mauretti, D. W. van der Schaft, M. J. Goumans, and C. V. Bouten. 2015. Behavior of CMPCs in unidirectional constrained and stress-free 3D hydrogels. *J Mol Cell Cardiol* 87:79-91.

Xing, Y., Z. He, J. N. Warnock, S. L. Hilbert, and A. P. Yoganathan. 2004. Effects of constant static pressure on the biological properties of porcine aortic valve leaflets. *Ann Biomed Eng* 32 (4):555-62.

Yap, C. H., H. S. Kim, K. Balachandran, M. Weiler, R. Haj-Ali, and A. P. Yoganathan. 2010. Dynamic deformation characteristics of porcine aortic valve leaflet under normal and hypertensive conditions. *Am J Physiol Heart Circ Physiol* 298 (2):H395-405.

Yip, C. Y., J. H. Chen, R. Zhao, and C. A. Simmons. 2009. Calcification by valve interstitial cells is regulated by the stiffness of the extracellular matrix. *Arterioscler Thromb Vasc Biol* 29 (6):936-42.

Young, C. J., L. A. Poole-Warren, and P. J. Martens. 2012. Combining submerged electrospray and UV photopolymerization for production of synthetic hydrogel microspheres for cell encapsulation. *Biotechnol Bioeng* 109 (6):1561-70.

Zhang, X., B. Xu, D. S. Puperi, Y. Wu, J. L. West, and K. J. Grande-Allen. 2015. Application of hydrogels in heart valve tissue engineering. *J Long Term Eff Med Implants* 25 (1-2):105-34.

Zhu, J., and R. E. Marchant. 2011. Design properties of hydrogel tissue-engineering scaffolds. *Expert Rev Med Devices* 8 (5):607-26.

Zimmermann, W. H., M. Didie, G. H. Wasmeier, U. Nixdorff, A. Hess, I. Melnychenko, O. Boy, W. L. Neuhuber, M. Weyand, and T. Eschenhagen. 2002. Cardiac grafting of engineered heart tissue in syngenic rats. *Circulation* 106 (12 Suppl 1):I151-7.

Zimmermann, W. H., I. Melnychenko, and T. Eschenhagen. 2004. Engineered heart tissue for regeneration of diseased hearts. *Biomaterials* 25 (9):1639-47.

Zimmermann, W. H., K. Schneiderbanger, P. Schubert, M. Didie, F. Munzel, J. F. Heubach, S. Kostin, W. L. Neuhuber, and T. Eschenhagen. 2002. Tissue engineering of a differentiated cardiac muscle construct. *Circ Res* 90 (2):223-30.

CHAPTER 5

Fibroblast growth factor 1 and fibroblast growth factor 2 in pathological stretched valve interstitial cells in 3D model

ABSTRACT

More than five million Americans suffer from heart valve disease annually, a condition that worsens cardiac function and gradually leads to heart failure if appropriate treatment is not performed on time. Currently no medicines can cure heart valve disease, leaving surgical intervention as the only viable option for patients at late stages of cardiac disease. Tremendous efforts have focused on studying how resident cells in the valves respond to pathological stimulation as well as the underlying mechanisms that regulate these responses in order to identify potential therapeutic targets for non-surgical treatment of valvular heart disease. Cardiac valve cells naturally reside in a complex three-dimensional environment under varying hemodynamics, which is difficult to replicate *in vitro.* As a result, most cell signaling studies in the field have traditionally been conducted on two-dimensional models or in the absence of hemodynamic forces. In aim 2, we reported the fabrication of a hydrogel scaffold that could be used to culture valve cells under dynamic mechanical stimulation in a valve-mimetic environment. This model, therefore appeared to be suitable for VIC signaling studies as it provided cells a three-dimensional environment with the ability to incorporate mechanical stretching stimulation. Utilizing this model, in this aim, we investigated the possible role of FGF1/FGF2 signaling in regulating valve cell activation under physiological and pathological stretching conditions as well as in mediating cell proliferation and metabolism via Akt/mTOR pathway. FGFR1 inhibitor was used to verify the involvement of FGFs. Using this model, we reported that 1) FGF1/FGF2 had similar effects on regulating valve cell phenotype and cellular activity as was seen under stretching stimulation alone; 2) Cells increased proliferation/metabolism under elevated cyclic stretch via Akt/mTOR pathway; 3) FGF1/FGF2 promoted cell proliferation at physiological conditions but mitigated it at pathological

conditions; and 4) FGF1/FGF2 was able to maintain cell quiescent phenotype. Overall, these results suggested that FGF1/2 may represent a possible therapeutic target for drug therapies for preventing heart valve disease progression.

1. INTRODUCTION

As the heart muscle contracts and relaxes, the valves open and shut, controlling unidirectional flow of blood. Throughout this dynamic process, resident valve cells actively remodel and maintain homeostasis by the intricate signaling networks between cells and their microenvironment. Malfunction of valve opening/closing due to disrupted homeostasis is associated with impaired cardiac function and gradually result in heart valve disease (Wang, Leinwand, and Anseth 2014). To prevent long-term damage to the heart, surgical intervention to replace heart valves is a must as currently there are no drug therapies to halt disease progression. Approximately, 67,500 aortic valve replacement procedures are performed every year in the U.S (Clark et al. 2012). Consequently, researchers have sought to understand the cellular and molecular processes of valvular diseases, hoping that it may possibly lead to nonsurgical treatment. *In vitro* cell/tissue culture systems and biomaterials scaffolds with/without application of mechanical forces have advanced our understanding of valvular diseases and provided insights into possible intracellular signaling pathways that regulate valve cell pathophysiology (Wang, Leinwand, and Anseth 2014).

In static two-dimensional (2D) culture conditions, Xu *et al* reported the association of serotonin signaling with valve disease. Specifically, treatment of sheep valve interstitial cell (VIC) with serotonin reportedly caused up-regulation of transforming growth factor- β1 (TGF-β1) activity which in turn caused increased synthesis of extracellular matrix (ECM) proteins (collagen and GAGs) as seen in heart valves of carcinoid syndrome patients (Jian et al. 2002; Xu et al. 2002). It was also reported that the serotonin-2A receptor subtype (5HTR2A) was involved in 5HT up-regulation of active TGF-β (Xu et al. 2002). Similarly, at the tissue level, Balachandran *et al* subjected aortic valve cusps to elevated cyclic stretch and reported the up-regulation of 5HTR2A

and 5HTR2B expression which was associated with increased proliferation and ECM production in response serotonin addition (Balachandran, Bakay, et al. 2011). TGF-β signaling activated VICs from a quiescent fibroblastic phenotype to a contractile myofibroblast phenotype, and was a key regulator of wound repair by VICs (Liu and Gotlieb 2008). Using a scratch wound model, a study showed that VICs at the wound edge produced TGF-β, which then enhanced wound repair through increasing cell activation, proliferation, wound repair and formation of stress fibers. Earlier studies reported the presence of TGF-β within calcific stenosis cusps that mediated the calcification of aortic VICs in culture through mechanisms involving apoptosis (Jian et al. 2003). Interestingly, Cushing *et al* reported that fibroblast growth factor 2 (FGF2) effectively blocked TGF-β1-mediated myofibroblast activation and also the development of pathological contractile and calcifying phenotypes in aortic valvular interstitial cells (Cushing et al. 2008). Similarly, FGF2 was found to promote VIC wound repair through the TGF-β/Smad2/3 signaling pathway (Han and Gotlieb 2011). Recently, the possible protective role of FGF2 on VICs has been tested directly in cell culture media and showed that FGF2-containing cell culture media was able to maintain and dedifferentiate the VICs back to a fibroblastic phenotype with phenotypic and functional characteristics ascribed to cells in the intact valve (Latif et al. 2015).

While 2D models are commonly used for growing cells, VICs naturally reside in a 3D matrix environment. Several pioneering experiments with cells cultured in or on hydrogels comprised of natural ECM proteins or synthetic biomaterials investigated the effect of matrix stiffness on valve cell phenotype. For instance, it was reported that VICs did not form calcified nodules on soft poly(ethylene glycol) (PEG) hydrogels while they had increased expression of calcification markers when cultured on tissue culture polystyrene (Benton, Kern, and Anseth 2008). Similarly, VICs cultured on soft PEG hydrogel did not adopt a myofibroblast phenotype in response to

TGF-β1 treatment (Wang et al. 2012). Soft hydrogels were shown to be able to preserve the quiescent phenotype of VICs compared to stiff plastic plates through down-regulation of PI3K/Akt pathway (Wang et al. 2013). Although these studies have provided more information about the role of microenvironment signals in regulating valve cell fate, an understanding about how valve cells respond to these cues as well as the possible signaling pathways that mediate cellular responses remains vague.

Hence, in this aim, we proposed to use a mechanically robust hydrogel scaffold to culture VICs in the presence of mechanical stretching conditions in order to study stretch-mediated cellular responses. Cells were subjected to 10% and 20% uniaxial cyclic stretch which represented physiological and pathological stretch conditions, respectively. We examined the activation of the Akt/mTOR pathway in response to stretch at different time points using western blot. We also supplemented stretched VICs with FGF1 and FGF2 and investigated the effect of FGFs on cell proliferation, metabolism and activation potential. FGFR1 inbibitor, PD166866, was also used to tease out the role of FGF1 versus FGF2. Our results suggested that cells up-regulated Akt/mTOR phosphorylation in response to elevated stretch and that this response was modulated in the presence of FGF1/FGF2. Akt/mTOR activation correlated with increased metabolism, proliferation and expression of activated phenotypic markers of cells at pathological stretch. Treatment with FGF1/FGF2 appeared to have protective effect on 20% stretched cells as it reversed all cellular responses. At physiological 10% stretch, FGF1/FGF2 seemed to have effect only on cell proliferation, but not cell phenotype. This study thus provides fundamental insights into valve cell pathophysiology under abnormal mechanical stretch and suggests the potential of FGF1/FGF2 as targets for drug therapies for the treatment of heart valve disease.

2. MATERIALS AND METHODS

2.1. Cell isolation and culture

Valve interstitial cells were isolated from fresh porcine hearts obtained from local abattoir (Cockrum's Custom Meat Processing and Taxidermy, AR). The heart was transported to the laboratory in ice-cold, sterile PBS solution and quickly dissected in the cell culture hood. All three aortic valve leaflets were collected and incubated in 1mg/ml collagenase solution (Worthington, NJ) for up to 3 hours at 37°C with frequent agitation. After collagenase digestion, 10% fetal bovine serum (FBS)-containing Dulbecco's Modified Eagle Medium (DMEM) was added to arrest enzymatic activity. The solution was filtered with the cell strainer 100μm pore size (Corning, NY) to remove any remaining tissue debris prior to centrifugation for 5 minutes at 4°C. The resulting cell pellet was re-suspended in the regular 10% FBS-containing cell culture media, plated in a flask and maintained in a 37°C incubator. Fresh media was changed at least every 3 days. Cells from passage 1-7 were used in all experiments.

2.2. Immunofluorescent staining

We were first interested in testing the effect of FGF1/FGF2 on valve cell phenotype in static 2D culture. Valve interstitial cells were seeded onto glass coverslips and divided into 3 groups which were supplemented with 3 different culture media, named as 10% FBS-containing medium, FGF1 medium and FGF2 medium (Peprotech, NJ). Specific reagents for these media formulations are listed in table 5.1. Cells were kept in culture for two weeks with frequent change of fresh media. At the end of second week, coverslips were fixed and stained with common phenotypic markers of VICs. Briefly, 4% PFA and 0.5% Triton X100 were used to fix and permeabilize the cells prior to 1 hour blocking in 5% BSA. Primary antibodies were added and incubated overnight, including α-SMA (1:200), vimentin (1:1500), calponin (1:1000), Ki67

(1:500) and osteopontin (1:200) (all from Abcam). The next day, appropriate secondary antibodies and DAPI (1:200) (to stain the nuclei) were added. These coverslips were then mounted onto glass slides and imaged. The sample preparation was repeated for another set of samples for multiphoton imaging. The image acquisition process is described in the redox imaging section.

Table 5.1: List of reagents used for 3 cell culture media

	FGF1 medium	**FGF2 medium**	**10% FBS-containing medium**
FGF1 or FGF2	50ng/ml FGF1	50ng/ml FGF2	N/A
FBS	2%	2%	10%
Antibiotics	1%	1%	1%
HEPES	1%	1%	1%
Insulin	50ng/ml	50ng/ml	N/A

2.3. Immunohistochemistry of healthy and diseased human heart valve leaflets

We next examined the presence of FGF1/FGF2 and their receptors in the healthy versus diseased heart valve leaflets. Four de-identified IRB-exempt paraffin-embedded sections of human aortic valve leaflets were obtained from the University of Arkansas for Medical Sciences tissue bank. Samples were divided into two categories depending on size of calcific lesions, namely (I) no lesion (n=3), (II) mild lesions (n=1). Sections were then immunostained using standard protocols against the following proteins: FGF1, FGF2, FGFR1, and FGFR2. Briefly, after deparaffinization and rehydration, sections were incubated in 10mM citrate buffer, pH 6 at 95°C for 10 minutes for antigen retrieval. The slides were then allowed to cool at room temperature for 20 minutes, followed by rinsing twice in Dulbecco's Phosphate Buffered Saline (dPBS,Gibco), 5 minutes each. Blocking was performed using either 20% goat serum or donkey serum (Life

Technologies) in dPBS for 1 hour at 37°C. Slides were incubated with primary antibody solution anti-FGF1 (Santa Cruz Biotechnology, 1:10), anti-FGF2 (Santa Cruz Biotechnology, 1:10), anti-FGFR1 (Abcam, 1:25), anti-FGFR2 (Abcam, 1:25) antibodies) with 2% goat/donkey serum in a humid chamber at room temperature for 2 hours. Following primary antibody incubation, the slides were washed in PBS thrice, 5 minutes each. The slides were then incubated with 1:100 secondary antibody (Alexa Fluor 488 or Alexa Fluor 594), 2% goat/donkey serum and 4',6-diamidino-2-phenylindole (DAPI) for 1 hour at room temperature in a humid chamber, away from light, followed by washing in dPBS thrice. A drop of Prolong Gold (Life Technologies) anti-fade mounting medium was used to coverslip the sections. Clear nail polish was used to seal the edges of the coverslip. Slides were then imaged using a standard epifluorescence microscope (Nikon Ti).

2.4. Pharmacological inhibition experiment

PD166866 (Sigma) was used to block FGFR1 (Panek et al. 1998) and validate the involvement of FGF1/FGF2 in mediating downstream cellular responses. Western blotting and standard MTT assays were carried out to determine the appropriate working concentrations of this inhibitor on VICs. For this purpose, we first tested FGFR1 inhibition on monolayer VICs. Cells were serum-starved overnight before the experiment. A total of 6 different concentrations of PD166866 were tested: 1, 10, 50, 100, 500 and 1000nM. Cells were incubated with the inhibitor for 2 hours, following which, 50ng/ml of FGF1 or FGF2 was separately administrated to the cells and left for 10 minutes before protein extraction took place using RIPA lysis buffer. Control samples included cells that received only FGF1 or FGF2 treatment, cells that received only inhibitor treatment at highest dose and cells that did not receive any treatment. BCA assay was carried out to determine protein concentration followed by western blot to examine the effect of FGFR1

inhibitor doses on Akt phosphorylation. The concentration that gave the least signal of phosphorylated Akt was chosen for the subsequent experiments.

The western blotting protocol is briefly as follows. Criterion 10% polyacrylamide gels (Bio-Rad) were loaded with at least 10 μg of protein and subject to electrophoresis for 1 hour at 150V constant voltage. The gel was transferred to PVDF membranes for western blotting analysis. Membranes were blocked for 2 hours at room temperature with blocking buffer (LiCor), and probed with phosphor-Akt antibody (Cell signaling, 1:200) and β-actin (Abcam, 1:200) and incubated overnight at 4°C. The next day, these membranes were washed and incubated with appropriate secondary antibody (Licor) and imaged using a Licor Odyssey scanner. These membranes were stripped with Stripping buffer (Licor) and re-probed with total Akt antibody (Cell signaling, 1:100) prior to incubation with secondary antibody and imaged again. Signaling was quantified by comparing the band intensity obtained for the phosphorylated protein and normalizing it with the intensity obtained for total protein. β-actin was used as an additional loading control.

For MTT assay, VICs were plated in a 96-well plate. All conditions were the same as in the western blot setup. After addition of inhibitor and ligands, cells were kept in culture for a further 3 days to accommodate the longer timescale of proliferation. At the end of day 3, cell media was discarded and 5mg/ml of MTT were added to the cells and incubated for 4 hours at 37°C until purple crystals formed as the result of enzymatic activity in active dividing cells. MTT solution was removed and DMSO was added to dissolve the crystals. Absorbance measurement was then taken at 570nm. This absorbance reading was proportional to the proliferation capacity of the cells, and was normalized against blank sample which had only DMEM-phenol red free, MTT and DMSO.

Mechanical stretching experiment

Matrigel-collagen hydrogel was used in all stretching experiments and its fabrication was reported in aim 2 (Lam et al. 2017). Valve interstitial cells were seeded into this hydrogel and allowed to grow for a day prior to the stretching experiment.

For all subsequent cell lysates used in western blot to detect protein phosphorylation, the hydrogel sample was first cut in half and processed in 2 different ways for protein collection (Figure 5.1). One half of the sample was immediately snap-frozen after stretch termination and RIPA lysis buffer was added. The solution was vortexed, centrifuged and supernatant was collected. This lysate was used to detect the transient expression of phosphorylated proteins. The second half of the hydrogel construct was treated with 1mg/ml of collagenase 1 and dispase 2 for 1 hour to degrade the hydrogel materials, thus releasing cells from the matrix. RIPA lysis buffer was then added to the cells for protein collection. This lysate was used to detect the stable expression of total protein.

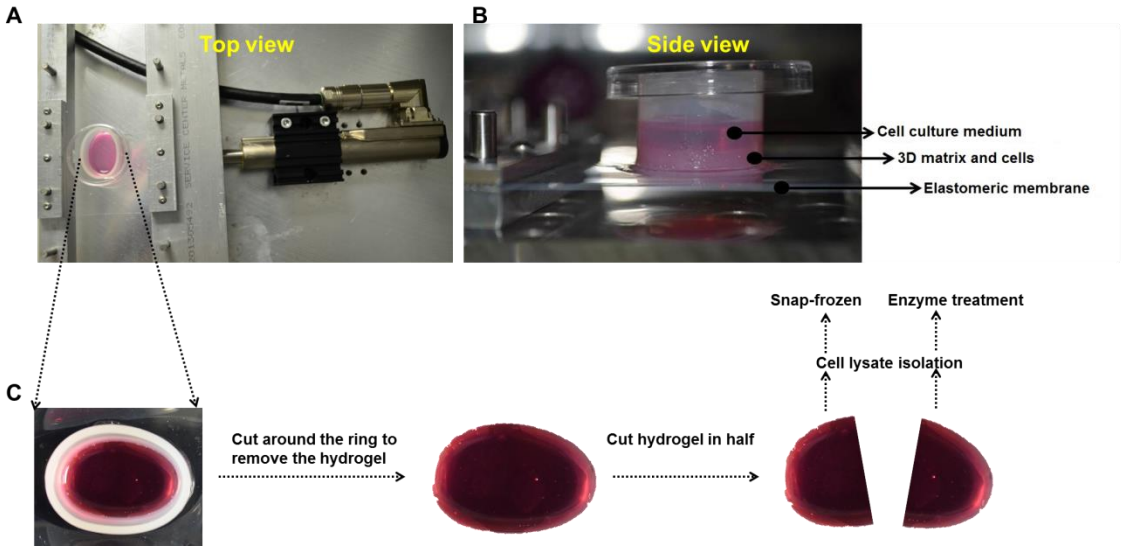

Figure 5.1: Schematic diagram showed representative images of a biostretcher device with a cell culture chamber (A, B) (figure was adapted from Lam et al. 2017) and 2 methods to collect cell lysate for phosphorylation study (C).

2.4.1. Experiment to measure changes in the phosphorylation level of Akt/mTOR at different time points

VICs were seeded into matrigel-collagen hydrogel and kept in culture overnight. The next day, these constructs were stretched uniaxially at either 10% or 20% which represented healthy and diseased conditions, respectively. Control samples were encapsulated VICs receiving no stretch. Validation of these stretch magnitudes could be found in our previous publication (Lam et al. 2017). Five different time points were examined, namely, 10 minutes, 1 hour, 6 hours, 24 hours and 48 hours. Immediately after the stretching was stopped at a certain time point, samples were taken out of the stretcher, washed briefly with PBS and divided into half with a scalpel. One half was immediately snap-frozen with liquid nitrogen and lysed with RIPA lysis buffer. The suspension was thoroughly mixed, centrifuged and supernatant was collected and stored at -80°C. The other half went through enzymatic treatment to disrupt the hydrogel and fully release the cells which were then collected after centrifugation. RIPA lysis buffer was added to the cell pellet and lysate was collected and stored. BCA assay were carried out to determine protein concentration.

For western blots, criterion 4-15% polyacrylamide gels (Bio-Rad) were loaded with at least 20 μg of protein and subject to electrophoresis for 1 hour at 150V constant voltage. The gel was transferred to PVDF membranes for western blotting analysis. Membranes were blocked for 2 hours at room temperature with blocking buffer (LiCor), and probed with appropriate primary antibodies and stored overnight at 4°C. In particular, membranes that had lysates from snap-frozen samples were probed with antibodies for phosphor-proteins, including phosphor-Akt (Cell signaling, 1:200), phosphor-mTOR (Abcam, 1:500) while membranes with enzyme treatment lysates were probed with antibodies for total proteins, including total Akt, total mTOR (Cell

signaling, 1:100). The next day, these membranes were washed and incubated with appropriate secondary antibody (Licor) and imaged using a Licor Odyssey scanner. Signaling was quantified by comparing the band intensity obtained for the phosphorylated protein and normalizing it with the intensity obtained for total protein. β-actin was used as loading control. The time point that yielded the strongest phosphorylation signal was then chosen for subsequent inhibition experiments. Although we used 'different lysates' to run western blot, these lysates indeed came from the same samples and we also used β-actin as loading control to ensure that all samples were loaded evenly.

2.4.2. Experiment to study the effect of FGF1/FGF2 signaling on Akt/mTOR signaling in stretched valve cells

For this experiment, a total of 13 different sample conditions were examined (Table 5.2). Cells were seeded as described above. After overnight culture, for samples that were treated with inhibitor, FGFR1 inhibitor at concentration determined by previous western blot and MTT assay was added to 6 samples and left for 24 hours. FGF1/FGF2 was added to the cells for 1 hour, followed by x hour stretching at 10% and 20% (x was determined by previous time point experiment). For samples that did not receive inhibitor treatment, FGF1/FGF2 was added directly to the cells and kept in culture for 1 hour before the stretch initiation. Protein collection and western blot were performed as previously described above.

Table 5.2: List of all conditions tested in the signaling study

Sample types	Without PD166866	With PD166866
10% stretch	10%	10% + PD166866
	10% + FGF1	10% + PD166866 + FGF1
	10% + FGF2	10% + PD166866 + FGF2
20% stretch	20%	20% + PD166866
	20% + FGF1	20% + PD166866 + FGF1
	20% + FGF2	20% + PD166866 + FGF2
No stretch	Control (No inhibitor treatment)	

2.5. Optical redox imaging and Second-harmonic generation imaging

Separate samples were prepared as described in table 5.2. For these experiments, as we were analyzing cell metabolism with redox imaging as in aim 1, the samples were allowed to stretch continuously for 24 hours before image acquisition to ensure cells have enough time to proliferate and actively start metabolic pathways. We were also interested in examining the collagen organization in these samples under the combined effects of FGFs treatment and stretch using simultaneous Second-harmonic generation imaging (SHG).

Before imaging, the cell culture chamber was placed carefully in a heated chamber to keep cells at 37°C throughout the procedure and imaging was taken using a custom-built resonant-scanning multiphoton microscopy platform with a 20X, 0.8 NA water immersion objective (Nikon, Japan) and a MaiTai ultrafast Ti:Sapphire tunable laser source (Spectra-Physics, Santa Clara CA).

The laser excitation source was tuned to 750nm (NADH fluorescence), 860nm (FAD fluorescence) and 800nm (Collagen). Laser power was kept constant throughout the experiment

and photomultiplier tube (PMT) gain was fixed at 90%. Images of a cuvette filled with 4ng/mL Rhodamine B (Sigma) were acquired via a 607nm/70nm bandpass filter, under identical conditions for both NADH and FAD acquisitions, to account for possible day-to-day variation in laser intensity. Images were analyzed using a custom MATLAB script and optical redox ratio was calculated using the following equation on a per pixel basis (Skala and Ramanujam 2010):

$$\text{Redox ratio} = \frac{[FAD]}{[NADH]+[FAD]}$$

[FAD] represents intensity of the FAD image normalized by the corresponding rhodamine intensity. [NADH] represents intensity of the NADH image normalized by the corresponding rhodamine intensity. After imaging, the samples were lysed with RIPA buffer and proceeded to BCA and western blot to detect the expression of phenotypic markers of VICs (i.e. calponin and α-SMA) and expression of heat shock protein 47 (hsp47).

2.6. Statistical analysis

All quantitative data were first analyzed for normality using the Anderson-Darling method. All normally distributed data were subsequently analyzed by one-way ANOVA followed by Holm-Sidak multiple pairwise comparisons. A p-value of less than 0.05 was used to indicate statistical significance differences between samples. Data was plotted as mean with standard error bars. In all the experiment, a replication of at least 3 different samples was performed.

3. RESULTS

3.1. FGF1 and FGF2 maintained VIC quiescent phenotype while promoted cell proliferation at 2D scale

FGF2 is becoming widely used in VIC cell culture media in order to maintain the cells in a quiescent state. In this experiment, we were interested in comparing the effect between FGF1 versus FGF2 on cell phenotype, using 10% FBS-containing medium as control. Immunostaining

fluorescence showed interesting observations. It appeared that cells in FGF1 and FGF2 media behaved in a different way than cells in 10% FBS-containing medium (Figure 5.2 A,B). Particularly, VICs expressed vimentin, a known quiescent marker, at a higher level in FGF1 and FGF2 media than in 10% FBS-containing medium while calponin was strongly expressed when cells were cultured in 10% FBS-containing medium as compared to those in FGF1 and FGF2 media. Other activated markers, α-SMA and osteopontin, were comparably expressed throughout the 3 media formulations. VICs also showed increased propensity for proliferation in the presence of FGF1 and FGF2 media as seen in Ki67 stained images. This observation was further supported by measurement of the optical oxidation-reduction ratio of NADH/FAD which correlates to the cellular metabolic activity. Redox ratio was significantly decreased in cells that were cultured in FGF1 and FGF2 media compared to cells that were kept in 10% FBS-containing medium. When comparing between FGF1 medium versus FGF2 medium, no significant differences were observed.

These observations suggested the possible role of FGF1/FGF2 in modulating VIC phenotype such that cell proliferation was promoted, while maintaining a quiescent phenotype. Hence, we were interested to examine further the role of FGF1/FGF2 on VIC phenotypee in a 3D model in the presence of mechanical stimulation.

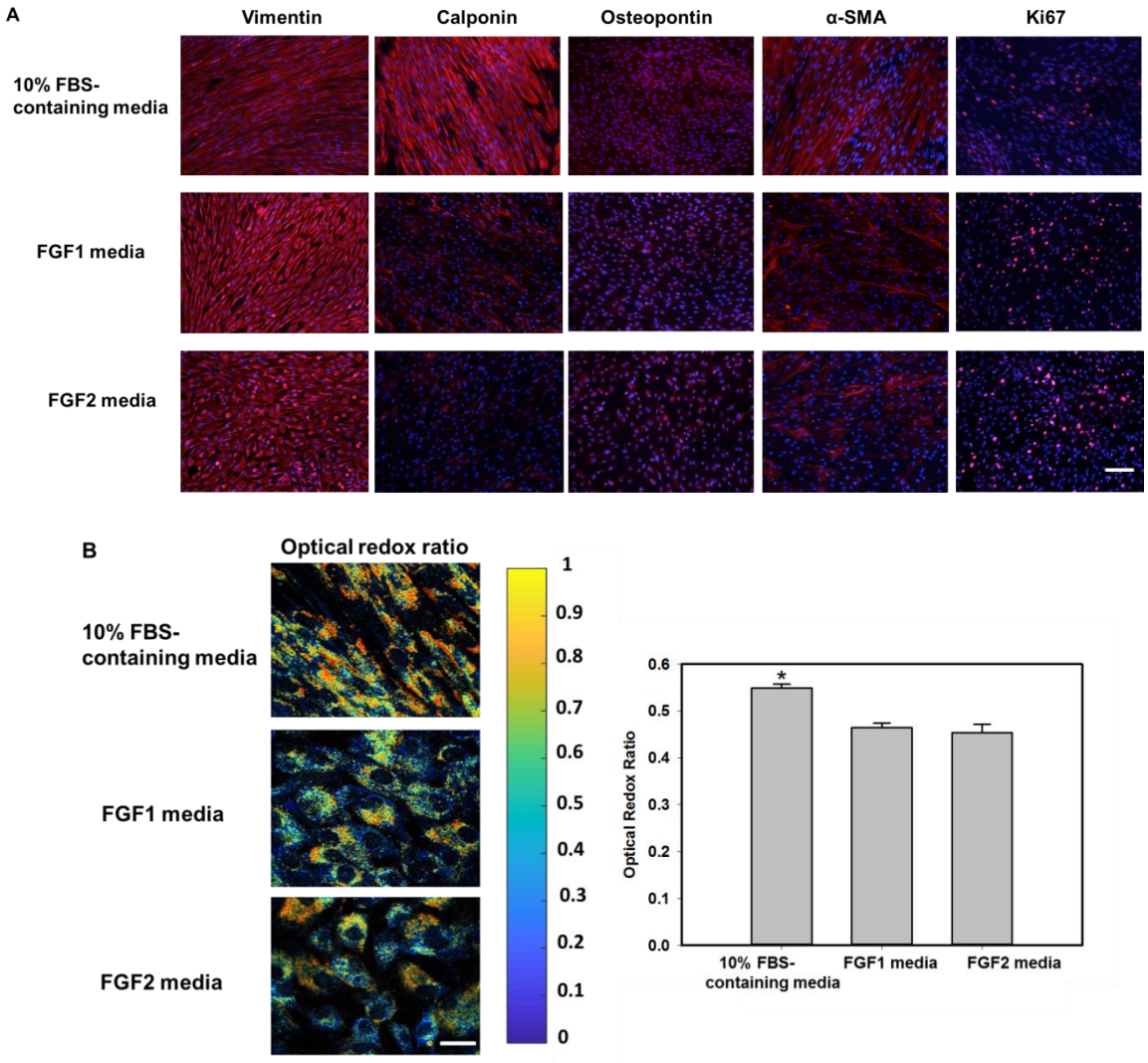

Figure 5.2: Immunofluorescent staining images for different proteins expressed when VICs were cultured in 3 different media, scale bar =100µm (A) and optical redox ratio, scale bar = 10µm (B), n=5, * $p<0.05$.

3.2. FGF1 and FGFR1 were moderately expressed in healthy and diseased valves while FGF2 was strongly expressed in diseased valves

Immunohistochemistry of human aortic valve leaflets showed expression of FGFR1 in both healthy and diseased valves while FGFR2 expression was low for all samples (Figure 5.3). This result consequently led us to a decision to target FGFR1 in the following inhibitor studies. Furthermore, FGF2 expression was high in healthy samples and calcific leaflets while FGF1

expression was high in healthy leaflets and low in diseased leaflets. This observation was intriguing, especially when compared to our monolayer staining data. At this point, we really wanted to see how FGF1/FGF2 impacted cells in a 3D model with the application of cyclic stretching.

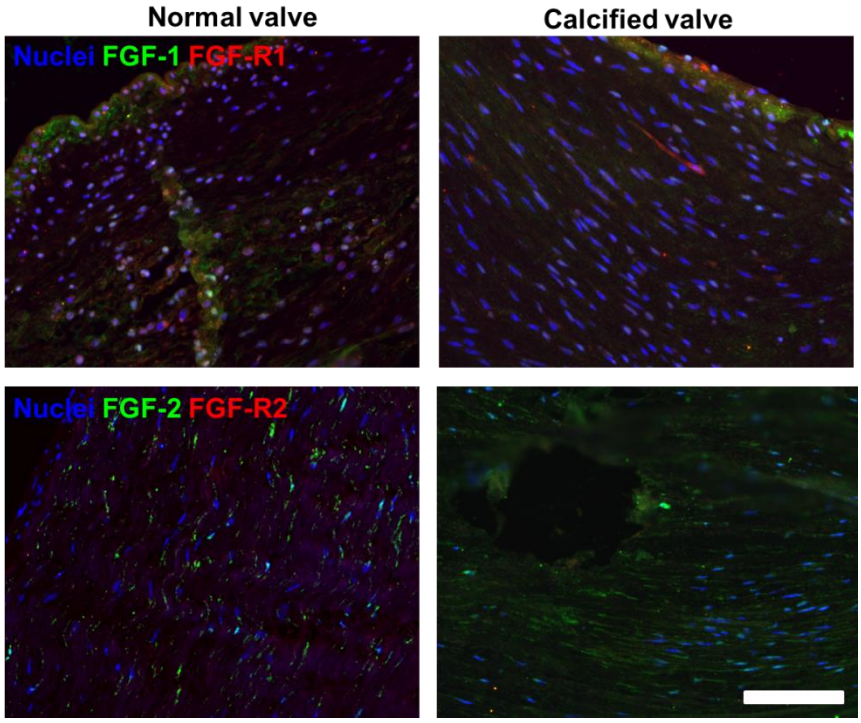

Figure 5.3: Immunohistochemistry staining of healthy and diseased valve leaflets, scale bar = 50µm.

3.3. The possible link between FGF1/FGF2 and Akt/mTOR pathway in stretched valve cells

3.3.1. Akt/mTOR phosphorylation was up-regulated at elevated stretch

Since monolayer VICs showed increased proliferation in FGFs-containing media, we decided to investigate the possible link between the FGF1/FGF2 and Akt/mTOR pathway in modulating VIC fate under abnormal mechanical forces. In order to do that, we first set out to determine the time point for detecting the phosphorylation event of Akt/mTOR in the mechanical stimulation experiment. VICs were cultured in 3D matrigel-collagen hydrogel and subjected to 10% and

20% uniaxial cyclic stretch to simulate physiological and pathological conditions, respectively. Unstretched samples served as controls. As showed in figure 5.4, the phosphorylation level of Akt/mTOR significantly increased at elevated stretch compared to normal stretch and control samples. The data suggested that the Akt/mTOR signaling became activated due to the effect of elevated cyclic stretching. Highest phosphorylation levels were seen at the 10 minute, 1 hour and 6 hour time points after the stretch initiation and slowly reduced thereafter. Based on this experiment, we decided to choose the 1 hour time point for subsequent phosphorylation experiments.

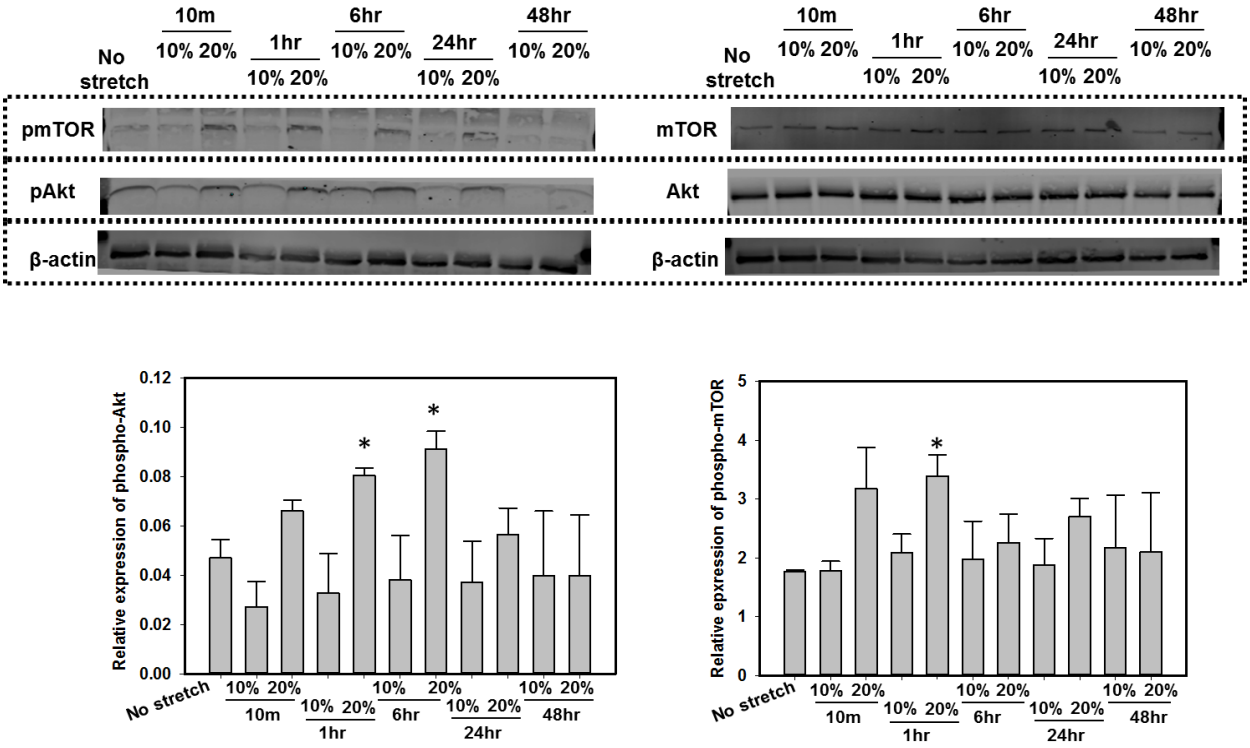

Figure 5.4: Representative western blot analysis of Akt/mTOR phosphorylation at different time points, n = 4, *p<0.05.

3.3.2. Opposite effect of FGF1 and FGF2 on cell proliferation at different stretch magnitudes

3.3.2.1. Determination working concentration of PD166866 - an FGFR1 inhibitor

As mentioned previously, we decided to target the FGFR1 only based on the IHC staining result in which only FGFR1 was expressed in valve cells together with FGF1 and FGF2. We used PD166866, an FGFR1 inhibitor (Panek et al. 1998), to validate the involvement of FGF1/FGF2 in mediating cellular behavior in response to mechanical stimulation. The appropriate working concentration of PD166866 was determined via western blotting and MTT assay on VIC monolayers. As shown in the western blotting results, adding small amount of PD166866 (i.e. 1nM and 10nM) did not seem to reduce Akt phosphorylation as compared to positive control which had only FGF1 or FGF2. Increased amount of PD166866 did decrease the level of phosphorylated Akt with highest effect seen at 1000nM. Untreated samples showed similar expression of phosphorylated Akt as in samples treated with the highest dose of PD166866 (Figure 5.5 A,B).

MTT assay further supported the previous dose determination study (Figure 5.5 C). In MTT, the absorbance at 570nm directly correlated to the metabolic activity of active cells and was used to assess cell proliferation. Addition of PD16686 significantly reduced cell proliferation capacity as seen in all samples that had PD166866 treatment as well as no treatment sample. Samples that had only FGF1 or FGF2 had significantly higher proliferation. We still did not see any difference between the effects of FGF1 versus FGF2 on Akt phosphorylation in this experiment.

Based on both western blot and MTT results, we chose 1000nM of PD166866 as our working concentration for subsequent experiments as it effectively blocked the Akt activation (phosphorylation) caused by FGF1/FGF2 stimulation.

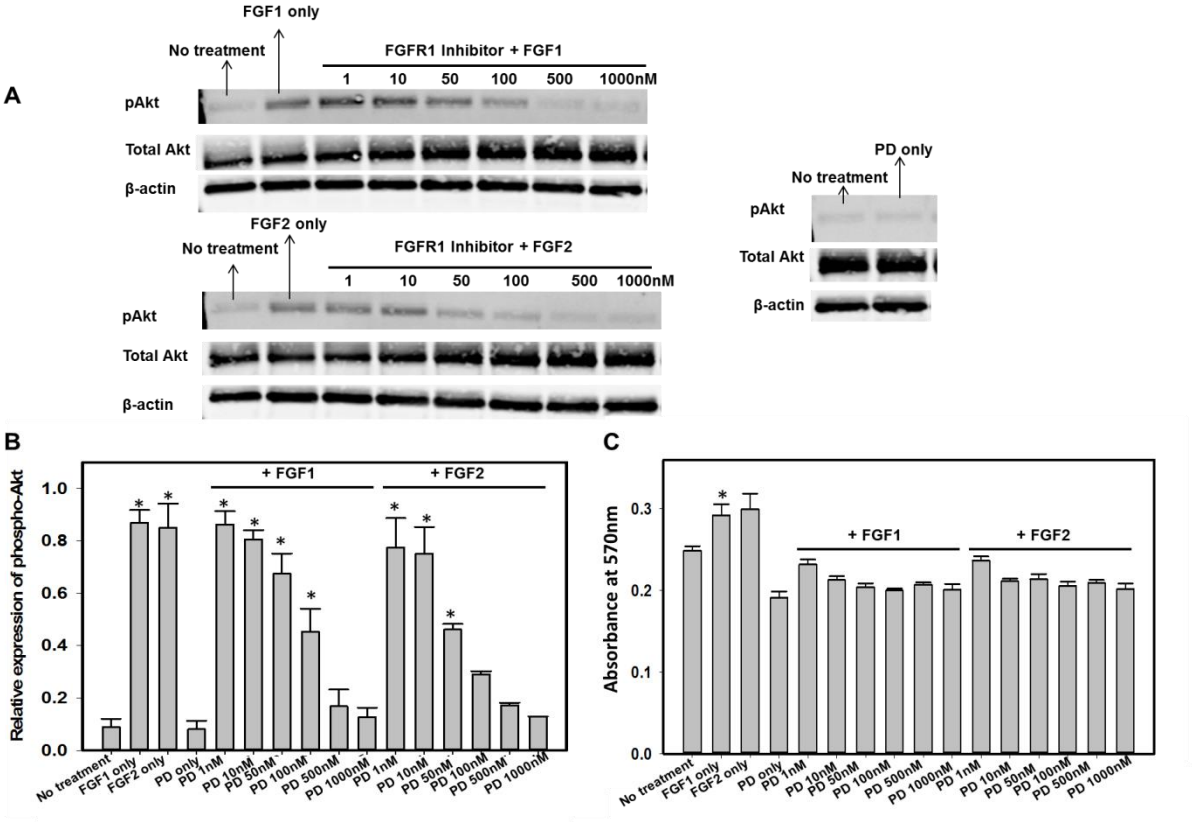

Figure 5.5: Representative western blot analysis of Akt phosphorylation in inhibitor study (A,B) and MTT assay (C), n=3, *p<0.05.

3.3.2.2. Stretch-dependent and opposite effects of FGF1 and FGF2 on Akt/mTOR pathway

To investigate the possible link between FGF-mediated cellular response under stretch stimulation and the Akt/mTOR pathway, we stretched the 3D cellular construct for 1 hour under various treatment conditions (table 5.2) and collected cell lysates for western blot analysis (Figure 5.6).

In the presence of FGFR1 inhibitor, the Akt/mTOR pathway was not activated as suggested by low expression of phosphorylated proteins observed throughout regardless the stretch magnitudes. In samples that were not treated with inhibitors, several observations were made. Cells at elevated cyclic stretch (20%) expressed more phosphorylated Akt/mTOR than cells at normal cyclic stretch (10%). Interestingly, when either FGF1 or FGF2 was added, at 20% stretch

the phosphorylation was significantly reduced while it was increased at 10% stretch. As before, FGF1 and FGF2 appeared to have very similar effects on stimulation of the Akt/mTOR pathway. Overall, it appeared that FGF1 and FGF2 mitigated the activation of Akt/mTOR pathway of VICs at 20% while they did the opposite at 10%. All these effects disappeared in the presence of PD166866, suggesting that FGF1/FGF2 was involved in regulating the activation of Akt/mTOR pathway in VICs in response to stretch stimulation.

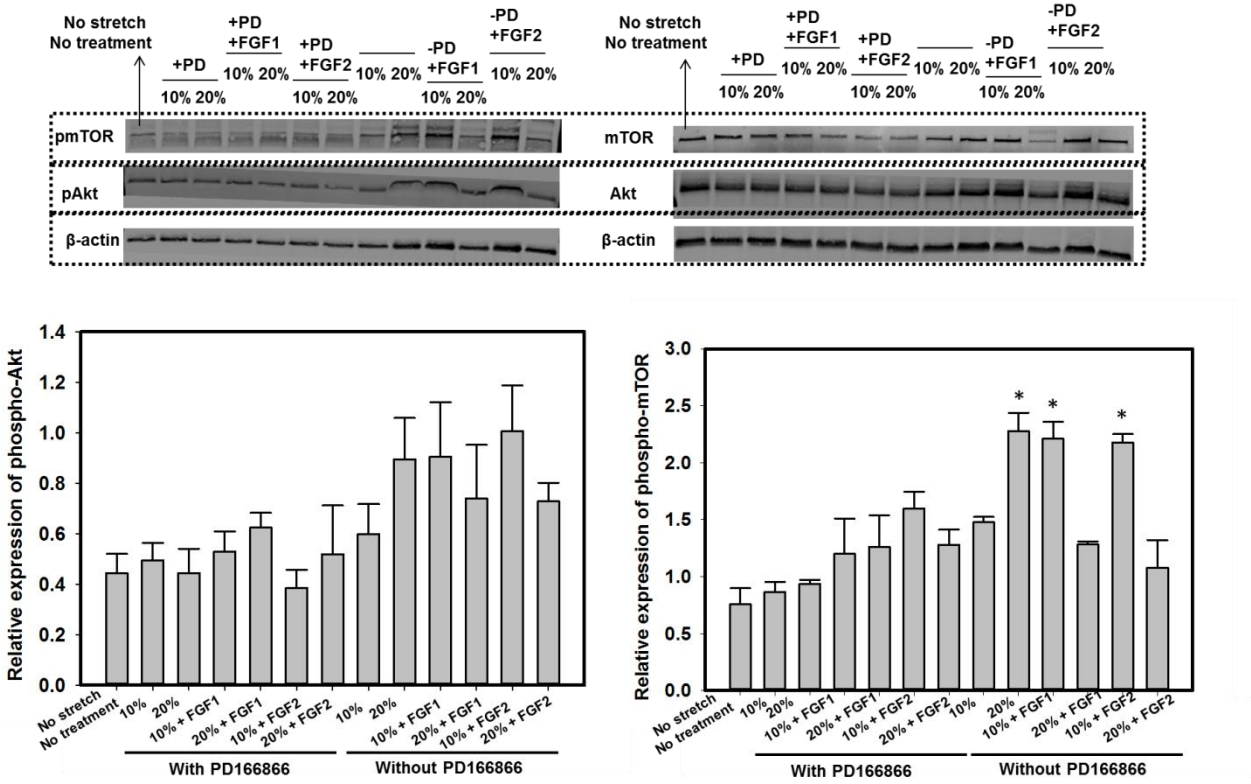

Figure 5.6: Representative western blot analysis of Akt/mTOR phosphorylation under the effects of FGF1/FGF2 and cyclic stretching, n=3, *p<0.05.

3.4. Activation of Akt/mTOR pathway correlated with cell metabolic activity under the effect of FGF1/FGF2

Since Akt/mTOR pathway directly regulates cellular proliferation (Yu and Cui 2016), we hypothesized that there would be a correlation between activation of Akt/mTOR pathway with the proliferation capacity of VICs under different treatment conditions. We used optical redox

ratio as the way to evaluable cell metabolic activity as well as proliferation potential of encapsulated stretched cells, based on our earlier results in aim 1 and 3.

We observed that in the presence of FGFR1 inhibitor, all treated samples exhibited increased redox ratios compared to 3 samples that did not receive FGFR1 inhibitor treatment (i.e. 20%, 10% + FGF1 and 10% + FGF2). This corresponded to the samples with low phosphorylation of Akt/mTOR from previous western blot data. Constructs at 20% stretch had significantly decreased redox ratio compared to 10% stretched samples. Addition of either FGF1 or FGF2 resulted in different response in VICs at 10% versus 20% stretch such that cells with FGF1 or FGF2 treatment under 10% had decreased redox ratio while cells with FGF1 or FGF2 under 20% had increased redox ratio. Again, we noticed that decreased optical redox ratio correlated with high level of phosphorylation of Akt/mTOR and increased optical redox ratio correlated with low level of phosphorylated Akt/mTOR. Overall, it appeared that an increase in proliferation caused by elevated cyclic stretch as seen in 20% sample was mitigated by the presence of FGF1 and/or FGF2. Interestingly, it seemed to be the opposite at 10% stretch when addition of FGF1 and/or FGF2 stimulated cell proliferation. These effects were eliminated in the presence of FGFR1 inhibitor (Figure 5.7).

We also examined possible collagen organization in these conditions using SHG imaging since VICs were the cells that were responsible for collagen production in the valve leaflets (Figure 5.8 A). We could not see any notable difference in the distribution of fiber alignment and intensity throughout the samples, which was likely due to the short culture time points investigated in this study. Western blot analysis of cell lysates from these samples for hsp47, the protein that was thought to involve in collagen maturation, also revealed little difference in the collagen production in cells (Figure 5.8 B). Although cells that were not treated with PD166866 and

experienced elevated stretch appeared to express higher level of hsp47 compared to the rest of the samples, we found no statistical significant difference across the samples.

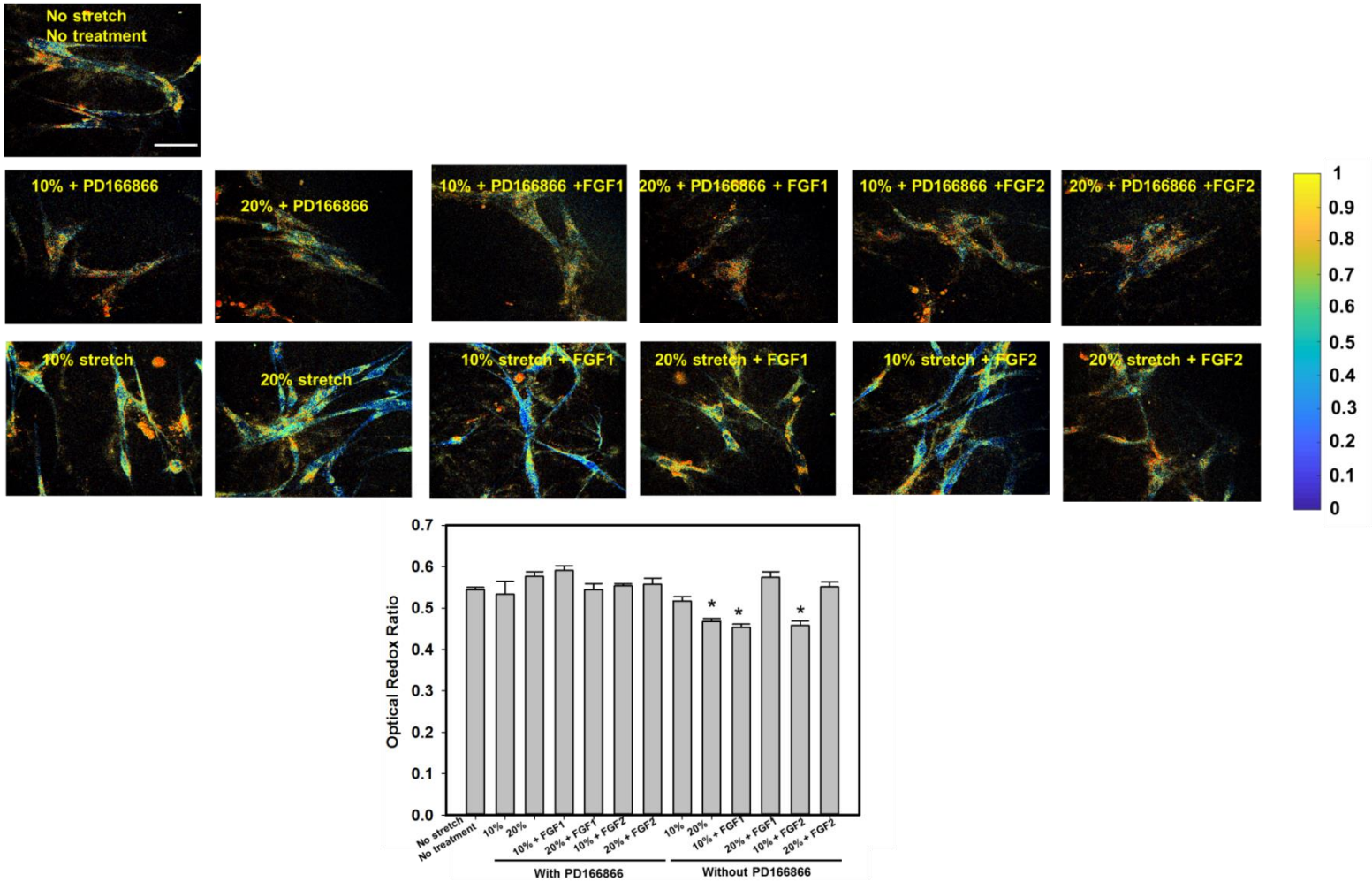

Figure 5.7: Representative optical redox ratio analysis, n=3-5, scale bar = 50µm, *p<0.05.

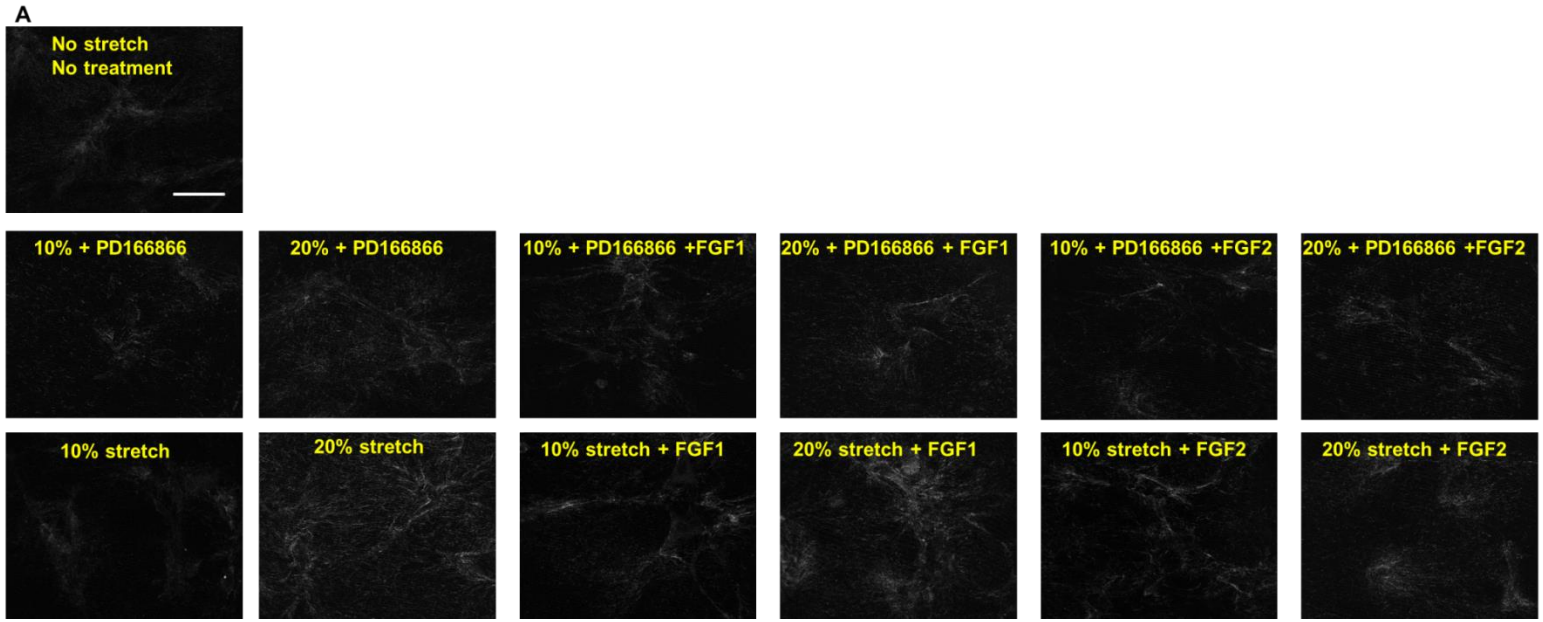
A
No stretch
No treatment
10% + PD166866
20% + PD166866
10% + PD166866 +FGF1
20% + PD166866 + FGF1
10% + PD166866 +FGF2
20% + PD166866 +FGF2
10% stretch
20% stretch
10% stretch + FGF1
20% stretch + FGF1
10% stretch + FGF2
20% stretch + FGF2

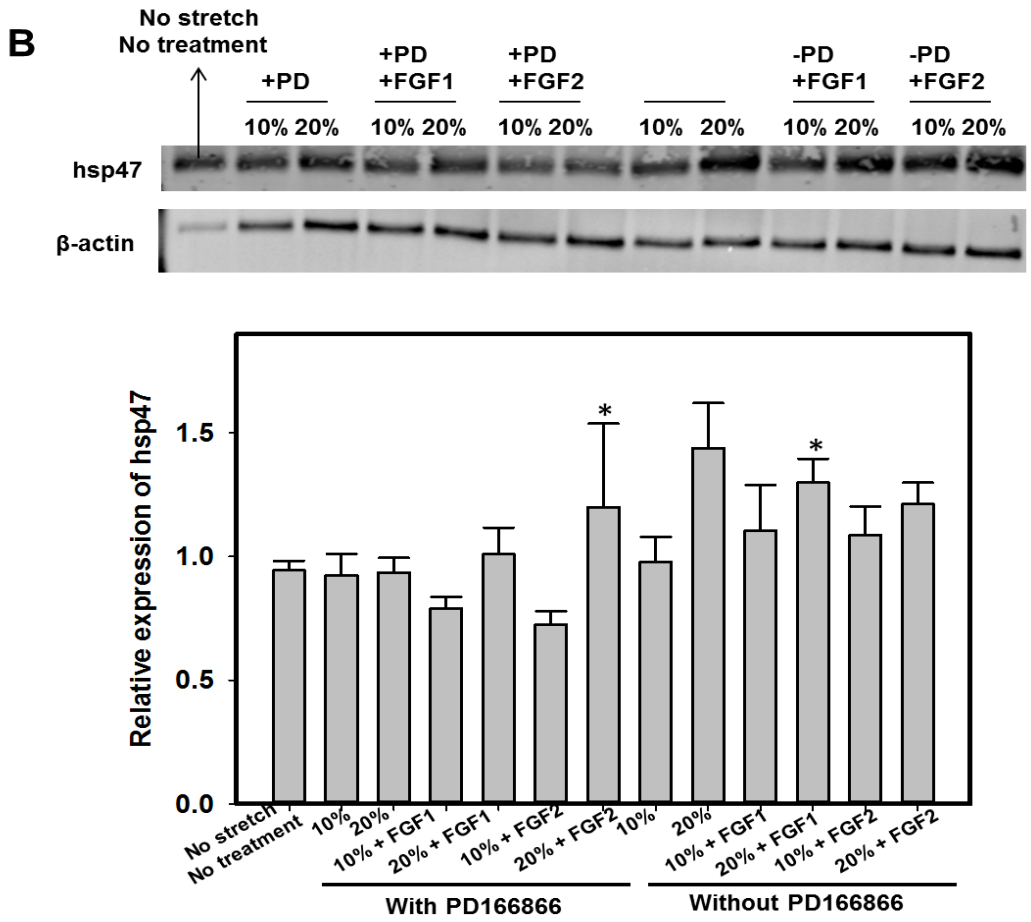

Figure 5.8: Representative SHG images (A) and western blot analysis of hsp47 (B), n=3, scale bar = 50μm.

3.5. Activation of Akt/mTOR pathway was coupled with changes in VIC phenotype under the effect of FGF1/FGF2

The difference in effect of FGF1 or FGF2 had on VICs via Akt/mTOR pathway at different stretch magnitudes led us to question whether cell phenotype was also modulated. Western blot to detect common phenotypic markers of VICs revealed an answer (Figure 5.9). We observed that FGF1 and FGF2 did act to keep cells from becoming activated at elevated cyclic stretch. Cells at 10% stretch only and cells in 10% stretch with FGF1/FGF2 treatment had similar expression level of α-SMA and calponin, common activated markers of VICs, suggesting that

10% stretch did not actively induce cell activation and that addition of FGF1/FGF2 to cells at 10% stretch only affected cell proliferation/metabolism but not cell phenotype. In contrast, cells at 20% stretch had significantly higher α-SMA and calponin compared to cells at 10% stretch and the presence of FGF1/FGF2 significantly reduced these expression as seen in 20% stretch samples with FGF1/FGF2 treatment. In the presence of FGFR1 inhibitor, all cells that experienced elevated stretch expressed higher amount of α-SMA and calponin, suggesting that FGF1 /FGF2 did take part in modulating VIC phenotype under pathological stretching condition.

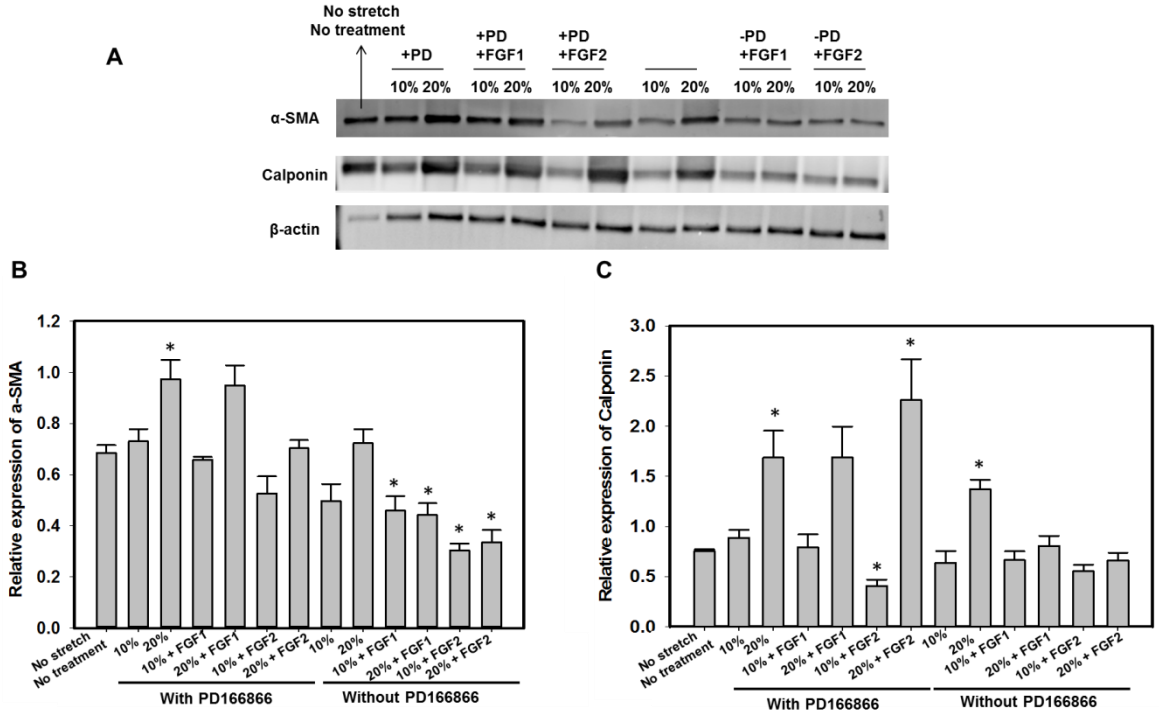

Figure 5.9: Representative western blot analysis of phenotypic markers of VICs (A), α-SMA (B) and calponin (C), n=3, *p<0.05.

4. DISCUSSION

The pathophysiological role of FGF family on VICs has been an ongoing study in the heart valve field, especially that of FGF2. Several studies had suggested the possible protective role of FGF2 on valve cells under pathological conditions which led to few recent studies where FGF2 was added to cell culture media to maintain VICs in a quiescent state *in vitro* (Latif et al. 2015; Han and Gotlieb 2011; Gotlieb, Rosenthal, and Kazemian 2002; Porras et al. 2017; Han and Gotlieb 2012). FGF1 and FGF2 belong to the FGF1 subfamily and they were both expressed in healthy and diseased aortic valve (Figure 5.3). It was also reported that FGF1/FGF2 expression was increased following myocardial infarction in rats (Zhao et al. 2011). Our immunofluorescent staining of VICs was in agreement with other studies, and suggested that FGF2 helped to maintain the quiescent phenotype of VICs as in native healthy valve (Latif et al. 2015). FGF1 appeared to have similar quiescent effects on VICs as similar profiles of cell phenotype was seen in both media formulations. Overall, FGF1 and FGF2 seemed to be able to preserve quiescent phenotype of VICs in culture. Interestingly, FGF1 and FGF2 not only kept VICs quiescent, they also appeared to increase cell proliferation, compared to cells cultured in 10% FBS-containing medium. This data was supported by optical redox imaging where cells in FGFs media displayed decreased optical redox ratio which suggested higher proliferative activity compared to cells in 10% FBS-containing medium with lower cell metabolism. Since FGF1 and FGF2 are considered as potent angiogenic factors and play important role in wound healing (Yun et al. 2010; Murakami and Simons 2008), it made sense to see that the presence of FGF in cell culture media promoted VIC proliferation although there was another study reported the reduction in proliferative capacity of VICs in FGFs media (Latif et al. 2015).

One of the hallmarks of VIC activation is an increase in proliferation, followed by intensive matrix remodeling which if not regulated, may result in pathological fibrosis, angiogenesis, chronic inflammation, and calcification (Liu, Joag, and Gotlieb 2007). A number of studies have demonstrated that the Akt/mTOR signaling cascade is associated with cardiac hypertrophy (Ikeda et al. 2015; Aoyagi and Matsui 2011). Akt is also involved in regulating the ability of oxidized low-density lipoprotein and lysophosphtydylcholine in upregulation of ECM protein production in human AVICs. Accumulation of ECM protein may contribute to the mechanism of valvular sclerosis associated with the development and progression of aortic stenosis (Cheng et al. 2017). PI3K/Akt signaling was reported to modulate the NF-κB pathway and its downstream target IL-6 which in turns affected the calcification process of VICs (El Husseini et al. 2014). This pathway, however, was not thoroughly examined in the heart valve context, especially under the effect of FGF1 and FGF2 in a 3D stretching model. Our data suggested that Akt/mTOR signaling activation-mediated FGF1/FGF2 was dependent on stretch magnitude and correlated with cellular optical redox ratio. Cells had higher level of phosphorylation of Akt/mTOR also displayed decreased optical redox ratio and vice versa. These effects were eliminated in the presence of FGFR1 inhibitor. Optical redox ratio recently has become widely used to assess the metabolic changes in cells during disease initiation and progression. Our previous study on single cells (aim1) reported that as cells became more elongated, the shape that mimicked pathological stretch, they decreased optical redox ratio which was associated with increased cell proliferation (Lam et al. 2016). Other studies reported a decrease in redox ratio was seen in cells undergoing differentiation (Quinn et al. 2013) or an increase in redox ratio after induction of cell death (Wang, Wei, and Guo 2009). Overall, it appeared that VICs responded to elevated stretch by activating Akt/mTOR pathway which increased cellular metabolic activity

and proliferative capacity as suggested by the reduced optical redox ratio. The treatment of FGF1 and FGF2 for cells under 20% stretch reversed those processes in which both phosphorylation and proliferation were reduced. In contrast, when VICs experienced physiological 10% stretch, they did not activate Akt/mTOR pathway but the addition of FGF1 and FGF2 significantly enhanced cell proliferation. These results suggested that FGF1 and FGF2 promoted cell proliferation physiologically while reduced cell proliferation in elevated cyclic stretch condition. It is worth to mention that these acute responses were observed only in the duration of 48 hours since the seeding time. This short time duration possibly explains why we did not observe any significant changes in collagen organization as well as collagen production in our experiment. Future studies may need to prolong the experimental duration to further study these responses.

VICs are known for their ability to become activated in response to pathological injury or abnormal hemodynamic/mechanical stretch. Activated VICs usually had increased expression of activated markers, α-SMA and calponin, while showing low expression of the quiescent, vimentin marker (Liu, Joag, and Gotlieb 2007). In our study, we observed that in treatment with FGF1 and FGF2, regardless the stretch magnitude, cells expressed lesser activated markers (i.e. 10% FGF1, 20% FGF1, 10% FGF2 and 20% FGF2 samples). In the presence of FGFR1 inhibitor, the effect of stretching became more pronounced as cells expressed more activated markers at elevated cyclic stretch. Additionally, VICs proliferated in 20% sample but decreased proliferation when treated with FGF1 and FGF2, suggesting that the presence of FGF1/FGF2 somehow ‘signaled’ the cells and reduced its proliferation propensity at least in the early phase of experiencing abnormal mechanical stretch. In the absence of FGF or in the presence of FGFR1 inhibitor, the effects of stretching became dominant as cells appeared to become activated and proliferated more at elevated stretch as compared to no stretch and 10% stretch.

Throughout the experiments, we could not detect any difference between the effect of FGF1 versus FGF2 on VICs. It was interesting to us to notice that although FGF1/FGF2 appeared to have similar effects on VICs in both monolayer and 3D culture model but its expression pattern was different in healthy versus calcified valves. Whether this suggested that there may be a need for a more complex cell culture model to closely mimic natural heart valve architecture and environment for teasing out the role of FGF1 and FGF2, or longer culture durations, may require further investigation.

With regard to western blotting experiments, we originally collected cell lysate by snap-freezing immediately after stretch termination and added lysis buffer directly to the frozen hydrogel. This method was necessary for the detection of the transient expression of phosphorylated proteins. However, we failed to detect expression of total proteins with this lysate. When we enzymatically treated the matrix for 1 hour, we were able to see total protein's expression but the transient expression of phosphorylated proteins were lost due to the long isolation procedure. As a result, to be able to both detect transient expression of phosphorylated proteins and stable expression of total protein from the same sample, we cut the hydrogel in half and processed separately. It is worth emphasizing that the two pieces of hydrogel came from exact same sample. They were only cut and processed right after stretch termination. We also used β-actin as loading control for every western blot, ensuring equal amount of lysates was loaded. Future experiments could optimize this protein isolation methodology for encapsulated cells in this 3D model. We also hope that in future experiments, we could extend the stretching duration to longer time points to further investigate the effect of FGFs on cell proliferation, metabolism and maybe other cellular remodeling endpoints.

5. CONCLUSIONS

We report here the possible involvement of FGF-mediated signaling in valve cell responses under stretching conditions via Akt/mTOR pathway. In our experiment, it appeared that FGF1 and FGF2 could modulate VIC phenotype under different mechanical stimulations. VICs appeared to be able to remain quiescent with high proliferative property in the presence of FGFs. When experiencing elevated stretch, VICs increased proliferation possibly as a way to compensate against extra load. When FGFs were added, cells started reducing proliferation. Cell proliferation also seemed to associate with the activation of Akt/mTOR pathway activation, cell metabolism and cell phenotype. Overall, this study provided fundamental information about how valve cells behave under abnormal stretch. Future studies need to investigate these phenomena at longer culture durations and to look into more cellular remodeling endpoints to get a more complete picture of what was going on with the cells when they experience abnormal stimulation in the context of FGF1/FGF2.

REFERENCES

Aoyagi, T., and T. Matsui. 2011. Phosphoinositide-3 kinase signaling in cardiac hypertrophy and heart failure. *Curr Pharm Des* 17 (18):1818-24.

Cheng, H., Q. Yao, R. Song, Y. Zhai, W. Wang, D. A. Fullerton, and X. Meng. 2017. Lysophosphatidylcholine activates the Akt pathway to upregulate extracellular matrix protein production in human aortic valve cells. *J Surg Res* 213:243-250.

El Husseini, D., M. C. Boulanger, A. Mahmut, R. Bouchareb, M. H. Laflamme, D. Fournier, P. Pibarot, Y. Bosse, and P. Mathieu. 2014. P2Y2 receptor represses IL-6 expression by valve interstitial cells through Akt: implication for calcific aortic valve disease. *J Mol Cell Cardiol* 72:146-56.

Gotlieb, A. I., A. Rosenthal, and P. Kazemian. 2002. Fibroblast growth factor 2 regulation of mitral valve interstitial cell repair in vitro. *J Thorac Cardiovasc Surg* 124 (3):591-7.

Han, L., and A. I. Gotlieb. 2011. Fibroblast growth factor-2 promotes in vitro mitral valve interstitial cell repair through transforming growth factor-beta/Smad signaling. *Am J Pathol* 178 (1):119-27.

Han, L., and A. I. Gotlieb. 2012. Fibroblast growth factor-2 promotes in vitro heart valve interstitial cell repair through the Akt1 pathway. *Cardiovasc Pathol* 21 (5):382-9.

Ikeda, M., T. Ide, T. Fujino, Y. Matsuo, S. Arai, K. Saku, T. Kakino, Y. Oga, A. Nishizaki, and K. Sunagawa. 2015. The Akt-mTOR axis is a pivotal regulator of eccentric hypertrophy during volume overload. *Sci Rep* 5:15881.

Lam, N. T., T. J. Muldoon, K. P. Quinn, N. Rajaram, and K. Balachandran. 2016. Valve interstitial cell contractile strength and metabolic state are dependent on its shape. *Integr Biol (Camb)* 8 (10):1079-1089.

Latif, N., A. Quillon, P. Sarathchandra, A. McCormack, A. Lozanoski, M. H. Yacoub, and A. H. Chester. 2015. Modulation of human valve interstitial cell phenotype and function using a fibroblast growth factor 2 formulation. *PLoS One* 10 (6):e0127844.

Liu, A. C., V. R. Joag, and A. I. Gotlieb. 2007. The emerging role of valve interstitial cell phenotypes in regulating heart valve pathobiology. *Am J Pathol* 171 (5):1407-18.

Murakami, M., and M. Simons. 2008. Fibroblast growth factor regulation of neovascularization. *Curr Opin Hematol* 15 (3):215-20.

Panek, R. L., G. H. Lu, T. K. Dahring, B. L. Batley, C. Connolly, J. M. Hamby, and K. J. Brown. 1998. In vitro biological characterization and antiangiogenic effects of PD 166866, a selective inhibitor of the FGF-1 receptor tyrosine kinase. *J Pharmacol Exp Ther* 286 (1):569-77.

Porras, A. M., N. C. van Engeland, E. Marchbanks, A. McCormack, C. V. Bouten, M. H. Yacoub, N. Latif, and K. S. Masters. 2017. Robust Generation of Quiescent Porcine Valvular Interstitial Cell Cultures. *J Am Heart Assoc* 6 (3).

Quinn, K. P., G. V. Sridharan, R. S. Hayden, D. L. Kaplan, K. Lee, and I. Georgakoudi. 2013. Quantitative metabolic imaging using endogenous fluorescence to detect stem cell differentiation. *Sci Rep* 3:3432.

Wang, H. W., Y. H. Wei, and H. W. Guo. 2009. Reduced nicotinamide adenine dinucleotide (NADH) fluorescence for the detection of cell death. *Anticancer Agents Med Chem* 9 (9):1012-7.

Yu, J. S., and W. Cui. 2016. Proliferation, survival and metabolism: the role of PI3K/AKT/mTOR signalling in pluripotency and cell fate determination. *Development* 143 (17):3050-60.

Yun, Y. R., J. E. Won, E. Jeon, S. Lee, W. Kang, H. Jo, J. H. Jang, U. S. Shin, and H. W. Kim. 2010. Fibroblast growth factors: biology, function, and application for tissue regeneration. *J Tissue Eng* 2010:218142.

Zhao, T., W. Zhao, Y. Chen, R. A. Ahokas, and Y. Sun. 2011. Acidic and basic fibroblast growth factors involved in cardiac angiogenesis following infarction. *Int J Cardiol* 152 (3):307-13.

CHAPTER 6

Conclusions, Limitations and Future Directions

1. CONCLUSIONS

Heart disease is the leading cause of death in the U.S., accounting for more than 600,000 American deaths each year (Kochanek et al. 2011). A population-based study reported that more than 13% of over 75 years suffer from some forms of valvular heart disease (VHD) (Nkomo et al. 2006) and 2-7% of the population in the western world of over 65 years with aortic stenosis (Spaccarotella, Mongiardo, and Indolfi 2011), the most common valve lesion in developed countries. Currently, there are no drug therapies that can cure or halt VHD progression. Without an aortic valve replacement, survival rates of patients with severe symptomatic aortic stenosis are as low as 50% at 2 years and 20% at 5 years after the onset of symptoms (Otto 2000).

As a result, tremendous efforts have been made to study heart valve biology and pathology in order to find drug therapies for VHD. Unfortunately, the complexity of heart valve architecture as well as the hemodynamic environment within the heart makes it extremely difficult for researchers to reproduce such conditions for *in vitro* studies. Consequently, most studies in the field were carried out in 2D or via use of the whole excised leaflets. Obviously, 2D culture model is not ideal because valve cells naturally reside in a 3D matrix environment which allows them to respond to biomechanical cues and exert forces through cell-cell, and cell-ECM matrix communication (Taylor et al. 2003). It is also impossible to apply mechanical forces onto currently existing 2D models. Using the whole excised leaflets, on the other hand, allows the application of certain mechanical forces onto the tissue while still preserving the natural architecture of the heart valve as well as all the cell populations and the interaction between the cells and the ECM (Balachandran et al. 2006; Sucosky et al. 2008; Sucosky et al. 2009; Sun, Chandra, and Sucosky 2012). The disadvantage of this approach is the inability to study and observe live cells, and the limited longer duration viability of whole tissues in an *ex vivo* setting.

It is also difficult to study cell type specific-mediated responses. A 3D scaffold appears to be a promising alternative not only for an *in vitro* culture model but also for generating living valve substitutes *in vitro* for tissue engineering application. However, the creation of a scaffold with similar composition, structure and mechanical properties to native leaflets is very challenging and requires tremendous efforts in finding appropriate biomaterials, cells and the availability of bioreactors for mechanical stimulation purpose (Zhang et al. 2015).

Overall, studies toward finding treatment therapies for heart valve disease are, in part, hindered by the challenges in recapitulating the dynamic structure and environment of the native heart valve. Our project set out to develop novel models to culture VICs *in vitro* and to study valve cell behavior under physiological and pathological conditions. In our study, VICs were examined both at the single cell and 3D cell levels in the presence of static and cyclic stretching conditions, respectively. These models are considered novel in the field and the information gained from these studies is expected to provide fundamental understanding of valve cell biology and pathology.

VICs are a dynamic population in the heart valve, whose primary function is to maintain leaflet structure and valve function (Taylor et al. 2003). VICs display different phenotypes depending on surrounding cellular and ECM signals. They are believed to remain quiescent in healthy leaflets. Upon experiencing abnormal conditions, they become activated and exhibit features of myofibroblasts such as increased contraction, prominent stress fiber, increased proliferation and ECM remodeling. These responses are considered important for wound repair process. However, if for some reasons, activated VICs persist with continued proliferation and ECM remodeling, this will detrimentally affect valve properties and physiological function (Wang, Leinwand, and Anseth 2014; Liu, Joag, and Gotlieb 2007).

In our single cell study, when single VICs were subjected to different ARs to mimic the deformation seen in stretched valve leaflets, we observed structural and functional changes in these cells which corresponded to features of activated VICs. It appeared that as VICs became more elongated (the deformation that seen when cells were stretched at pathological 20%), they started to re-organize their cytoskeletal organization such that more stress fibers were expressed in the circumferential direction. These cells also significantly increased contractility, metabolism and proliferation in response to shape alteration. Although this single-cell model did not account for the role of hemodynamic mechanical forces, by just manipulating cell shape, we were able to study cell behavior at the smallest functional scale, the single cell. The result from this study encouraged us to continue looking into the signaling regulation on valvular cells using a 3D model that better represented the microenvironment of the natural heart valve.

The matrigel-collagen hydrogel scaffold is not a new model in other fields (Zimmermann, Melnychenko, and Eschenhagen 2004; Zimmermann et al. 2002; van Marion et al. 2015; Dewitt et al. 2009) but its combination is novel in the heart valve field, although independent use of matrigel and collagen has been previous reported (Butcher and Nerem 2004; Gupta et al. 2007; Arevalos et al. 2016). This 3D scaffold was thoroughly examined biologically and mechanically with respect to using it for culturing VIC in the presence of cyclic stretching. The mixture of matrigel and collagen created a porous scaffold with good bioactivity and strong mechanical properties that was able to sustain cyclic stretching for 48 hours in culture. Compared to existing 3D models in the field, the matrigel-collagen scaffold could serve as another promising alternative to be used for *in vitro* study. Its application potential is immediately tested in the last part of our project where it is used to study the role of FGF1/FGF2 in mediating cell proliferation in response to elevated cyclic stretch. Using this matrigel-collagen scaffold, we were able to

apply uniaxial cyclic stretch onto the cells while providing cells with a rich ECM matrix environment. The significant finding of this study is to show the protective role of FGF1/FGF2 on VICs at pathological stretch, in part, via the Akt/mTOR pathway and modulation of VIC phenotype. As shown in our experiments, VICs up-regulated Akt/mTOR in response to elevated cyclic stretch. This upregulation was also coupled with increased metabolism, proliferation and increased expression of activated markers. Upon treatment with FGF1/FGF2, these responses were reversed, clearly suggesting the potential application of FGF1/FGF2 as therapeutic target for treatment of valvular heart disease.

2. LIMITATIONS AND FUTURE DIRECTIONS

This study has some limitations that we would like to address. First, we only looked at acute responses of cells upon experiencing altered shape and/or mechanical stimulation (i.e. 24 hours and 48 hours). Longer duration needs to be done to further examine these responses in order to obtain more clinically relevant data as the valve disease progression usually takes months or years to develop. Second, due to technical limitations, we were only able to carry out these studies in the presence of solely uniaxial cyclic stretching which is not a perfect simulation of *in vivo* condition, but accepted widely in the field. However, to our knowledge, there are no existing models that could mimic the mechanics of the actual heart valve. Last, it is author's hope that more end-point assays could be done with regard to the signaling study to fully investigate the role of FGF1/FGF2 on valve cell pathophysiology. These additional experiments will be the focus of future directions for this project.

REFERENCES

Arevalos, C. A., J. M. Berg, J. M. Nguyen, E. L. Godfrey, C. Iriondo, and K. J. Grande-Allen. 2016. Valve Interstitial Cells Act in a Pericyte Manner Promoting Angiogensis and Invasion by Valve Endothelial Cells. *Ann Biomed Eng* 44 (9):2707-23.

Balachandran, K., S. Konduri, P. Sucosky, H. Jo, and A. P. Yoganathan. 2006. An ex vivo study of the biological properties of porcine aortic valves in response to circumferential cyclic stretch. *Ann Biomed Eng* 34 (11):1655-65.

Butcher, J. T., and R. M. Nerem. 2004. Porcine aortic valve interstitial cells in three-dimensional culture: comparison of phenotype with aortic smooth muscle cells. *The Journal of heart valve disease* 13 (3):478-85; discussion 485-6.

Dewitt, D. D., S. N. Kaszuba, D. M. Thompson, and J. P. Stegemann. 2009. Collagen I-matrigel scaffolds for enhanced Schwann cell survival and control of three-dimensional cell morphology. *Tissue engineering. Part A* 15 (10):2785-93.

Gupta, V., J. A. Werdenberg, T. L. Blevins, and K. J. Grande-Allen. 2007. Synthesis of glycosaminoglycans in differently loaded regions of collagen gels seeded with valvular interstitial cells. *Tissue Eng* 13 (1):41-9.

Kochanek, K. D., J. Xu, S. L. Murphy, A. M. Minino, and H. C. Kung. 2011. Deaths: preliminary data for 2009. *Natl Vital Stat Rep* 59 (4):1-51.

Liu, A. C., V. R. Joag, and A. I. Gotlieb. 2007. The emerging role of valve interstitial cell phenotypes in regulating heart valve pathobiology. *Am J Pathol* 171 (5):1407-18.

Nkomo, V. T., J. M. Gardin, T. N. Skelton, J. S. Gottdiener, C. G. Scott, and M. Enriquez-Sarano. 2006. Burden of valvular heart diseases: a population-based study. *Lancet* 368 (9540):1005-11.

Otto, C. M. 2000. Timing of aortic valve surgery. *Heart* 84 (2):211-8.

Spaccarotella, C., A. Mongiardo, and C. Indolfi. 2011. Pathophysiology of aortic stenosis and approach to treatment with percutaneous valve implantation. *Circ J* 75 (1):11-19.

Sucosky, P., K. Balachandran, A. Elhammali, H. Jo, and A. P. Yoganathan. 2009. Altered shear stress stimulates upregulation of endothelial VCAM-1 and ICAM-1 in a BMP-4- and TGF-beta1-dependent pathway. *Arterioscler Thromb Vasc Biol* 29 (2):254-60.

Sucosky, P., M. Padala, A. Elhammali, K. Balachandran, H. Jo, and A. P. Yoganathan. 2008. Design of an ex vivo culture system to investigate the effects of shear stress on cardiovascular tissue. *J Biomech Eng* 130 (3):035001.

Sun, L., S. Chandra, and P. Sucosky. 2012. Ex vivo evidence for the contribution of hemodynamic shear stress abnormalities to the early pathogenesis of calcific bicuspid aortic valve disease. *PLoS One* 7 (10):e48843.

Taylor, P. M., P. Batten, N. J. Brand, P. S. Thomas, and M. H. Yacoub. 2003. The cardiac valve interstitial cell. *Int J Biochem Cell Biol* 35 (2):113-8.

van Marion, M. H., N. A. Bax, M. C. van Turnhout, A. Mauretti, D. W. van der Schaft, M. J. Goumans, and C. V. Bouten. 2015. Behavior of CMPCs in unidirectional constrained and stress-free 3D hydrogels. *J Mol Cell Cardiol* 87:79-91.

Wang, H., L. A. Leinwand, and K. S. Anseth. 2014. Cardiac valve cells and their microenvironment--insights from in vitro studies. *Nat Rev Cardiol* 11 (12):715-27.

Zhang, X., B. Xu, D. S. Puperi, Y. Wu, J. L. West, and K. J. Grande-Allen. 2015. Application of hydrogels in heart valve tissue engineering. *J Long Term Eff Med Implants* 25 (1-2):105-34.

Zimmermann, W. H., I. Melnychenko, and T. Eschenhagen. 2004. Engineered heart tissue for regeneration of diseased hearts. *Biomaterials* 25 (9):1639-47.

Zimmermann, W. H., K. Schneiderbanger, P. Schubert, M. Didie, F. Munzel, J. F. Heubach, S. Kostin, W. L. Neuhuber, and T. Eschenhagen. 2002. Tissue engineering of a differentiated cardiac muscle construct. *Circ Res* 90 (2):223-30.

APPENDIX

Appendix 1: Fabrication of the matrigel-collagen hydrogel

Rat tail collagen type I and reduced growth factor matrigel were both purchased from Corning, NY.

Collagen hydrogel was made by adding appropriate amount of PBS to make up a desired concentration. 0.1M NaOH was last added to neutralize and allow for polymerization.

Mixed matrigel-collagen hydrogel was made as follows:

- Calculate how much of each reagent was needed based on table 3.1.
- Start adding the reagents together, beginning with matrigel, followed by collagen, PBS (if needed) and 0.1M NaOH.
- Mixed gently to avoid bubble and incubated at 37°C for at least 30 minutes. Note that all the procedures were performed on ice.

Table 3.1: Summary of the samples used in the study

	Matrigel	Collagen 1 mg/ml	Collagen 2 mg/ml	M-C 0.5 mg/ml	M-C 1mg/ml	M-C 1.5 mg/ml	M-C 2 mg/ml
Matrigel (v/v)	100%	None	None	80%	65%	55%	45%
Collagen	None	1mg/ml	2mg/ml	0.5mg/ml	1mg/ml	1.5mg/ml	2mg/ml
NaOH	None	Yes	Yes	Yes	Yes	Yes	Yes

Valve interstitial cells were encapsulated into the mixed matrigel-collagen as follow:

- Trypsinize the cells and count to obtain desired seeding density.
- Centrifuge the solution at 500RCF for 5 minutes. Discard the supernatant. Do not disturb the cell pellet. Quickly proceed to next step.
- Start adding hydrogel ingredients to the cell pellet, beginning with matrigel, followed by collagen, PBS (if needed) and 0.1M NaOH.
- Gently mix by pipetting.

- Transfer the mixture onto the cell chamber (the cell chamber was UV-Ozone treatedduring trypsinization process).
- Allow polymerization for at least 30 minutes. After 30 minutes, top off the hydrogel with cell culture media and return the chamber back to the incubator. Note that all the procedures were performed on ice.

Appendix 2: Protocol for controlling the biostretcher

Step 1: Initiate the LinMot program

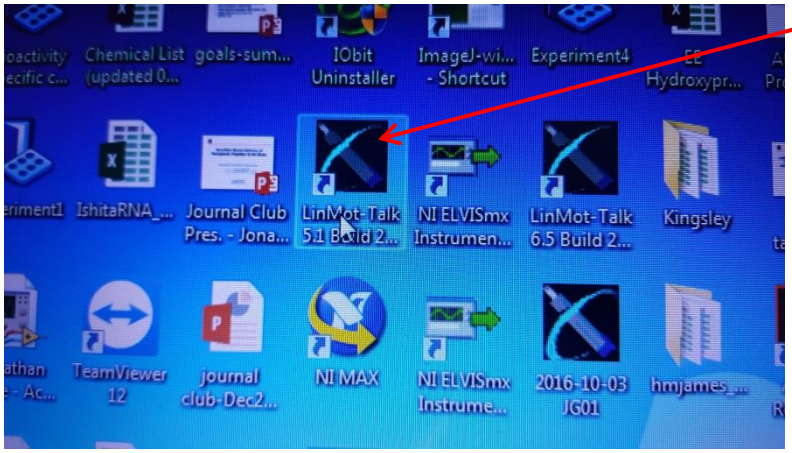

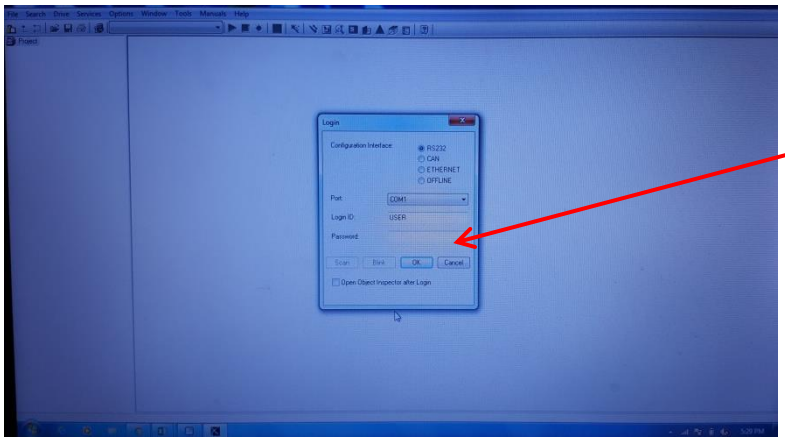

Step 2: Set up desired parameters

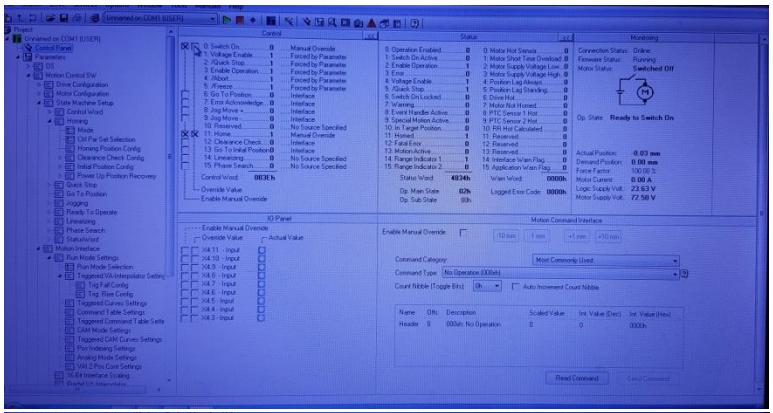

Control Panel Screen

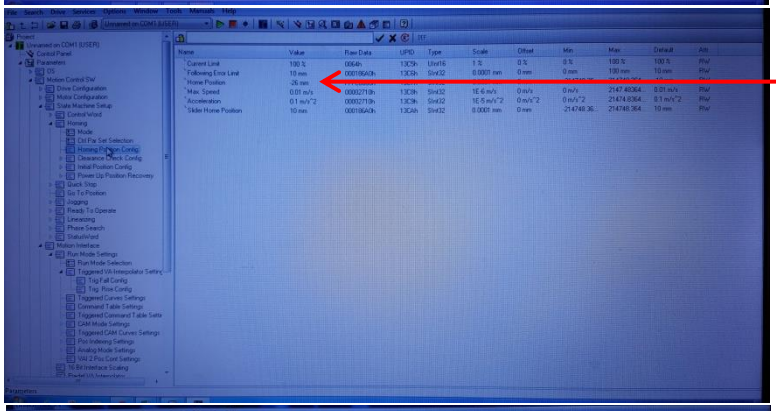

Edit desired homing position

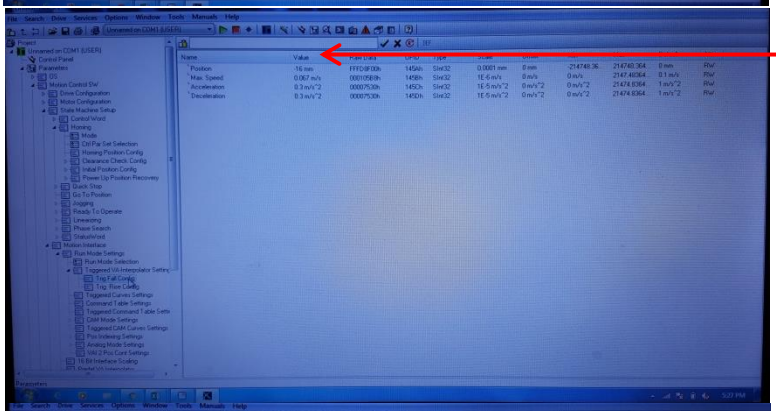

Edit desired Trig Fall position

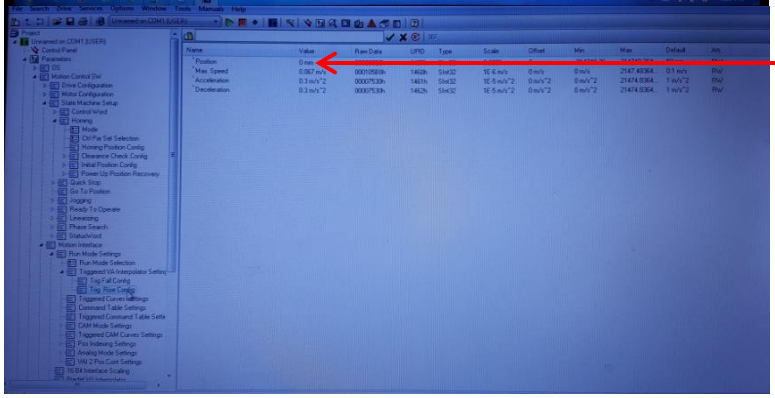

Edit desired Trig Rise position

Step 3: Initiate the stretch

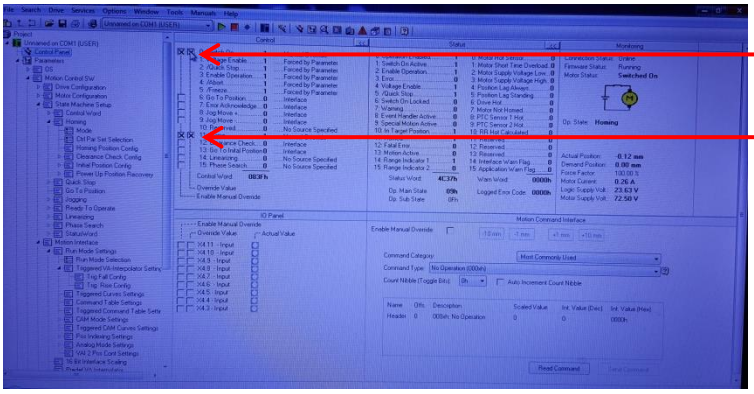

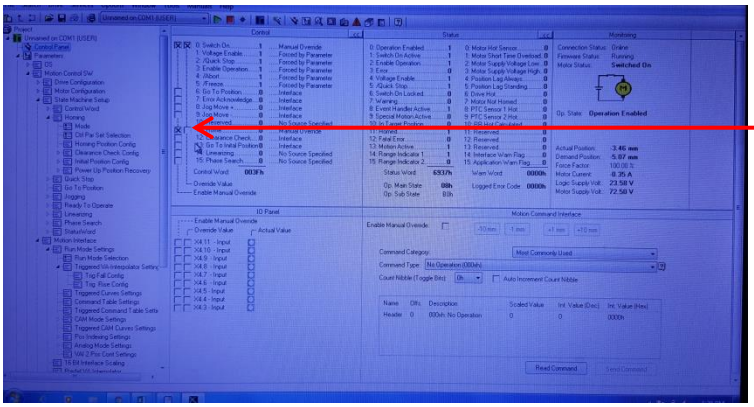

Step 4: Terminate the stretch

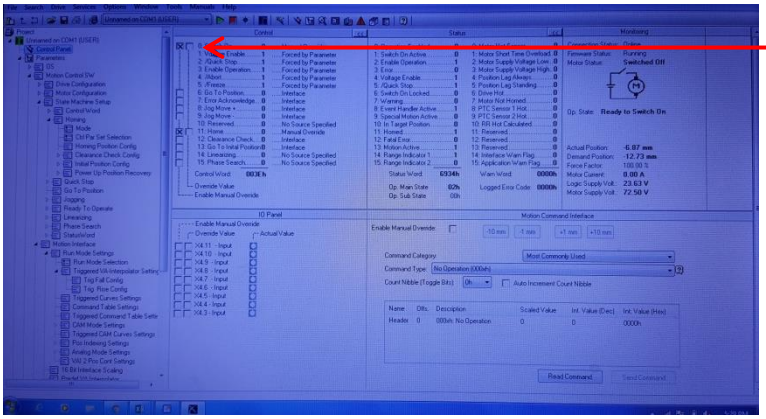

Appendix 3: dilution ratio of antibody

Antibody/Dye	Vendor	Dilution ratio
Phalloidin	Life Technologies	1:200
DAPI	Life Technologies	1:200
Ki67	Abcam	1:500
ERK1/2	Cell Signaling	1:50
pERK1/2	Cell Signaling	1:500
α-SMA	Abcam	1:200
Vimentin	Abcam	1:1500
SM-MHC	Millipore	1:20
β-actin	Abcam	1:200
Calponin	Abcam	1:1000
Fibronectin	Abcam	1:500
Osteopontin	Abcam	1:200
FGF1	Santa Cruz Biotechnology	1:10
FGF2	Santa Cruz Biotechnology	1:10
FGFR1	Abcam	1:25
FGFR2	Abcam	1:25
Akt	Cell Signaling	1:100
pAkt	Cell Signaling	1:200
mTOR	Cell Signaling	1:100
pmTOR	Abcam	1:500
Hsp47	Enzo Life Sciences	1:1000

Appendix 4: Biosafety Committee research approval

March 1, 2018

MEMORANDUM

TO:	Dr. Kartik Balachandran
FROM:	Bob Beitle, Acting Biosafety Committee Chair
RE:	Protocol Modification
PROTOCOL #:	16005
PROTOCOL TITLE:	Role of risk factors such as smoking and diabetes on cardiovascular cells
APPROVED PROJECT PERIOD:	Start Date August 13, 2015 Expiration Date August 12, 2018

The Institutional Biosafety Committee (IBC) has approved your request, dated January 30, 2018, to modify Protocol # 16005, "Role of risk factors such as smoking and diabetes on cardiovascular cells".

The IBC appreciates your assistance and cooperation in complying with University and Federal guidelines for research involving hazardous biological materials.